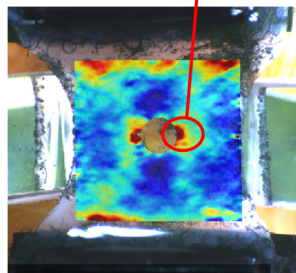


# Mechanical Characterization of Tissue Engineered Fibrous Cap Constructs

Towards the Development of an In Vitro  
Atherosclerotic Disease Model

**Sheila M. Serra**  
MSc Thesis  
Biomedical Engineering





# Mechanical Characterization of Tissue Engineered Fibrous Cap Constructs

Towards the Development of an In Vitro Atherosclerotic Disease Model

by

Sheila M. Serra

to obtain the degree of Master of Science  
at the Delft University of Technology,  
to be defended publicly on Wednesday, September 23, 2020 at 10:00.

Student number: 4778421

Supervisors: Dr. ir. Frank Gijzen (Erasmus MC)  
Dr. Tamar Wissing (Erasmus MC)

Dr. ir. Lidy Fratila-Apachitei (TU Delft)  
Prof. Dr. ir. Amir A. Zadpoor (TU Delft)

An electronic version of this thesis is available at <http://repository.tudelft.nl/>.



# Preface

For my Master's research graduation project, I was given the opportunity to work on a recently developed project at Erasmus Medical Center in collaboration with the Eindhoven University of Technology. The overall aim of this project is to create an *in vitro* reproducible human-like vulnerable plaque in order to study atherosclerotic plaque rupture mechanics, nearly impossible to study inside the body due to its stochastic nature.

Due to the COVID-19 pandemic, the study could not be completed in the way we originally planned, introducing a strain gradient during culture to the tissue engineered constructs and linking histology to mechanical properties, therefore the topic changed in order to work from home. The experimental facilities were no longer available during this time, therefore the focus of this project shifted to the constructs that had been created and mechanically tested before the lockdown. In this study, the mechanical testing data obtained was used for investigating the mechanical behavior of differently strained constructs during culture and different clamping mechanisms during testing, as well as for performing digital image correlation in order to observe local strain patterns leading to rupture. Therefore, the study shifted to a more exploratory nature, containing a few limitations.

*Sheila Serra*  
*Delft, September 2020*



# Acknowledgements

This project was completed thanks to the assistance and encouragement from a few people. First and foremost, I would like to thank my daily supervisor, Tamar Wissing, for taking me onto this project and teaching me as much as she could about tissue engineering in the limited time available. She was extremely helpful and was always happy to answer my million questions. I would also like to thank Michiel Manten from the Instrumentation department for manufacturing the redesigned clamps I sketched on short notice. I am also very grateful to Robert Beurskens for providing the assistance and tools needed to fix the outdated Flexcell system, although unfortunately I ended up not using it for my project due to the COVID-19 pandemic. He was always there to lend a helping hand and we had some nice hallway chats. Also, thanks to Ali Akyildiz for occasionally meeting to brainstorm ideas and give input for my project. I would like to thank my TU Delft supervisor, Lidy Fratila-Apachetei, for providing guidance during my project and always responding to my emails quickly.

Last but not least, I would like to thank my amazing quarantine supervisor, Frank Gijzen, for providing continuous support and advice during these unprecedented times so that I could complete my thesis project in time. He was helpful in thinking out loud with me (virtually and face-to-face) and pushed me to think about matters more analytically.

I am extremely grateful for the guidance and encouragement from all of my colleagues in the Cardiovascular Biomechanics department at Erasmus MC, as well the support and patience from my friends and family. The overall help from all of the people mentioned above allowed me to successfully complete my thesis project.



# Abstract

Atherosclerosis is a widespread disease characterized by the formation of a plaque within the inner most layer of the arterial wall. This plaque is comprised of a lipid-rich pool containing little to no collagen covered by a collagenous fibrous cap which serves as a barrier containing the plaque from rupture. Plaque rupture is an often fatal phenomenon, not yet fully understood, which can result in arterial blockage causing myocardial infarction or stroke depending on rupture location. Whether a plaque will rupture depends on many interrelated aspects; the biological composition of the plaque, the mechanical properties of these components, and how they are mechanically loaded. The collagenous matrix is the main load bearing structure of the plaque cap, therefore affects plaque stability and should be further investigated. Due to the various limitations when studying *ex vivo* and *in vivo* human plaques as well as the significant difference in plaque development in animal models, an *in vitro* atherosclerotic plaque cap model is necessary to systematically study plaque rupture mechanics.

In this study, a simplified collagenous fibrous cap model with a soft inclusion (SI) was developed. The effect of intermittent uniaxial straining (IS) versus no straining (static) during culture was investigated as intermittent straining during culture is linked to an increase in alignment of collagen fibers in the loading direction, which is seen in human fibrous caps. The constructs were mechanically tested with two different clamp designs (commercial and redesigned), to investigate the differences in mechanical behavior and to improve the clamping technique. The local strain patterns were studied using digital image correlation (DIC) preceding rupture.

Although there was higher compaction observed in the IS constructs when compared to the static constructs, the mechanical behavior of the IS and static constructs tested in the commercial clamps were comparable. However, DIC analysis demonstrated that the static constructs in the commercial clamps showed homogeneous  $\epsilon_{xx}$  extension behavior, whereas the IS constructs showed a symmetric “C-shaped” compressive pattern, signifying a possible difference in microstructure. Additionally, the redesigned clamps displayed a consistent two bump rupture pattern correlating to rupture near the SI, as well as higher measured force at comparable stretch, not seen with the commercial clamps. The redesigned clamps demonstrated an improvement in the testing method when compared to the commercial clamps by exhibiting better load transmission from clamp to tissue, creating more homogeneous strain distribution within the region of interest and leading to more consistent rupture near the SI. Interestingly, high  $\epsilon_{yy}$  values were observed at the rupture location in both the redesigned and commercial clamps, possibly demonstrating a linkage between high  $\epsilon_{yy}$  extension behavior and rupture location. In this study, collagenous constructs with an integrated SI were successfully created exhibiting mechanical properties within the range found in literature and rupturing near the SI-tissue interface, therefore these findings can serve as a guide for future experiments in the development of an atherosclerotic plaque cap *in vitro* model.



# Contents

<b>Preface</b>	<b>i</b>
<b>Acknowledgements</b>	<b>iii</b>
<b>Abstract</b>	<b>v</b>
<b>Table of Contents</b>	<b>vii</b>
<b>List of Figures</b>	<b>xi</b>
<b>List of Tables</b>	<b>xvii</b>
<b>Nomenclature</b>	<b>xix</b>
<b>1 Introduction</b>	<b>1</b>
1.1 Motivation . . . . .	2
1.2 Aims of the study . . . . .	4
<b>2 Materials and Methods</b>	<b>5</b>
2.1 Tissue Engineered Constructs . . . . .	6
2.1.1 Cell Culture . . . . .	6
2.1.2 Engineered Fibrous Cap Models . . . . .	7
2.1.3 Including Previously Created Constructs . . . . .	9
2.2 Mechanical Testing . . . . .	10
2.2.1 Experimental Setup . . . . .	10
2.2.2 Clamp Redesign . . . . .	12
2.3 Digital Image Correlation . . . . .	13
2.4 Data Analysis . . . . .	14
2.4.1 Compaction Analysis . . . . .	14
2.4.2 Global Mechanical Analysis . . . . .	14
2.4.3 Creating Regions for DIC Analysis . . . . .	17
2.4.4 Image Analysis Selection . . . . .	19
2.4.5 Finite Element Analysis Model: Illustrative Example . . . . .	19
2.4.6 Strain Measures . . . . .	20
2.4.7 Statistical Analysis . . . . .	21

<b>3</b>	<b>Results</b>	<b>22</b>
3.1	Tissue Engineered Constructs . . . . .	22
3.2	Global Mechanical Behavior . . . . .	24
3.2.1	Effect of Straining Protocol: Static vs IS Constructs . . . . .	24
3.2.2	Effect of Clamp Design: Commercial vs Redesigned Clamps . . . . .	25
3.3	Local Strain Patterns . . . . .	27
3.3.1	Finite Element Analysis Model: Illustrative Example . . . . .	28
3.3.2	Effect of Straining Protocol: Static vs IS Constructs . . . . .	30
3.3.3	Effect of Clamp Design: Commercial vs Redesigned Clamps . . . . .	32
3.3.4	Quantification of Local Strain Patterns . . . . .	34
3.4	Rupture Behavior . . . . .	40
<b>4</b>	<b>Discussion</b>	<b>43</b>
4.1	Tissue Engineered Constructs . . . . .	43
4.2	Global Mechanical Behavior . . . . .	44
4.2.1	Effect of Straining Protocol: Static vs IS Constructs . . . . .	44
4.2.2	Effect of Clamp Design: Commercial vs Redesigned Clamps . . . . .	45
4.2.3	Comparison to human atherosclerotic fibrous caps . . . . .	46
4.3	Local Strain Patterns . . . . .	46
4.3.1	Effect of Straining Protocol: Static vs IS Constructs . . . . .	46
4.3.2	Effect of Clamp Design: Commercial vs Redesigned Clamps . . . . .	47
4.4	Rupture Behavior . . . . .	48
4.5	Limitations . . . . .	49
<b>5</b>	<b>Concluding Remarks</b>	<b>51</b>
5.1	Conclusion . . . . .	51
5.2	Future recommendations . . . . .	52
<b>Appendix A Protocols</b>		<b>57</b>
A.1	Creating Fibrin-based TE Constructs . . . . .	57
A.2	Mechanical Testing . . . . .	62
<b>Appendix B Clamp Redesign Specifications</b>		<b>69</b>
<b>Appendix C Ncorr Software</b>		<b>71</b>
C.1	Introduction . . . . .	71
C.2	Mathematical Algorithm . . . . .	71
C.3	Program Work Flow . . . . .	75
C.3.1	Starting Ncorr and using multithreading . . . . .	75
C.3.2	Setting the reference and current image(s) . . . . .	76
C.3.3	Setting the region of interest . . . . .	76
C.3.4	Selecting parameters and performing RG-DIC analysis . . . . .	77
C.3.5	Formatting displacements . . . . .	80
C.3.6	Strain analysis . . . . .	81
C.3.7	Plotting and obtaining data . . . . .	82

<b>Appendix D DIC Parameter Analysis</b>	<b>84</b>
D.1 Subset Size and Strain Radius Selection . . . . .	84
D.2 2D Correlation Coefficient Maps . . . . .	86
D.3 Optimizing Speckle Pattern . . . . .	86
D.4 Optimizing Parameter Selection . . . . .	87
<b>Appendix E Supplementary Results</b>	<b>88</b>
E.1 Linking local strain patterns to global behavior . . . . .	88
E.2 X-Y displacement/strain maps for all constructs . . . . .	89
E.3 Average X-Y strain plots across all constructs . . . . .	101
E.4 X-Y strain variation example . . . . .	113
E.5 Scatter plots: average X-Y regional strain . . . . .	115
E.6 DIC analysis: SI region example . . . . .	120
<b>Appendix F Matlab code</b>	<b>121</b>
F.1 Tissue Culture Analysis . . . . .	121
F.1.1 Plotting average compaction . . . . .	121
F.2 DIC Parameter Analysis . . . . .	123
F.2.1 Subset size and strain radius selection . . . . .	123
F.2.2 2D correlation coefficient maps . . . . .	127
F.3 Data Analysis . . . . .	128
F.3.1 Determining the image for each construct at 10% average mid cap Y strain . . . . .	128
F.3.2 Plotting the average $\epsilon_{xx}$ , $\epsilon_{yy}$ and $\epsilon_{xy}$ values across the width of the constructs . . . . .	129
F.3.3 Determining the average $\epsilon_{xx}$ , $\epsilon_{yy}$ and $\epsilon_{xy}$ values for the 8 regions . .	134
F.3.4 Plotting the actuator Y displacement vs Y force and calculating the tangential stiffness for each construct . . . . .	136
F.3.5 Statistical analysis . . . . .	139



# List of Figures

1.1	Vulnerable plaque structure. Atherosclerotic plaques form in the intima layer and when the fibrous cap strength exceeds the arterial stresses, rupture occurs and a thrombus can form, blocking blood flow through the lumen. *Image courtesy of Tamar Wissing . . . . .	1
1.2	Collagen fiber direction a) collagen orientation vector plot of a human fibrous cap longitudinal section b) corresponding rose plot shows predominately longitudinal alignment in the cap with respect to the lumen [6] and c) multiphoton image of a vascular TE construct subjected to 3 weeks of uniaxial intermittent straining shows longitudinal alignment in direction of load and high collagen and SMCs production (green:collagen, blue: smooth muscle cells) [5] . . . . .	3
1.3	The goal of the in vitro atherosclerotic fibrous cap model is to systematically add relevant biological components that influence rupture such as the collagenous structure created by smooth muscle cells, microcalcifications, macrophages, and a combination of these factors in order to simulate in vivo rupture mechanics *Image courtesy of Tamar Wissing . . .	3
2.1	Overview of study methods . . . . .	6
2.2	The Velcro strips were cut with 15x5 mm dimensions and two were pasted 10 mm apart within the culture wells: a) top view of the reference used to place the Velcro's at the correct location within the wells b) one Velcro strip has been pasted using the reference under the well, another strip will be pasted in the dotted white region . . . . .	7
2.3	An example of a static construct on day 0 after seeding the fibrin-cell matrix between two PDMS bars (a) and on day 7 after including the SI (b) . . . .	9
2.4	Adapted protocol used for culturing the constructs. The control group included the statically cultured constructs (n=4). Intermittent straining was performed on group 1 (n=4) for one week after two weeks of static culturing (0.5 Hz, 4-5% strain, 1 hr on + 3 hrs off) [5] . . . . .	9

2.5	The Flexcell system subjected the constructs to uniaxial intermittent straining via a vacuum system on each side of the loading post where the construct has been seeded (Flexcell Int, McKeesport, PA): a) side view schematic of Flexcell system b) top view of a intermittently strained construct within the Flexcell system. Note: graphite particles were applied to the construct to track strain pattern . . . . .	10
2.6	Commercial uniaxial tensile tester with the components referred to [CellScale Biomaterial Testing, Waterloo, Canada] . . . . .	11
2.7	A construct mounted into two different clamping mechanisms for mechanical testing: a) commercial clamps b) redesigned clamps; top clamp shows how the construct is snugly fit onto the sandpaper groove before tightening the top piece . . . . .	12
2.8	Comparison of the original clamps and redesigned clamps: side and top view of the original clamps (a & c), side and top view of the redesigned clamps (b & d). The redesigned clamps were created specifically to avoid failure at the Velcro/clamp edge by evenly redistributing the stresses within the grip. *Images depict only one of the two clamps in the system . . . . .	13
2.9	The 5-parameter Mooney Rivlin material model was determined as the best fit model to the experimental stretch (x) vs stress (y) data and the material constants for each construct were obtained using the Curve Fitting Toolbox in MATLAB. This figure shows an example of one of the static constructs tested in the redesigned clamps . . . . .	16
2.10	The rectangular shaped ROI mask drawn over the top of a construct for DIC analysis. The ROI excludes the SI region and tissue regions near the clamps which contain Velcro fiber artefacts . . . . .	17
2.11	Subdivided regions of the constructs for DIC analysis which include right and left sides with the center of SI as the origin, top and bottom shoulders, and the mid cap region. The grey dotted lines represent the right and left sides of the SI. The box region enclosed by the green dotted lines is where the average $\epsilon_{yy}$ was calculated per image. The box extends from the top and bottom of the SI and 20% away from the edge and SI. The right or left side was chosen per construct based on which side displayed the most $\epsilon_{yy}$ field homogeneity within the region. The image number in which an average value of 10% $\epsilon_{yy}$ in the green box was used for data analysis . . . . .	18
2.12	The average $\epsilon_{xx}$ and $\epsilon_{yy}$ values were calculated per each region; 4,5: right/left of SI (mid cap), 2,7: top/bottom of SI (shoulders), 1,3,6,8: outside shoulder regions . . . . .	18
2.13	Image # (15 Hz) vs average mid cap $\epsilon_{yy}$ until rupture. A red marker has been placed at approximately $\epsilon_{10\%}$ for each construct. The image # of this location was used for analysis in order to normalize the local strain fields and minimize the variables between the constructs . . . . .	19
3.1	Comparison of construct compaction on day 21 with different culturing protocol: a) statically cultured construct showed less compaction in X direction b) IS construct showed more compaction in X direction . . . . .	22

3.2	Quantitative comparison of static and IS construct compaction percentage and standard deviation in the X, Y and Z directions (refer to coordinate system in Figure 3.1) on day 21. Note: negative values represent shrinkage and positive represent expansion, dotted line represents no change . . . . .	23
3.3	Images taken with a Brightfield microscope on day 21, before mechanical testing, to observe the collagen migration into the soft inclusion: a) static construct b) IS construct *Images courtesy of Tamar Wissing . . . . .	24
3.4	Y force vs actuator Y displacement plots of the IS and static constructs tested in the commercial clamps until rupture. This plot is proportional to the nominal engineering stress vs strain plot: Dotted curves represent the IS constructs, solid lines represent the static constructs, red represents rupture which occurred at the clamp edge, black represents rupture which occurred near the SI . . . . .	25
3.5	Y force vs actuator Y displacement plots of all statically cultured constructs until rupture. This plot is proportional to the nominal engineering stress vs strain plot: Solid curves represent the constructs tested in the redesigned clamps, dotted curves represent the constructs tested in the commercial clamps, red represents rupture which occurred at the clamp edge, black represents rupture which occurred near the SI . . . . .	26
3.6	Y force vs actuator Y displacement plots of all static (black) and all IS (red) constructs until rupture: solid lines represent the new clamps, dotted lines represent the commercial clamps. This plot is proportional to the nominal engineering stress vs strain plot . . . . .	27
3.7	Finite element analysis results of 2D hyperelastic model reported as logarithmic strain (symmetry applied about Y-Z plane) . . . . .	29
3.8	X and Y displacement and strain maps at $\epsilon_{10\%}$ for a static and IS construct tested in the commercial clamps . . . . .	31
3.9	Two constructs which displayed different behavior from the other constructs: a) $\epsilon_{xx}$ of a static construct tested in commercial clamps (gradient-like) b) $\epsilon_{yy}$ of an IS construct tested in commercial clamps (diagonally shifted behavior) . . . . .	32
3.10	X and Y displacement and strain maps at $\epsilon_{10\%}$ for two static constructs tested in the commercial clamps (left) and redesigned clamps (right) . . . . .	33
3.11	X and Y average strain plots running along the width of an IS construct, excluding the SI for the mid cap and shoulder regions, subdivided into left/right and top/bottom regions. The normal X and Y strains are presented in the first and second rows, respectively, as well as the XY shear strain in the last row. The grey dotted lines enclose the left and right most side boundaries of the SI region . . . . .	35
3.12	Average $\epsilon_{xx}$ (a), $\epsilon_{yy}$ (b), and $\epsilon_{xy}$ (c) from different regions of an IS construct (refer to Figure 2.12 for corresponding regions); blue: right and left sides of SI in mid cap region, green: top and bottom sides of SI in shoulder region, red: remaining shoulder regions, excluding edges . . . . .	37

3.13	Comparisons of average $\epsilon_{xx}$ between construct types and clamps used: a) left/right SI in mid cap region b) shoulder regions, excluding edges c) top/bottom SI in shoulder region; Note: (R) redesigned clamps, (C) commercial clamps *:p<0.05. . . . .	38
3.14	Comparisons of average $\epsilon_{yy}$ between construct types and clamps used: a) left/right SI in mid cap region b) shoulder regions, excluding edges c) top/bottom SI in shoulder region; Note: (R) redesigned clamps, (C) commercial clamps **:p<0.005. . . . .	39
3.15	Comparisons of average $\epsilon_{xy}$ between construct types and clamps used: a) left/right SI in mid cap region b) shoulder regions, excluding edges c) top/bottom SI in shoulder region; Note: (R) redesigned clamps, (C) commercial clamps *:p<0.05. . . . .	40
3.16	X and Y strain maps taken immediately before rupture observed during uniaxial tensile testing: IS constructs tested in the commercial clamps show rupture near the clamp edges (2/4) and near the SI (2/4), static construct in commercial clamps show rupture near the clamps only (4/4) . . . . .	41
3.17	X and Y strain maps taken immediately before rupture observed during uniaxial tensile testing: static constructs tested in redesigned clamps show rupture near the SI (2/3) and clamp region (1/3) . . . . .	42
A.1	How to properly paste the sandpaper onto the clamps for gripping the constructs during tensile testing *Image courtesy of Tamar Wissing . . . . .	65
A.2	Proper positioning of the construct in the redesigned clamps. The soft inclusion should still be visible. The Velcro should fit snugly into the groove. *Image courtesy of Tamar Wissing . . . . .	66
A.3	Measure and save 10 thickness values across the construct on both sides *Image courtesy of Tamar Wissing . . . . .	67
B.1	Schematic drawing of clamp redesign with dimensions (mm). Top, side, back, and orthogonal views. Material used: PVC plastic . . . . .	70
C.1	Finding initial guess process: a) reference subset selected b) convolution with the current image to find the normalized cross correlation c) array of correlation coefficient values are output, maximum value is located d) subset location is recovered with respect to the first image [27] . . . . .	72
C.2	Approach used by the RG-DIC algorithm in Ncorr. The path flows from the seeding point in the direction of the lowest $C_{LS}$ for each step. [27] . . . . .	74
C.3	Main start window of the Ncorr GUI . . . . .	75
C.4	Reference and current images are set as seen under Program State . . . . .	76
C.5	Uploaded .jpg file of ROI is set as seen under Program State . . . . .	77
C.6	Selecting the subset size and subset spacing in the RG-DIC Parameters window . . . . .	78
C.7	The selected seeding points, which equal to number of cores selected under RG-DIC Parameters (4). It is important that the seeds are placed so that the regions are subdivided somewhat symmetrically as seen in this figure . . . . .	79

C.8	Seed placement preview window. The user must make sure that the seeds do not travel outside the current image as the sample deforms and that they converge properly by checking that the correlation coefficient remains low and the number of iterations remain below the cutoff . . . . .	80
C.9	Selection of scaling to 0.0093 mm/pixel and correlation coefficient cutoff, $C_{LS} \leq 0.7$ . . . . .	81
C.10	Selection of strain radius=5. The least squares plane fit is shown in the right window . . . . .	82
C.11	Lagrangian strain plot in the x direction . . . . .	83
D.1	Green-Lagrangian strain maps in the X direction derived from Ncorr allow a visual comparison of the different parameter sizes. The parameter values of the middle column were chosen for this construct, as it contained the least amount of noise and smoothing effect, which was quantitatively verified with the parameter analysis method mentioned and shown in Figure 3.9 . . . . .	85
D.2	X displacement and strain plots across half a construct from the lumen area to the SI comparing a) subset sizes and b) strain radii sizes. A subset size of 35 pixels and strain radius of 5 were chosen for this construct, as these values demonstrated the most optimal balance between noise and oversmoothing when analyzing the average relative differences between each parameter curve . . . . .	85
D.3	2D correlation coefficient maps generated in MATLAB: static constructs tested in redesigned clamps (a-c), static constructs tested in commercial clamps (d-g) and IS constructs tested in commercial clamps (h-k). SI was not analyzed due to weak correlation in this region for most constructs. green: strong correlation $0 < C_{LS} \leq 0.5$ , blue: moderately strong correlation $0.5 < C_{LS} \leq 0.7$ , yellow: weak correlation $0.7 < C_{LS} < 1.0$ , red: bad data $1.0 \leq C_{LS}$ . The green and blue regions were included in the analysis (moderately strong to strong correlation) . . . . .	86
E.1	Y force vs actuator Y displacement plots of all static (black) and all IS (red) constructs until rupture: solid lines represent the new clamps, dotted lines represent the commercial clamps. This plot is proportional to the nominal engineering stress vs strain plot. Black dots depict the location of $\epsilon_{10\%}$ as determined by DIC analysis . . . . .	89
E.2	Static construct tested in redesigned clamps (1/3) . . . . .	90
E.3	Static construct tested in redesigned clamps (2/3) . . . . .	91
E.4	Static construct tested in redesigned clamps (3/3). Inadequate speckle pattern was applied therefore DIC was not comprehensive . . . . .	92
E.5	Static construct tested in commercial clamps (1/4) . . . . .	93
E.6	Static construct tested in commercial clamps (2/4) . . . . .	94
E.7	Static construct tested in commercial clamps (3/4) . . . . .	95
E.8	Static construct tested in commercial clamps (4/4) . . . . .	96
E.9	IS construct tested in commercial clamps (1/4) . . . . .	97
E.10	IS construct tested in commercial clamps (2/4) . . . . .	98

E.11 IS construct tested in commercial clamps (3/4)	99
E.12 IS construct tested in commercial clamps (4/4)	100
E.13 Static construct tested in redesigned clamps (1/3)	102
E.14 Static construct tested in redesigned clamps (2/3)	103
E.15 Static construct tested in redesigned clamps (3/3)	104
E.16 Static construct tested in commercial clamps (1/4)	105
E.17 Static construct tested in commercial clamps (2/4)	106
E.18 Static construct tested in commercial clamps (3/4)	107
E.19 Static construct tested in commercial clamps (4/4)	108
E.20 IS construct tested in commercial clamps (1/4)	109
E.21 IS construct tested in commercial clamps (2/4)	110
E.22 IS construct tested in commercial clamps (3/4)	111
E.23 IS construct tested in commercial clamps (4/4)	112
E.24 Static construct tested in commercial clamps (1/1)	114
E.25 Static constructs	115
E.26 Static constructs	116
E.27 Static constructs	117
E.28 IS constructs	118
E.29 IS constructs	119
E.30 Static construct tested with commercial clamps including the SI region: a) $\epsilon_{xx}$ map b) $\epsilon_{yy}$ map	120

# List of Tables

- 3.1 The estimated tangential moduli, engineering stresses and stretch ratios at the  $\epsilon_{10\%}$  locations for the static constructs tested in the redesigned clamps;  $TM_{10\%}$ = tangential modulus,  $\sigma_{10\%}$ = stress,  $\lambda_{10\%}$  = stretch, Note: data does not include the static construct with the inadequate speckle pattern . 26



# Nomenclature

## Greek Symbols

$\epsilon_{10\%}$	Average of 10% $\epsilon_{yy}$ in the mid cap region
$\epsilon_{xx}$	Green-Lagrangian strain in x direction
$\epsilon_{xy}$	Green-Lagrangian shear strain in xy direction
$\epsilon_{yy}$	Green-Lagrangian strain in y direction

## Abbreviations

$C_{CC}$	Zero mean normalized cross correlation coefficient
$C_{LS}$	Least-squares correlation coefficient
ACA	$\epsilon$ -amino caproic acid
DIC	Digital image correlation
FEA	Finite element analysis
GUI	Graphic user interface
IC-GN	Inverse compositional Gauss-Newton
IS	Intermittently strained
PBS	Phosphate-buffered saline
PDMS	Polydimethylsiloxane
RG-DIC	Reliability guided digital image correlation
ROI	Region of interest
SI	Soft inclusion
TE	Tissue engineered



# 1

## Introduction

Atherosclerosis is a global cardiovascular disease and is one of the most common causes of mortality, often leading to myocardial infarctions and strokes. Atherosclerosis refers to the formation of inflamed fatty lesions, also known as plaques, within the intimal layer, the inner most layer of the arterial wall. The plaque is sealed from the blood stream by a collagen rich fibrous cap. The collagen structure is the main load-bearing structure of the plaque which regulates stiffness and provides its strength. Plaque rupture often leads to thrombosis in the arterial lumen which can lead to blockage either at the site of rupture, or further downstream. The fibrous cap of a vulnerable plaque contains various collagen types but is most abundant in collagen type I and III, which account for approximately ninety percent of the collagen in the cap. In the cap, collagen is synthesized by the vascular smooth muscle cells [1]. An imbalance can occur between collagen synthesis and matrix degradation within the cap by macrophages which may lead to rupture.

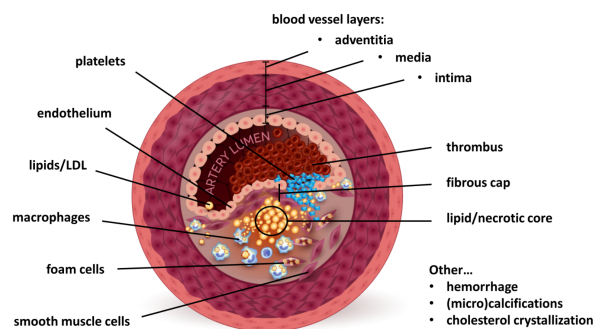


**Figure 1.1:** Vulnerable plaque structure. Atherosclerotic plaques form in the intima layer and when the fibrous cap strength exceeds the arterial stresses, rupture occurs and a thrombus can form, blocking blood flow through the lumen. \*Image courtesy of Tamar Wissing

Thin cap fibroatheromas, also known as vulnerable plaques, are known to be the precursor to rupture. These type of fibroatheromas are defined as containing a thin collagen rich fibrous cap, a large necrotic core containing dead cells and little to no collagen, sparse vascular smooth muscle cells within the cap, and macrophage infiltration as part of the inflammatory response (Figure 1.1) [2]. Many biological processes are involved leading to plaque rupture, but in the end, it's a mechanical event in which the local mechanical stresses experienced by the cap exceed the local tissue strength. To properly understand and predict plaque rupture, gaining more insight in the tissue mechanics and failure mode, which is determined by the biological composition and its mechanical properties, is necessary.

## 1.1 Motivation

Understanding atherosclerotic plaque rupture mechanics is of great clinical interest and can aid in saving many lives. Predicting the exact time of rupture is currently impossible due to the variety of interrelated factors that are involved in plaque rupture and the stochastic nature of the process. Due to the existing knowledge gap and limitations in human *in vivo* and *ex vivo* models as well as in animal models, the need for a controllable *in vitro* atherosclerotic model is evident, in order to properly study plaque formation, properties, and ultimately rupture mechanics. Collagen is known to be the most important load bearing component of fibrous caps, therefore comprehending the mechanical properties of collagen in human atherosclerotic arteries will lay a foundation for creating a simplified mechanically representative model to systematically investigate plaque rupture [3].

By first focusing on the collagen content, structure, and mechanical properties, the basis of the *in vitro* model can be made. In order to simulate a fibrous cap model, the alignment of collagen fibers in the direction of loading is necessary to replicate. In a study investigating tissue engineered (TE) heart valves, vascular TE constructs were subjected to uniaxial straining during culture. It was observed that the collagen fibers reoriented along the direction of the load, matching what is seen in plaque caps (Figure 1.2) [4],[5]. Collagen alignment in the loading direction results in a decrease of strength in the fibrous cap in the direction perpendicular to the load making it more prone to rupture [6]. In the study, it was demonstrated that the amount of time of straining significantly affects the collagen composition and mechanical properties of the constructs, therefore in order to simulate a less structured fibrous plaque cap, the straining time protocol must be altered accordingly.

Including a soft inclusion (SI) in the model to represent the mechanical stiffness of a necrotic core is also of interest in order to investigate the mechanical effects surrounding the SI. Additionally, other important biological components can be added to the model, such as macrophages and micro-calcifications, which also influence the collagen structure and stresses within the plaque (Figure 1.3). The overall goal this thesis project is working towards is to systematically control and add different components to the model in order to cover the complete spectrum of plaques and variability seen *in vivo*.

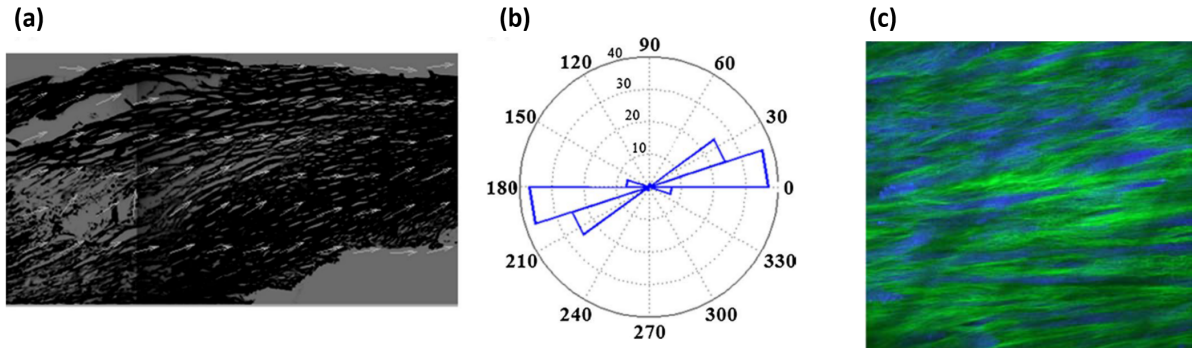


**Figure 1.2:** Collagen fiber direction a) collagen orientation vector plot of a human fibrous cap longitudinal section b) corresponding rose plot shows predominately longitudinal alignment in the cap with respect to the lumen [6] and c) multiphoton image of a vascular TE construct subjected to 3 weeks of uniaxial intermittent straining shows longitudinal alignment in direction of load and high collagen and SMCs production (green:collagen, blue: smooth muscle cells) [5]

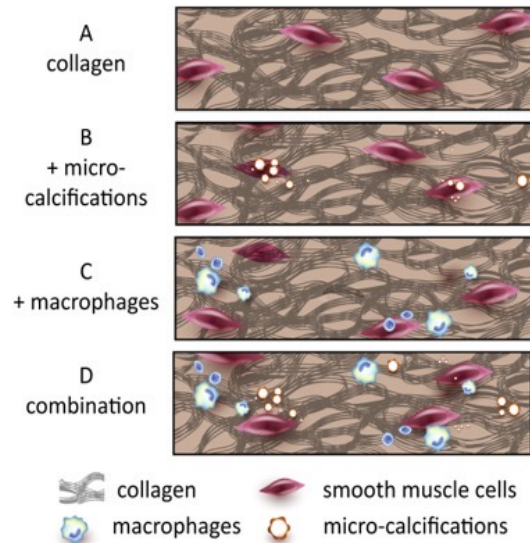


**Figure 1.3:** The goal of the in vitro atherosclerotic fibrous cap model is to systematically add relevant biological components that influence rupture such as the collagenous structure created by smooth muscle cells, micro-calcifications, macrophages, and a combination of these factors in order to simulate in vivo rupture mechanics \*Image courtesy of Tamar Wissing

## 1.2 Aims of the study

The overarching aim of this project is to aid in the development towards a reproducible *in vitro* atherosclerotic fibrous cap model in order to systematically study plaque rupture mechanics. The aims of this study are the following:

1. Create TE collagenous constructs containing a SI subjected to different straining protocol during culture: generate collagen rich constructs to simulate a simplified model of an atherosclerotic fibrous cap and subject them to different straining methods during culture.
2. Subject the constructs to mechanical testing and investigate their global mechanical behavior leading to rupture: investigate the effects of straining methods during culture on global mechanical behavior as well as the effect of clamp design.
3. Investigate local strain patterns of the constructs undergoing mechanical testing: perform digital image correlation (DIC) analysis on the constructs from the images obtained from mechanical testing.
4. Investigate rupture behavior of the constructs: utilize DIC analysis to study local strain patterns in the constructs immediately before rupture to relate to rupture location.

# 2

## Materials and Methods

This chapter will cover the methodology carried out in this study, which was divided into four parts. In part one, collagenous constructs were created by culturing them with isolated human myofibroblast cells derived from the vena sephena magna. The tissue engineering experiments included cell culture, creating a temporary fibrin-based matrix, seeding the cell-matrix between Velcro strips, and either statically culturing them or subjecting them to uniaxial intermittent straining (IS) during culture. In part two, mechanical testing was performed on the TE collagenous constructs utilizing uniaxial tensile tests. In part three, DIC analysis was performed to study the local strain patterns of the constructs leading to rupture using the images taken during tensile testing. In part four, data analysis was performed on the constructs, including compaction behavior before mechanical testing as well as on the data gathered from the tensile tests. This recorded test data was used to compare the global and local mechanical behavior of the differently strained constructs as well as to investigate the effect of clamp design on mechanical behavior. An overview of the methods used in this study can be seen in Figure 2.1.

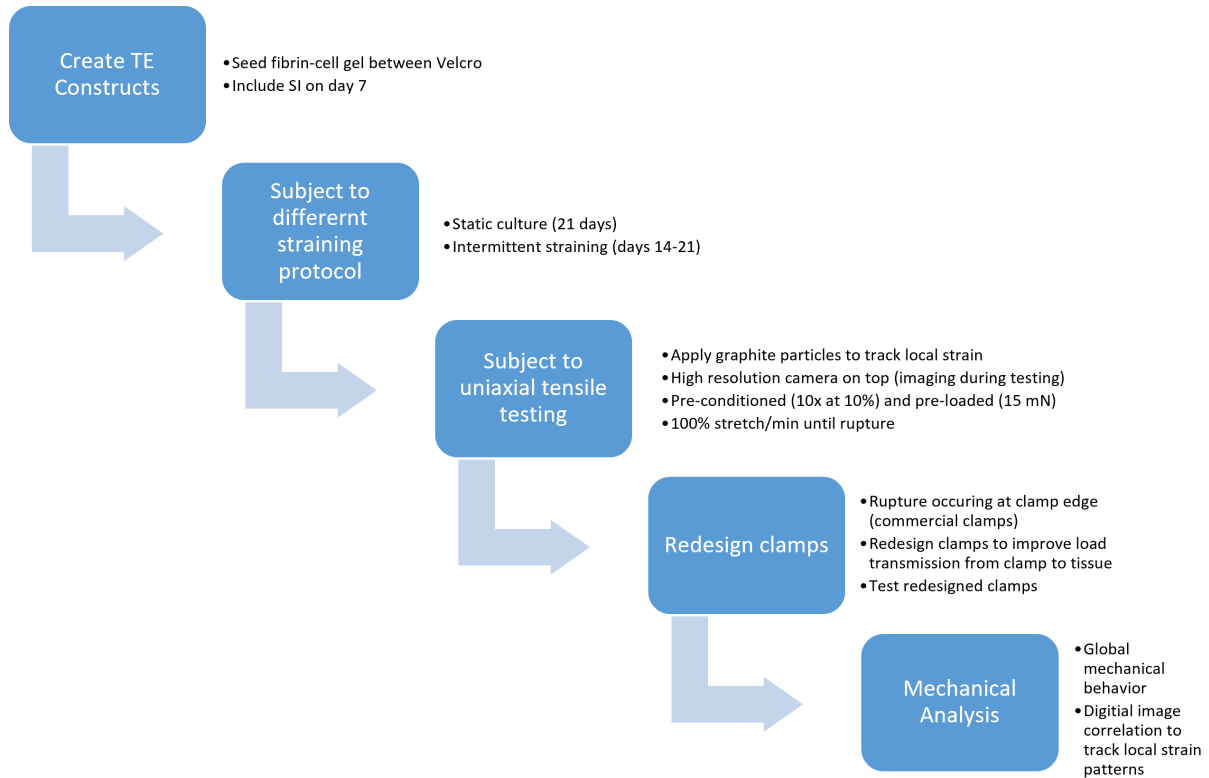


Figure 2.1: Overview of study methods

## 2.1 Tissue Engineered Constructs

### 2.1.1 Cell Culture

Vascular cells such as myofibroblasts are often used to create tissue engineered cardiovascular constructs. Specifically, human vena saphena derived myofibroblasts (HVSCs) are known to produce excellent *in vitro* collagen and tissue strength, and are easily accessible as well [7]. Due to these factors, these cells were selected for creating the collagenous constructs.

For the cell culturing experiments, vascular-derived myofibroblasts were acquired from the human vena saphena magna of a sixty-three year old woman donor after coronary by-pass surgery according to Dutch guidelines for secondary use material [8],[9]. The cells were isolated according to established protocols and stored in liquid nitrogen until usage [7]. The cells ( $0.5 \times 10^6$ ) were cultured in growth medium consisting of Advanced Dulbecco's Modified Eagle Medium [ $\alpha$ -DMEM; Gibco, Carlsbad, CA], supplemented with 10% fetal bovine serum [FBS; Greiner Bio-One, Monroe, NC], 1% penicillin streptomycin [PenStrep; Lomza, Belgium] and 1% GlutaMax [Gilco, Carlsbad, CA]. The cells were cultured at 37°C in a humidified 95/5% air/CO<sub>2</sub> incubated environment. The growth

medium was renewed every 2-3 days. The cells were passaged when they reached about 80% confluency, which refers to the percentage of the culture flask surface covered with adherent cells. Confluency above 80% can trigger intracellular mechanisms to occur such as changes in gene expression or causing the cells to die off, thereby effecting the results of the experiment [10]. Once approximately 80% confluency was observed for each passage, the cells were washed with phosphate-buffered saline (PBS), dislodged with Trypsin-EDTA solution [Life Technologies, Thermo Fisher Scientific, Inc., USA], checked to see if they were loosened under the microscope (rounded), centrifuged, resuspended in new medium, and added to new containers. The cells were counted after passage 7 (approximately 3 weeks).

### 2.1.2 Engineered Fibrous Cap Models

For the preparation of the molds in which the cells were seeded into, two 15x5 mm Velcro strips (nylon fabric with many tiny hooks) were placed on each side of the seeding location per construct. This allows the cells to integrate into the strips and provide a grip for mechanical testing. The hard sides of the Velcro strips were carefully glued 10 mm apart onto each well of the cell culture plate using medical adhesive silicone [Silastic; DOW Corning, USA] (Figure 2.2). The silicone glue was allowed to dry overnight in an oven at 60°C and sterilized by adding 70% ethanol to the wells and incubated for 30 min. They were washed 3x with PBS and placed under ultraviolet light for 30 min. Rectangular polydimethylsiloxane (PDMS) bars (10x4x4 mm) were created by mixing a silicon elastomer base and a curing agent and were sterilized using 70% ethanol. These bars were placed between the Velcro strips, on each side in order to prepare a mold for the fibrin-cell suspension to solidify during the initial phase of the culturing process, and were removed on day 5 (Figure 2.3).

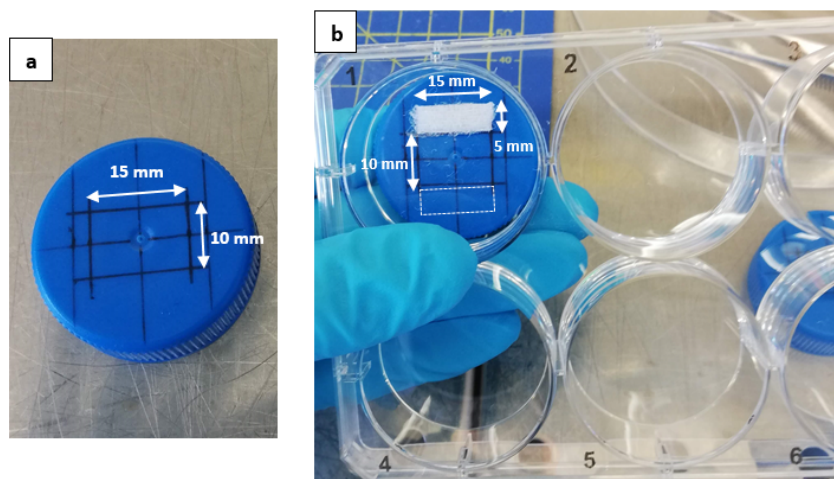


**Figure 2.2:** The Velcro strips were cut with 15x5 mm dimensions and two were pasted 10 mm apart within the culture wells: a) top view of the reference used to place the Velcro's at the correct location within the wells b) one Velcro strip has been pasted using the reference under the well, another strip will be pasted in the dotted white region

After counting the total number of cultured cells grown, the fibrin-based matrix was created, each construct seeded with 675,000 cells. The protocol used can be found in Appendix A. Using fibrin gel as a cell carrier has been studied as a method that can offer several advantages. Seeding the cells with fibrin (temporary matrix) allows the cells to create their own mature extracellular matrix [9]. Therefore, in this study, twelve fibrin-based constructs were created in order to provide a temporary support matrix for the myofibroblasts to proliferate and produce their own matrix. To produce the fibrin matrix, the cells previously cultured were added to 10 IU/mL of bovine thrombin [Sigma, St. Louis, MO]. 10 mg/mL of bovine fibrinogen [Sigma, St. Louis, MO] was then added to the thrombin-cell suspension.

The fibrin-cell suspension was seeded between the two Velcro strips and two PDMS bars, as well as on top of the Velcro strips, and incubated for 30 minutes in the incubator to gelate. The culture medium was added to the culture plate consisting of growth medium supplemented with L-ascorbic acid 2-phosphate (vitamin C, 0.25 mg/ml) and  $\epsilon$ -Amino Caproic Acid (ACA, 1 mg/ml). Vitamin C and ACA were added to the medium to stimulate collagen synthesis and slow down the fibrin degradation, respectively. The medium was replaced every 3 days with ACA being added for the first 7 days, to allow cells to deposit their first matrix [8],[9].

The fibrin-based constructs were first exposed to 7 days of static culture to achieve mechanical integrity. On day 7, 2 mm centered holes were created in the constructs using a sterile biopsy puncher in order to create a SI representative of the low stiffness necrotic core in arterial plaque. The same concentrations of 10mg/ml fibrinogen and 10u/ml thrombin were mixed to create the fibrin gel for the SI, excluding the HVSCs. The holes in the constructs were filled with the newly made fibrin gel, allowed to solidify for 15 minutes in an incubator, and then fresh medium was added to the wells without ACA. The stiffness of the fibrin-based gel SI created was approximately 0.5-1.0 kPa [11]. The SI should be substantially less stiff than the tissue constructs because the HVSCs produce their own collagenous matrix over time which increases the structural integrity of the tissue. Figure 2.3 displays a construct on the day of seeding and on the day of creating the SI. The constructs continued to be statically cultured for 14 more days at 37°C in a humidified 95/5% air/CO<sub>2</sub> incubated environment. The constructs were sacrificed on day 21 for mechanical testing or fixation for future histology analysis.

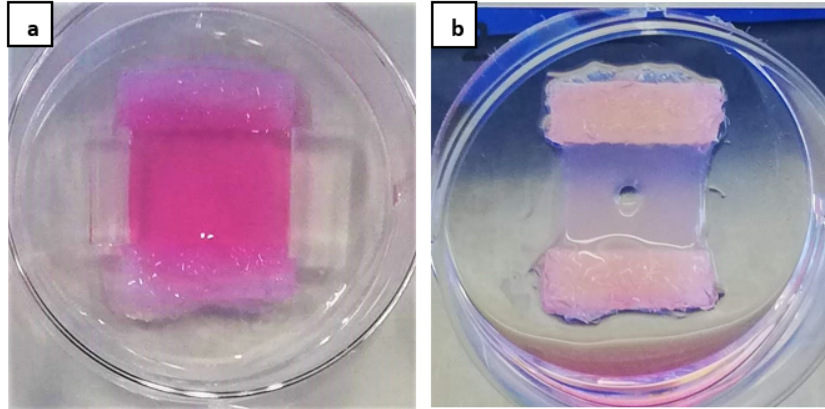


**Figure 2.3:** An example of a static construct on day 0 after seeding the fibrin-cell matrix between two PDMS bars (a) and on day 7 after including the SI (b)

### 2.1.3 Including Previously Created Constructs

As mentioned in the preface, a few limitations were encountered during this project due to the COVID-19 pandemic, such as time restrictions and limited lab accessibility. Due to these limitations, the analysis performed in this project utilized 3 of the constructs created in the experimental batch mentioned above, as well as 4 static and 4 intermittently strained constructs created previously. All static constructs followed the same protocol mentioned above and all constructs included a centered SI.

Uniaxial intermittent straining during culture was introduced on day 14 using the Flexcell FX-4000T system (Flexcell Int, McKeesport, PA), as shown in Figure 2.4. One week of intermittent straining was applied to the 4 constructs via a vacuum system on the left and right sides and consisted of one hour of 4% strain and three hours of 0% strain (Figure 2.5). Three weeks of intermittent straining has been shown to significantly increase collagen production in vascular tissue engineered constructs, however one week was used in this protocol as the fibrous cap typically contains less amount of collagen overall when compared to normal arterial tissue [5].

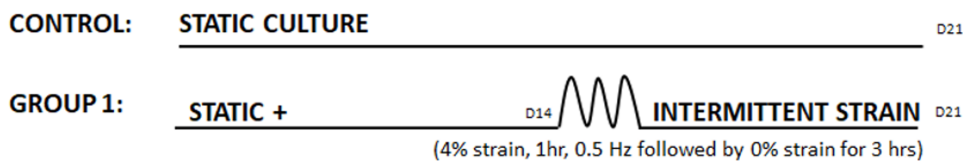


**Figure 2.4:** Adapted protocol used for culturing the constructs. The control group included the statically cultured constructs (n=4). Intermittent straining was performed on group 1 (n=4) for one week after two weeks of static culturing (0.5 Hz, 4-5% strain, 1 hr on + 3 hrs off) [5]

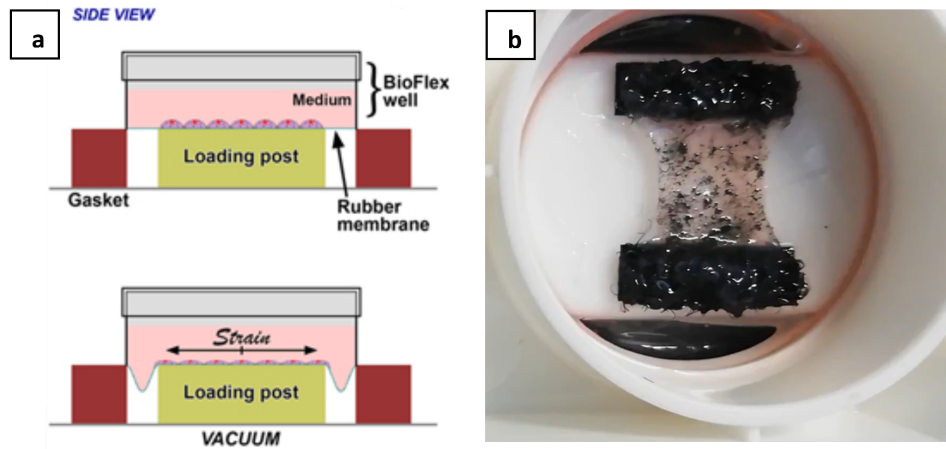


**Figure 2.5:** The Flexcell system subjected the constructs to uniaxial intermittent straining via a vacuum system on each side of the loading post where the construct has been seeded (Flexcell Int, McKeesport, PA): a) side view schematic of Flexcell system b) top view of a intermittently strained construct within the Flexcell system. Note: graphite particles were applied to the construct to track strain pattern

## 2.2 Mechanical Testing

### 2.2.1 Experimental Setup

A commercial biaxial tester [CellScale Biomaterial Testing, Waterloo, Canada] was used to perform the uniaxial tensile testing with two 5 newton (N) load cells (Figure 2.6). Two identical clamps, that were included with the system, were used to secure the constructs in place, with the edge of the Velcro aligning with the edge of the clamp. Black graphite specks removed from sandpaper were manually applied on top of the tissue samples using cotton swabs for digital image correlation analysis. The constructs were lowered into a pre-warmed (37°C) bath of PBS to simulate physiological conditions. A high resolution camera and lens were included in the testing setup and were located directly above the constructs, used to capture 15 images per second during testing. Two adjustable light sources were also included and positioned above the construct, at angles that did not obstruct the camera view.



**Figure 2.6:** Commercial uniaxial tensile tester with the components referred to [CellScale Biomaterial Testing, Waterloo, Canada]

The system was first calibrated with a spring of 5 N stiffness. The constructs were pre-loaded to approximately 15 mN measured in the Y-direction in order to remove slack and subsequently pre-conditioned 10x with 10% strain in order to produce repeatable behavior [12]. The tensile tests were performed at a strain rate of  $100\% \text{ min}^{-1}$  until failure. The forces experienced in the tissue constructs were recorded during testing. The mechanical testing protocol can be found in Appendix A. Figure 2.7 displays a construct mounted in the mechanical testing setup with the commercial clamps (originally used) and with the redesigned clamps.

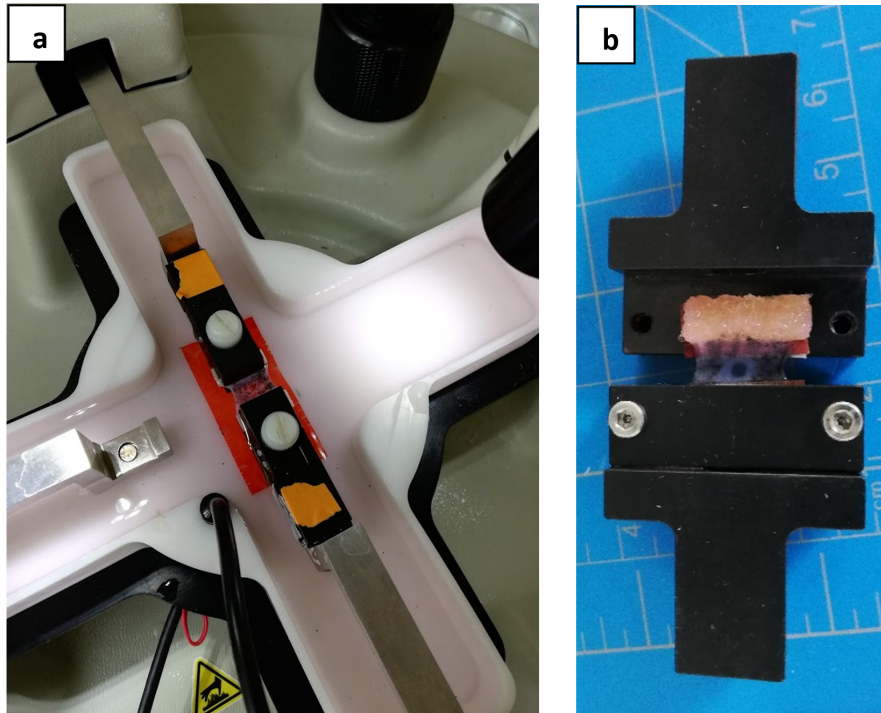


**Figure 2.7:** A construct mounted into two different clamping mechanisms for mechanical testing: a) commercial clamps b) redesigned clamps; top clamp shows how the construct is snugly fit onto the sandpaper groove before tightening the top piece

### 2.2.2 Clamp Redesign

It was observed that the rupture location for each construct occurred at the interface between the tissue and Velcro/clamp edge. Therefore, it was predicted that the clamps that came with the mechanical testing setup could be causing a stress concentration within the clamping mechanism, ultimately causing rupture of the constructs to occur at the Velcro/clamp edge. To test this hypothesis, special clamps were designed and manufactured to redistribute the stresses within the clamps and improve the load transmission from the clamps to tissue. The redesign concept can be seen in Figure 2.8 and the specifications of the redesigned clamps can be found in Appendix B. Sandpaper and foam tape were used to grip the tissue with more of an even stress distribution as opposed to the concentrated clamping mechanism apparent in the system clamps [13]. Also, in the redesign, 2 mm of the tissue from the Velcro on each side was gripped onto with the new clamps, in order to provide sufficient grip. The grip heights also differed for the Velcro and tissue due to the different thicknesses of these features, which was incorporated into the design. In this thesis report, the system clamps will be referred to as the commercial clamps and the newly manufactured clamps will be referred to as the redesigned clamps.

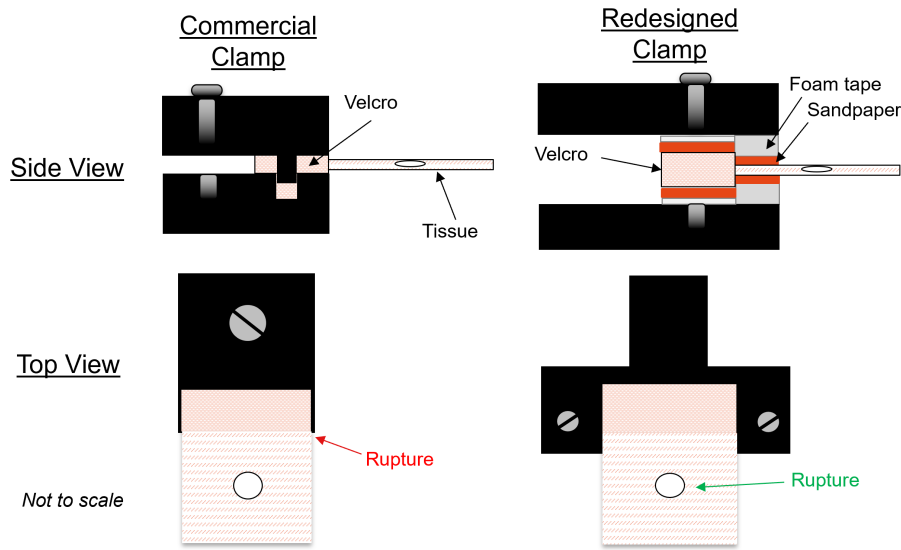


**Figure 2.8:** Comparison of the original clamps and redesigned clamps: side and top view of the original clamps (a & c), side and top view of the redesigned clamps (b & d). The redesigned clamps were created specifically to avoid failure at the Velcro/clamp edge by evenly redistributing the stresses within the grip. \*Images depict only one of the two clamps in the system

## 2.3 Digital Image Correlation

Two-dimensional DIC was performed on the images captured by the high resolution camera (15 images per second) in order to calculate the local displacement and strain fields on the constructs. The MATLAB open-source software Ncorr was used to perform DIC analyses (see Appendix C). The images included began after the pre-loading and pre-conditioning phase and ended immediately before rupture was observed. Each image was correlated with the first image of the set, which was referred to as the reference image that was undeformed. Using the first image as the reference image is the common method for materials that do not experience high strains (200-300%) [14]. Since the constructs in this project only stretched approximately 20-30% before rupture, this method was used.

In DIC, the region of interest is broken down into multiple subsets of a selected size. The relative positions of these subsets are then compared as the sample deforms and are used to calculate displacements and derive the strain fields. The optimal subset size selected for each TE constructs in this project were determined using a parameter analysis method which reduced noise and minimized smoothing, described in Appendix D. A trade-off must be made when selecting the parameters between smoothing of the data to decrease noise and accuracy. The Green-Lagrangian strains were calculated using a technique in which least squares plane fitting was performed on a region of displacement data (determined by the selected strain radius) [15]. The displacement gradients were then calculated and used to determine the strains (this study reports the Green-Lagrangian strains). The method for computing the Green-Lagrangian strains is included in Appendix C.

To verify the appropriate parameter selection, 2D correlation coefficient maps were generated in MATLAB using the stored correlation coefficient data  $C_{CC}$  from the DIC parameter analyses. The mathematics behind this quality matching process can be seen in Appendix C and the procedure to generate the 2D correlation coefficient maps for each construct can be seen in Appendix D. In this study, a  $C_{CC}$  cutoff value was chosen for the final analyses which included values correlating to a moderate-strong agreement in grayscale values, especially near the SI.

## 2.4 Data Analysis

### 2.4.1 Compaction Analysis

Tissue compaction represents the amount of shrinkage in a certain direction. Images were taken of each construct on a grid background on day 21, before performing mechanical testing, in order to calculate the compaction. The final thickness values across the construct's length before testing were recorded using a digital microscope [Keyence VHX-500FE, Itasca, IL] and averaged. The initial thickness values were estimated using the total seeding volume and area dimensions. The average compaction in X, Y and Z directions were calculated for the static and IS constructs using ImageJ [16] and plotted in MATLAB [2017b MathWorks, Massachusetts, USA]. The code can be found in Appendix E.

### 2.4.2 Global Mechanical Analysis

To investigate the global mechanical behavior of the constructs, the actuator Y displacement and global Y force values measured in the tissue constructs were recorded and plotted. These values are proportional to the nominal engineering stress and strain values. The tangential moduli were calculated, as a measure of stiffness, for the constructs tested in the redesigned clamps at the location of the actuator Y displacement value in which the  $\epsilon_{10\%}$  was recorded, further elaborated on in the next section.

To convert from actuator Y displacement ( $\Delta Y$  in  $\mu\text{m}$ ) to stretch ratio ( $\lambda$ ), Equation 2.1 was used, where  $L_o$  represents the original length ( $\mu\text{m}$ ) of the construct before testing. To convert from Y force ( $F_y$  in mN) to nominal engineering stress ( $\sigma$  in kPa), Equation 2.2 was used, where  $A_o$  represents the original cross sectional area ( $\text{m}^2$ ).  $A_o$  was determined by multiplying the average initial thickness values of each construct on day 21 before mechanical testing by the initial width at the maximum compaction location.

$$\lambda = 1 + \frac{\Delta Y}{L_o} \quad (2.1)$$

$$\sigma = \frac{F_y}{A_o} \quad (2.2)$$

In order to calculate the tangential moduli for each construct, a few material models (i.e. Neo-Hookean, Mooney-Rivlin) were fit to the stretch-stress data in ABAQUS and the best fit was selected. The 5-parameter Mooney-Rivlin strain energy density function fit the data best (Figure 2.9). This function can be used to characterize non-linear, hyperelastic materials with up to 100% deformation typically, and the constructs in this study did not exceed 40% before rupture [17]. The strain energy density function equation is shown below (Equation 2.3).

$$\begin{aligned} W = c_{10}(I_1 - 1) + c_{01}(I_2 - 1) + c_{20}(I_1 - 1)^2 + c_{02}(I_2 - 1)^2 \\ + c_{11}(I_1 - 1)(I_2 - 1) + \frac{1}{d}(J - 1)^2 \end{aligned} \quad (2.3)$$

where  $I_1$  is the first invariant,  $I_2$  is the second invariant,  $J$  is the Jacobian of the deformation gradient tensor,  $c_{10}$ ,  $c_{01}$ ,  $c_{20}$ ,  $c_{02}$  and  $c_{11}$  are material constants. In this study, incompressibility is assumed therefore  $J=1$ . Through derivation of the above equation, the Second Piola Kirchhoff uniaxial nominal stress equation can be derived with respect to stretch (shown in Equation 2.4).

$$\begin{aligned} \sigma = 2c_{10}\left(\lambda - \frac{1}{\lambda}\right) + 2c_{01}\left(1 - \frac{1}{\lambda^3}\right) + 6c_{11}\left(\lambda^2 - \lambda - 1 + \frac{1}{\lambda^2} + \frac{1}{\lambda^3} - \frac{1}{\lambda^4}\right) \\ + 4c_{20}\lambda\left(1 - \frac{1}{\lambda^3}\right)\left(\lambda^2 + \frac{2}{\lambda} - 3\right) + 4c_{02}\left(2\lambda + \frac{1}{\lambda^2} - 3\right)\left(1 - \frac{1}{\lambda^3}\right) \end{aligned} \quad (2.4)$$

The stretch-stress data sets for each construct were fit to the 5-parameter Mooney-Rivlin stress equation (derivative of the strain energy density function with respect to strain) by using the curve fitting toolbox in MATLAB in order to obtain the material constants. Next, equation 2.3 was differentiated with respect to the stretch ratio ( $\lambda$ ), the obtained material constants were placed in the differentiated equation 2.5, and the tangential modulus was calculated for the static constructs tested in the redesigned clamps at a specified stretch, as well as the nominal engineering stress and stretch values. The MATLAB code can be seen in Appendix E.

$$TM = 2c_{10} + \frac{2c_{10}}{\lambda} + \frac{6c_{01} - 18c_{11} + 4c_{20}(3\lambda^6 - 6\lambda + 6)}{\lambda^4} + 12c_{11}\lambda + \frac{24c_{11}}{\lambda^5} - \frac{12c_{11}}{\lambda^3} - 6c_{11} - 12c_{20} + \frac{4c_{02}(2\lambda^2 - 9\lambda^2 + 5)}{\lambda^6} + 8c_{02} \quad (2.5)$$

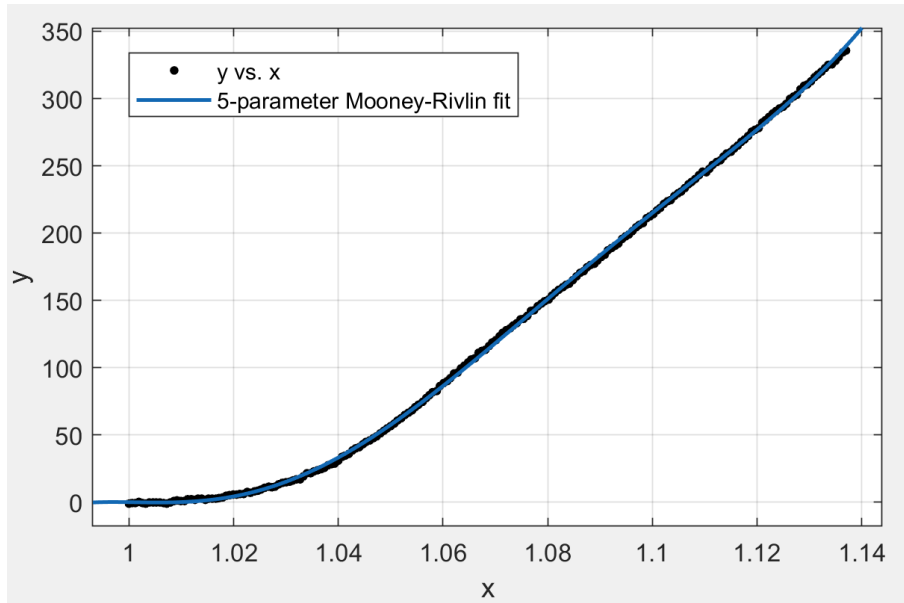


**Figure 2.9:** The 5-parameter Mooney Rivlin material model was determined as the best fit model to the experimental stretch ( $x$ ) vs stress ( $y$ ) data and the material constants for each construct were obtained using the Curve Fitting Toolbox in MATLAB. This figure shows an example of one of the static constructs tested in the redesigned clamps

### 2.4.3 Creating Regions for DIC Analysis

A box-shaped region of interest (ROI) was selected for each construct for DIC analysis, excluding the clamp edge regions which contained loose Velcro fibers, as well as the SI region (Figure 2.10). The focus of the analysis was on the tissue region around the SI. This binary mask region was drawn using Photopea, an open-source online photo editor.

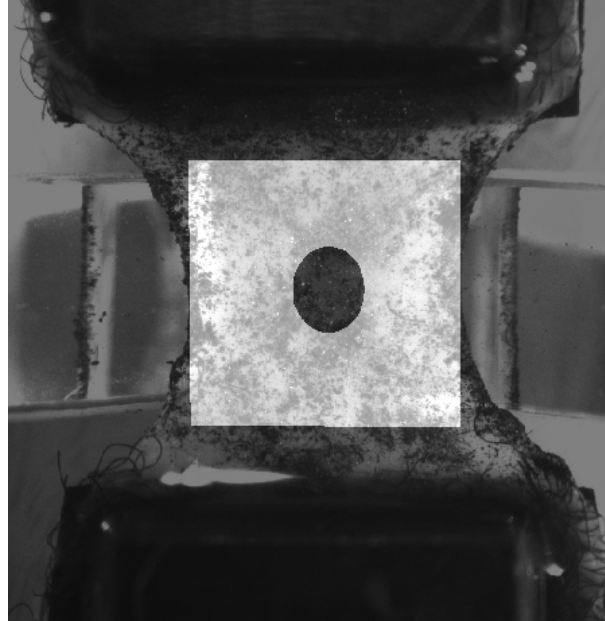


**Figure 2.10:** The rectangular shaped ROI mask drawn over the top of a construct for DIC analysis. The ROI excludes the SI region and tissue regions near the clamps which contain Velcro fiber artefacts

The constructs were subdivided into right and left sides with respect to the center of the SI, as well as top shoulder, bottom shoulder, and mid cap regions, also seen in Figure 2.11. To study the local strain patterns, the static and IS constructs were compared investigating the shoulder regions versus the mid cap region on both sides of the SI. Plots were generated in MATLAB by averaging the  $\epsilon_{xx}$  and  $\epsilon_{yy}$  values per pixel across the constructs within these regions mentioned above with the origin located at the center of the SI. The X and Y displacement and strain maps were also generated in Ncorr to give a more visual and local representation of these plots. Furthermore, the average  $\epsilon_{xx}$  and  $\epsilon_{yy}$  values of each of the regions shown in Figure 2.12 were calculated in MATLAB per construct to investigate the mid cap and shoulder regions surrounding the SI. The left and right edges of the constructs were excluded due to visible artefacts observed with DIC.

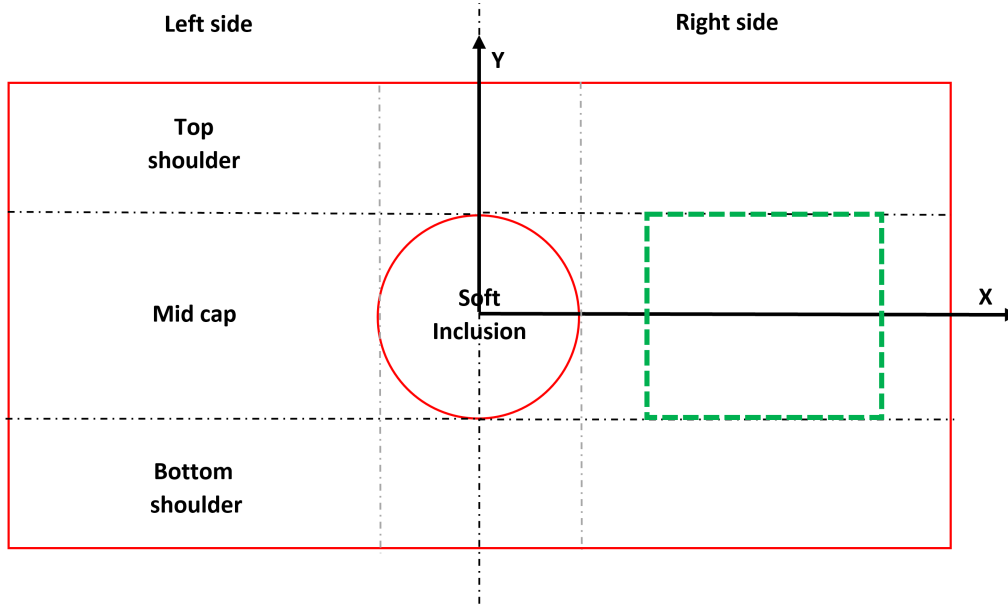


**Figure 2.11:** Subdivided regions of the constructs for DIC analysis which include right and left sides with the center of SI as the origin, top and bottom shoulders, and the mid cap region. The grey dotted lines represent the right and left sides of the SI. The box region enclosed by the green dotted lines is where the average  $\epsilon_{yy}$  was calculated per image. The box extends from the top and bottom of the SI and 20% away from the edge and SI. The right or left side was chosen per construct based on which side displayed the most  $\epsilon_{yy}$  field homogeneity within the region. The image number in which an average value of 10%  $\epsilon_{yy}$  in the green box was used for data analysis

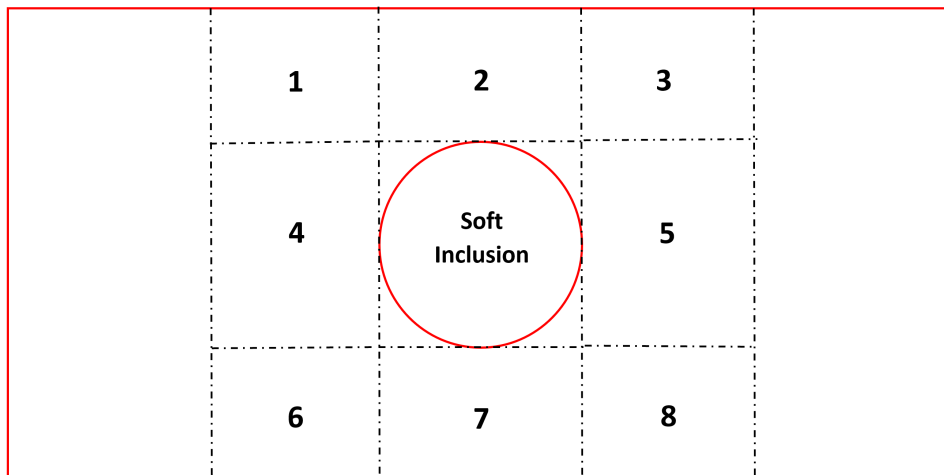


**Figure 2.12:** The average  $\epsilon_{xx}$  and  $\epsilon_{yy}$  values were calculated per each region; 4,5: right/left of SI (mid cap), 2,7: top/bottom of SI (shoulders), 1,3,6,8: outside shoulder regions

### 2.4.4 Image Analysis Selection

Using the DIC output data acquired per construct after running analysis in Ncorr, the image number in which an average of 10%  $\epsilon_{yy}$  in the mid cap region (referred to as  $\epsilon_{10\%}$ ) was determined per construct using MATLAB (region specified in Figure 2.11). This was performed in order to minimize the effect of the the different clamps used on the static constructs when looking at local strain behavior and tangential moduli. The image number where  $\epsilon_{10\%}$  occurred was used for the analysis of each construct. The image number differed for each construct (Figure 2.13). This normalizing method allowed a more direct comparison to be made at  $\epsilon_{10\%}$ , which is approximately the maximum amount of physiological circumferential strain experienced by the mid cap region in a fibrous plaque [18].

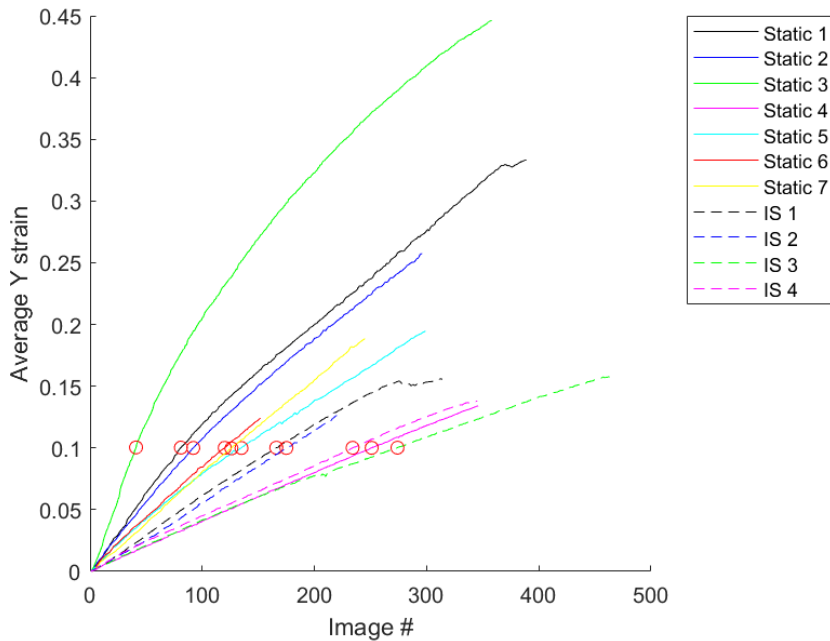


**Figure 2.13:** Image # (15 Hz) vs average mid cap  $\epsilon_{yy}$  until rupture. A red marker has been placed at approximately  $\epsilon_{10\%}$  for each construct. The image # of this location was used for analysis in order to normalize the local strain fields and minimize the variables between the constructs

### 2.4.5 Finite Element Analysis Model: Illustrative Example

In order to give the reader an illustrative example of the expected local displacement and strain patterns surrounding the SI when undergoing uniaxial loading, a simplified finite element analysis (FEA) model was created in ABAQUS [Dassault Systèmes, Rhode Island, USA]. This model was meant to solely demonstrate how pulling a material with a centered hole in two opposite directions affects the local properties, focusing on the region surrounding the SI. For simplicity purposes, the model was assumed to be rectangular, two-dimensional, hyperelastic non-linear, homogeneous, isotropic, and incompressible.

Hyperelastic models have been used often for modeling tissue due to the non-linear behavior exhibited at high strains [19]. A few different hyperelastic material models were fit to Treloar’s experimental uniaxial, biaxial, and planar test data for a rubber material and analysed to see which material models were stable (i.e. Neo-Hookean, Mooney-Rivlin) [20]. The Mooney-Rivlin isotropic hyperelastic material model was chosen because it fit the data reasonably well up to 100% stretch and the model was not stretched more than 30%. Half of a 6x15 mm construct was modeled with a 2 mm hole located in the center. Symmetry was applied about the Y-Z plane. The model was seeded with a seed size of 0.25 and CPS4 elements were used (4-node bilinear plane stress quadrilateral). The model was fixed at a central node at the edge of the hole and a Y displacement of 1 mm was applied to both a central node at the top and at the bottom of the model, in opposite directions to represent uniaxial tensile testing. A standard static solver was used and the X and Y displacement and strain fields were created.

### 2.4.6 Strain Measures

Logarithmic strain (true strain) is the default output variable in ABAQUS for nonlinear material, and is especially used for large deformations as it calculates incremental strain. Although this FEA model outputs logarithmic strain as the default strain measure, the Green-Lagrangian strain measure seen in DIC analysis is a comparable measure for small deformations [21]. Green-Lagrangian strain is less of an intuitive measure for modeling as it is obtained from the deformation gradient and using it in constitutive equations can introduce challenges when interpreting the results or material constants of the model [21]. Green-Lagrangian strain is a more optimal measure for DIC as it allows for discontinuous analysis (i.e. cracks), accounts for any rigid body rotation, and provides more accurate results based on the deformation tensors. The Green-Lagrangian strain equations used in DIC analysis for the normal X, Y and shear XY directions can be found in Appendix C.

When investigating global mechanical behavior of the constructs, the Y actuator displacement was presented which is proportional to the stretch through Equation 2.1. Stretch is one of the most often used strain measures recorded in literature. Often it is most convenient for researchers to normalize the strain data in order to characterize the material.

Each measure of strain can be mapped to one another through the following equations below, where stretch is represented by  $\lambda$ , logarithmic strain is represented by  $\epsilon_{LE}$ , and Green-Lagrangian strain is represented by  $\epsilon_{GL}$ .  $L_o$  represents the original length and  $l$  represents the final length.

$$\lambda = \frac{l}{L_o} \quad (2.6)$$

$$\epsilon_{LE} = \ln(\lambda) \quad (2.7)$$

$$\epsilon_{GL} = \frac{1}{2}(\lambda^2 - 1) \quad (2.8)$$

### 2.4.7 Statistical Analysis

Statistical analysis was carried out between the static constructs (using the commercial and redesigned clamps), as well as with the IS constructs, reporting the average  $\epsilon_{xx}$ ,  $\epsilon_{yy}$ , and  $\epsilon_{xy}$  in the mid cap and shoulder regions. All statistical data were generated using MATLAB. The p value < 0.05 was used as the cutoff for statistical significance in this study. The data sets for each sample were assessed for normality using the Shapiro-Wilk test, as this test is appropriate for small sample sizes [22]. If  $p > 0.05$ , the data was determined as normally distributed. Then the data sets being compared were put through Levene's test for homogeneity of variances [23]. If the variances were homogeneous, then an independent two-sample t test was used. If  $p < 0.05$  for the Shapiro-Wilk test, then the data set was determined as not normally distributed and a non-parametric test of two independent samples test was considered. Statistical analysis was not carried out if the data set contained  $n < 3$ .

# 3

## Results

### 3.1 Tissue Engineered Constructs

Collagenous constructs including a soft inclusion with both culture procedures were successfully created. The constructs varied in compaction rate by day 21. Tissue compaction in the X direction was observed to be much greater in the IS constructs (approx. 45%) than in the static constructs (approx. 15%) (Figures 3.1 and 3.2). A large percentage of compaction in the Z direction was observed for both types of constructs (approx. 80%), however minimal compaction in the Y direction was observed for both constructs (Figure 3.2).

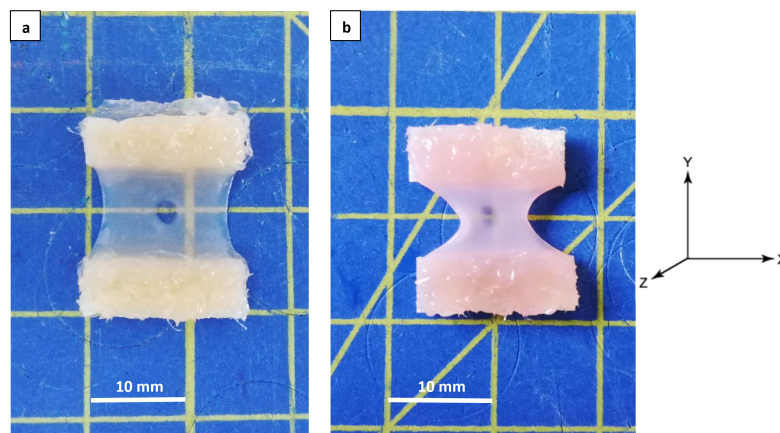


**Figure 3.1:** Comparison of construct compaction on day 21 with different culturing protocol: a) statically cultured construct showed less compaction in X direction b) IS construct showed more compaction in X direction

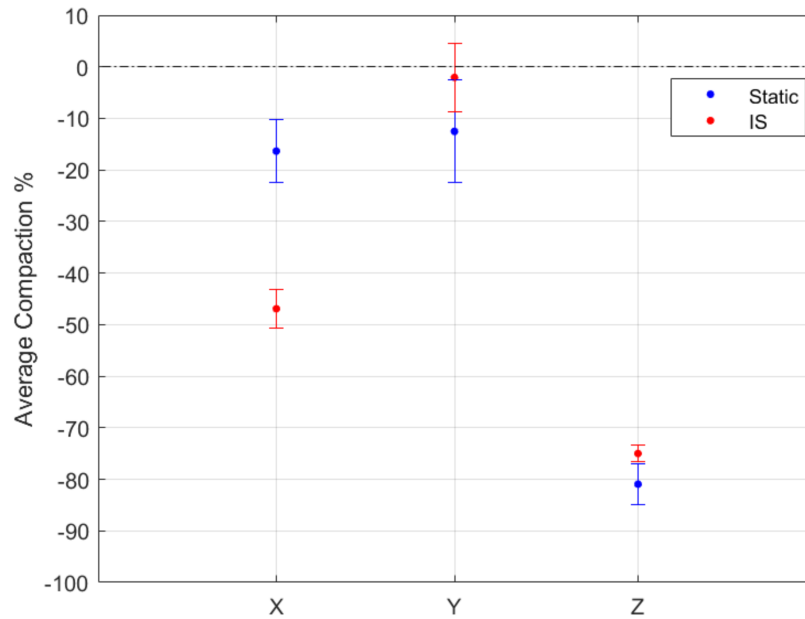


**Figure 3.2:** Quantitative comparison of static and IS construct compaction percentage and standard deviation in the X, Y and Z directions (refer to coordinate system in Figure 3.1) on day 21. Note: negative values represent shrinkage and positive represent expansion, dotted line represents no change

The SI's were well integrated in the constructs by day 21 as cells of the fibrin-matrix infiltrated all SI's, irrespective of the loading protocol applied (Figure 3.3). The observed gradient in cell number will affect the amount of collagen deposited going from the artificial fibrous cap to the SI (mimicking the fibrous cap-lipid pool transitions seen *in vivo*) [2].

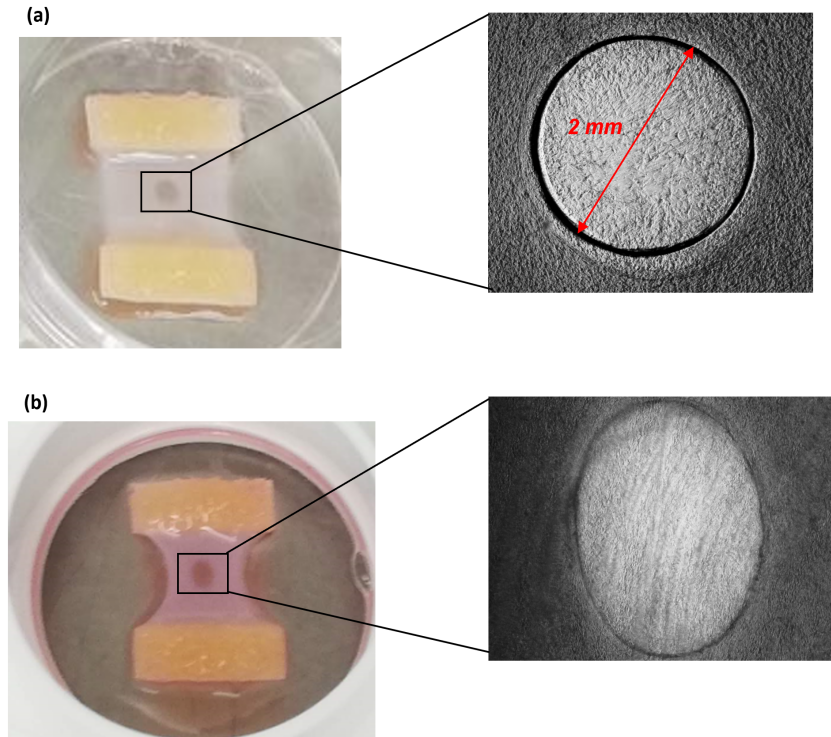


**Figure 3.3:** Images taken with a Brightfield microscope on day 21, before mechanical testing, to observe the collagen migration into the soft inclusion: a) static construct b) IS construct \*Images courtesy of Tamar Wissing

## 3.2 Global Mechanical Behavior

In this section, the results of the uniaxial tensile tests that were performed on the statically cultured ( $n=4$ ) and IS constructs ( $n=4$ ) in the commercial clamps, as well as the static constructs in the redesigned clamps ( $n=3$ ), are presented. This section will report the effect of straining protocol on global mechanical behavior for the static and IS constructs tested in the commercial clamps, as well as the effect of the clamp redesign on the mechanical behavior of the static constructs.

### 3.2.1 Effect of Straining Protocol: Static vs IS Constructs

The actuator Y displacement vs Y force measured in the IS and static tissue constructs tested in the commercial clamps are plotted (Figure 3.4). These constructs exhibit a comparable mechanical behavior pattern, with the exception of the varying maximum Y force/Y displacement experienced before rupture (Y force ranging from approx. 1000-2500 mN). Rupture at the clamp edge was seen in all constructs, except in 2 out of 4 of the IS constructs in which rupture occurred near the SI.

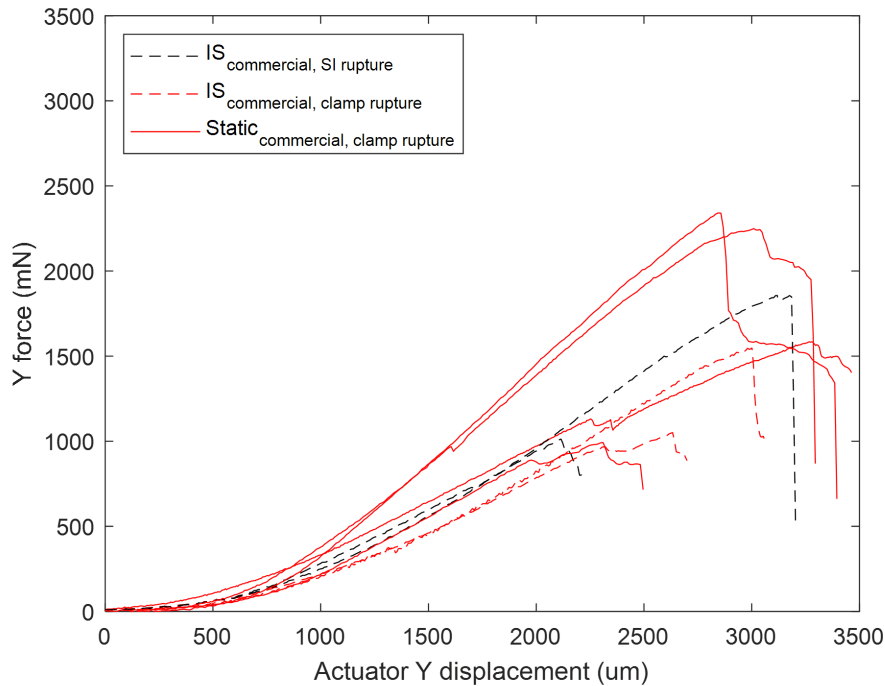


**Figure 3.4:** Y force vs actuator Y displacement plots of the IS and static constructs tested in the commercial clamps until rupture. This plot is proportional to the nominal engineering stress vs strain plot: Dotted curves represent the IS constructs, solid lines represent the static constructs, red represents rupture which occurred at the clamp edge, black represents rupture which occurred near the SI

### 3.2.2 Effect of Clamp Design: Commercial vs Redesigned Clamps

The actuator Y displacement vs Y force measured in all statically cultured tissue constructs are plotted (Figure 3.5). This graph is proportional to the nominal engineering stress vs strain plot. It was observed that the static constructs tested in the commercial clamps all lead to rupture at the clamp edge, displaying a sudden decrease in Y force at rupture, followed by a plateau and decrease again. This rupture pattern was not observed in the static constructs tested in the redesigned clamps. Two out of three of these constructs displayed a two-bump pattern, linked to the initial rupture on one side of the SI (first bump) and the second rupture on the other side (second bump). The other static construct tested with the redesigned clamp ruptured at the clamp edge resulting in a sudden decrease in measured Y force. Moreover, a higher Y force at comparable stretch values was observed in the static constructs tested in the redesigned clamps when compared to the commercial clamps, most apparent after approximately 25% stretch ( $250 \mu\text{m}$  actuator Y displacement). Accordingly, the maximum Y force values before rupture were also approximately doubled for the constructs in the redesigned clamps, and located at a lower stretch value than the commercial clamps.

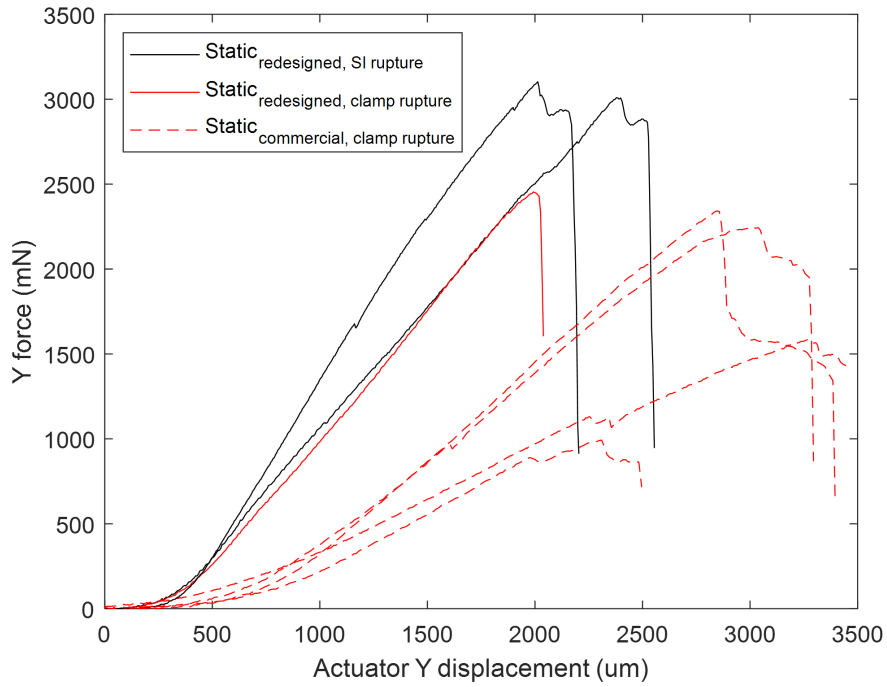


**Figure 3.5:** Y force vs actuator Y displacement plots of all statically cultured constructs until rupture. This plot is proportional to the nominal engineering stress vs strain plot: Solid curves represent the constructs tested in the redesigned clamps, dotted curves represent the constructs tested in the commercial clamps, red represents rupture which occurred at the clamp edge, black represents rupture which occurred near the SI

The calculated stretch ratios, nominal engineering stresses, and tangential moduli of the static constructs tested in the redesigned clamps at the  $\epsilon_{10\%}$  locations are listed in Table 3.1. Refer to Appendix F for the code used to extract these values. One of the three constructs was excluded from analysis due to an inadequate speckle pattern applied, which is necessary to calculate the  $\epsilon_{10\%}$  location with DIC in order to carry out DIC analysis. A large difference was observed in tangential modulus between the two constructs, approximately 2 MPa. The stretch and engineering stress values at the region of  $\epsilon_{10\%}$  for each construct was comparable.

**Table 3.1:** The estimated tangential moduli, engineering stresses and stretch ratios at the  $\epsilon_{10\%}$  locations for the static constructs tested in the redesigned clamps;  $TM_{10\%}$  = tangential modulus,  $\sigma_{10\%}$  = stress,  $\lambda_{10\%}$  = stretch, Note: data does not include the static construct with the inadequate speckle pattern

	Static (redesigned) n=2
$TM_{10\%}$ (MPa)	4, 2
$\sigma_{10\%}$ (kPa)	75, 60
$\lambda_{10\%}$	1.05, 1.06

The actuator Y displacement vs Y force measured in all 7 of the static and all 4 of the IS tissue constructs are plotted until their rupture points (Figure 3.6). All constructs demonstrated non-linear behavior. The commercial clamps displayed less steep curves as well as lower maximum Y force when compared to the redesigned clamps, although they reached higher stretch values overall. No significant difference was observed in mechanical behavior between the static and IS constructs tested in the commercial clamps.

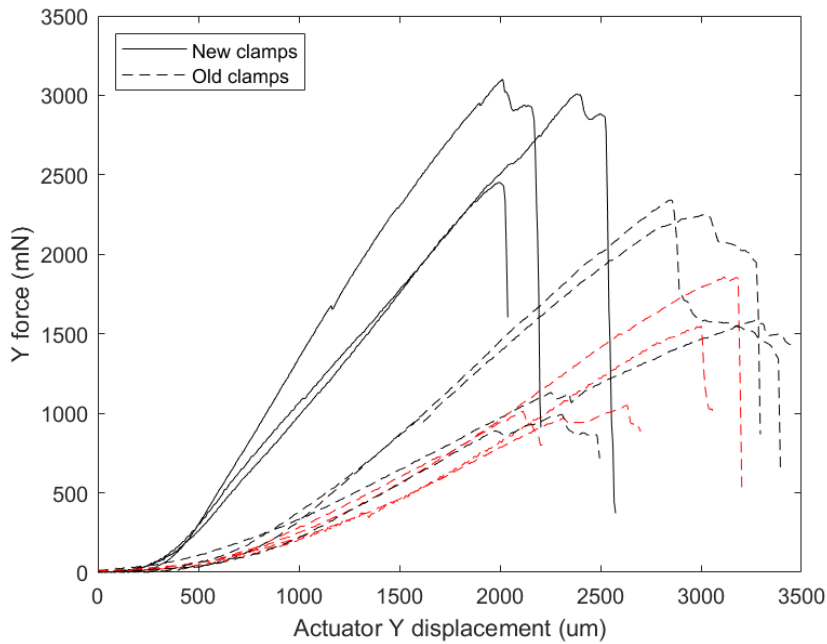


**Figure 3.6:** Y force vs actuator Y displacement plots of all static (black) and all IS (red) constructs until rupture: solid lines represent the new clamps, dotted lines represent the commercial clamps. This plot is proportional to the nominal engineering stress vs strain plot

### 3.3 Local Strain Patterns

Digital image correlation analysis was carried out on the images obtained during mechanical testing for each of the constructs to investigate local strain patterns for the different clamping and straining techniques, and how they may relate to rupture. A normalizing method was used to select the images for analysis to allow a more direct comparison between constructs. A simplified 2D hyperelastic finite element model was created to serve as an illustrative example of what the expected displacement and strain fields would look like when undergoing uniaxial tensile testing. Appendix D explains the parameter selection analysis method in order to carry out DIC analysis.

### 3.3.1 Finite Element Analysis Model: Illustrative Example

The displacement and strain field outputs of the simple hyperelastic FEA model were generated (Figure 3.7). Symmetry was applied about the Y-Z plane. A gradient pattern was observed in the X and Y displacement as approaching the SI. Higher X logarithmic strain was observed at the top and bottom of the SI (extension), whereas lower Y logarithmic strain was seen in these regions. Whereas, lower X logarithmic strain was observed at the right and left sides of the SI (compression) and higher Y logarithmic strain was seen at these regions. There is an apparent inverse pattern between X and Y strain surrounding the SI. A symmetric positive and negative XY shear strain pattern was also observed at the sides of the SI.

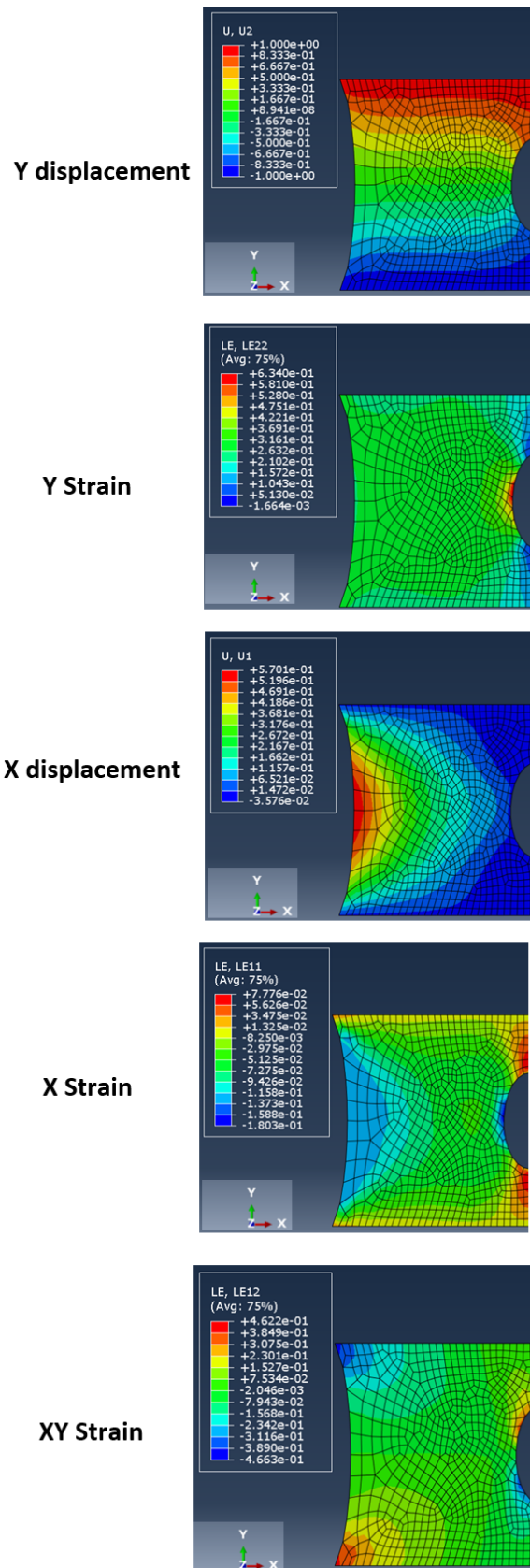


**Figure 3.7:** Finite element analysis results of 2D hyperelastic model reported as logarithmic strain (symmetry applied about Y-Z plane)

### 3.3.2 Effect of Straining Protocol: Static vs IS Constructs

A few observations can be noted from the X and Y displacement and strain maps generated via DIC analysis (Figure 3.8). It can be seen that the Y displacement field shows symmetric behavior in both the static and IS constructs, as was also observed in the FEA model. Furthermore, in both constructs, higher  $\epsilon_{yy}$  (extension) was seen at the left and right sides of the SI and a lower  $\epsilon_{yy}$  was seen at the top and bottom of the SI. High  $\epsilon_{yy}$  values also occurred near both clamp edges. Overall symmetric behavior can be seen in both constructs. An inverse trend for  $\epsilon_{xx}$  was observed in for both constructs, which agree with the FEA model results. On the top and bottom of the SI, high  $\epsilon_{xx}$  values (extension) were exhibited, whereas the right and left sides of the SI exhibited negative  $\epsilon_{xx}$  values (compression). The  $\epsilon_{xy}$  behavior of the constructs showed a comparable diagonal symmetric trend, especially surrounding the SI region. One key difference between constructs was the X extension noticed at the edges of the IS construct as opposed to compression observed in the static constructs. There was also an apparent symmetric “C” shaped trend observed in the IS constructs for  $\epsilon_{xx}$  as opposed to the homogeneous behavior seen in the static constructs.

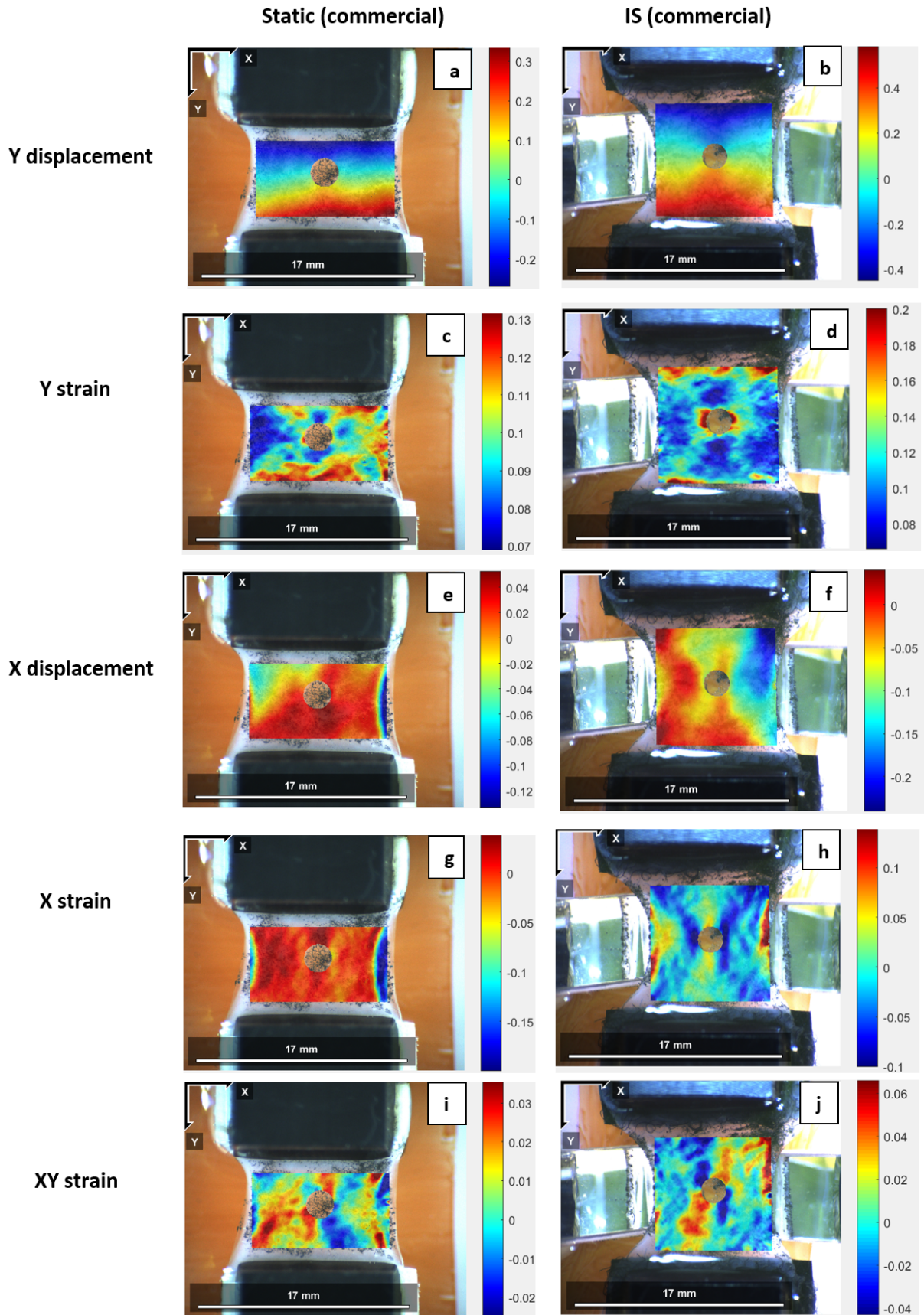


**Figure 3.8:** X and Y displacement and strain maps at  $\epsilon_{10\%}$  for a static and IS construct tested in the commercial clamps

All constructs behaved similarly to the examples shown above, with the exception of 2 constructs (1 IS and 1 static in commercial clamps) which did not follow the same X displacement and  $\epsilon_{xx}$  trends as the other constructs (Figure 3.9). One static construct tested with the commercial clamps displayed a large gradient-like behavior in the X direction and one IS construct exhibited a very different behavior than the other IS constructs, as if it was shifted diagonally while undergoing mechanical testing.

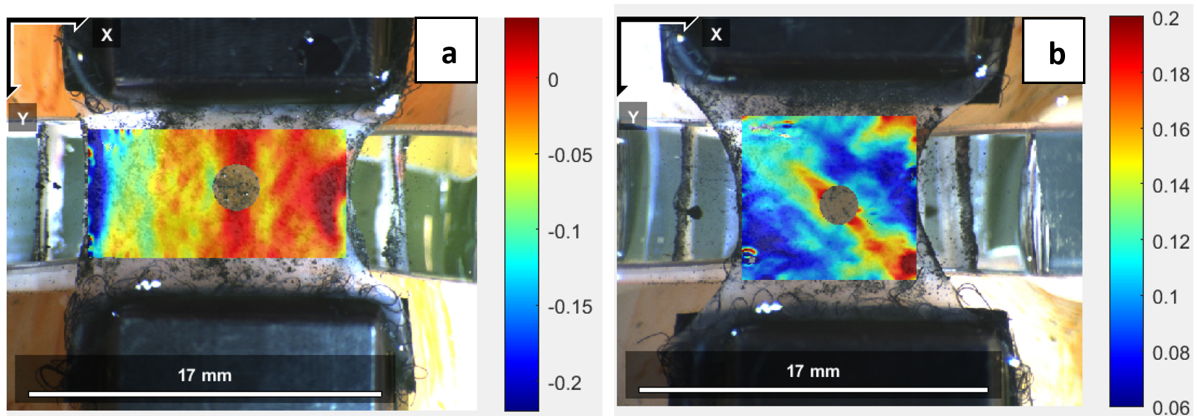


**Figure 3.9:** Two constructs which displayed different behavior from the other constructs: a)  $\epsilon_{xx}$  of a static construct tested in commercial clamps (gradient-like) b)  $\epsilon_{yy}$  of an IS construct tested in commercial clamps (diagonally shifted behavior)

### 3.3.3 Effect of Clamp Design: Commercial vs Redesigned Clamps

The strain pattern behavior of the static constructs tested in the commercial clamps and redesigned clamps showed similar trends, with a few exceptions (Figure 3.10). Overall symmetric behavior can be seen in both clamp designs, although the redesigned clamps displayed more homogeneity throughout the construct, especially when looking at the  $\epsilon_{yy}$  behavior. Both clamp designs displayed compressive  $\epsilon_{xx}$  behavior at the edges, not observed in the IS constructs.

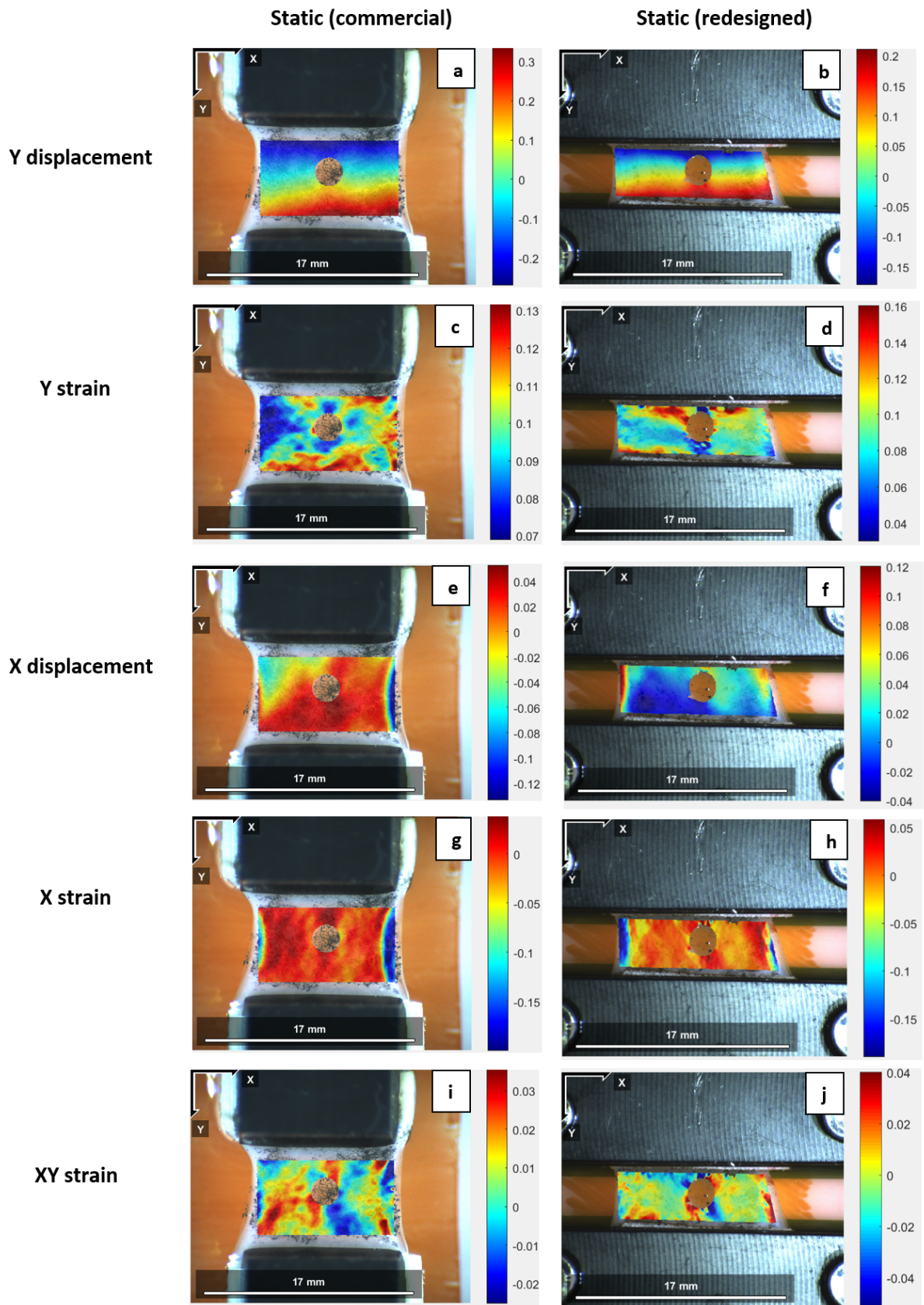


**Figure 3.10:** X and Y displacement and strain maps at  $\epsilon_{10\%}$  for two static constructs tested in the commercial clamps (left) and redesigned clamps (right)

### 3.3.4 Quantification of Local Strain Patterns

Additionally, X and Y average strain plots were generated across the mid cap and shoulder regions for all constructs (Figure 3.11 shows an example of the IS construct from Figure 3.8). It can be verified with these plots that the top and bottom of the SI in the mid cap region experienced high  $\epsilon_{xx}$  extension and the immediate left and right sides of the SI experienced  $\epsilon_{xx}$  compression. In the shoulder regions, this trend was also observed, although the compression values were less. For the average  $\epsilon_{yy}$ , the opposite trend mentioned previously could be verified as well, where the top and bottom of the SI in the mid cap region experienced low  $\epsilon_{yy}$  extension and the immediate left and right sides of the SI experienced a high  $\epsilon_{yy}$  extension peak. It is apparent that within the shoulder regions, the peak values were much less. The  $\epsilon_{xy}$  also showed symmetric behavior about zero, where an inverse trend is seen in the shoulders region surrounding the SI for the right/left sides. Overall, symmetric behavior was observed in the constructs for the right and left sides as well as the top and bottom shoulders. The remaining X and Y average strain plots for all constructs can be seen in Appendix E and display similar trends as previously mentioned.

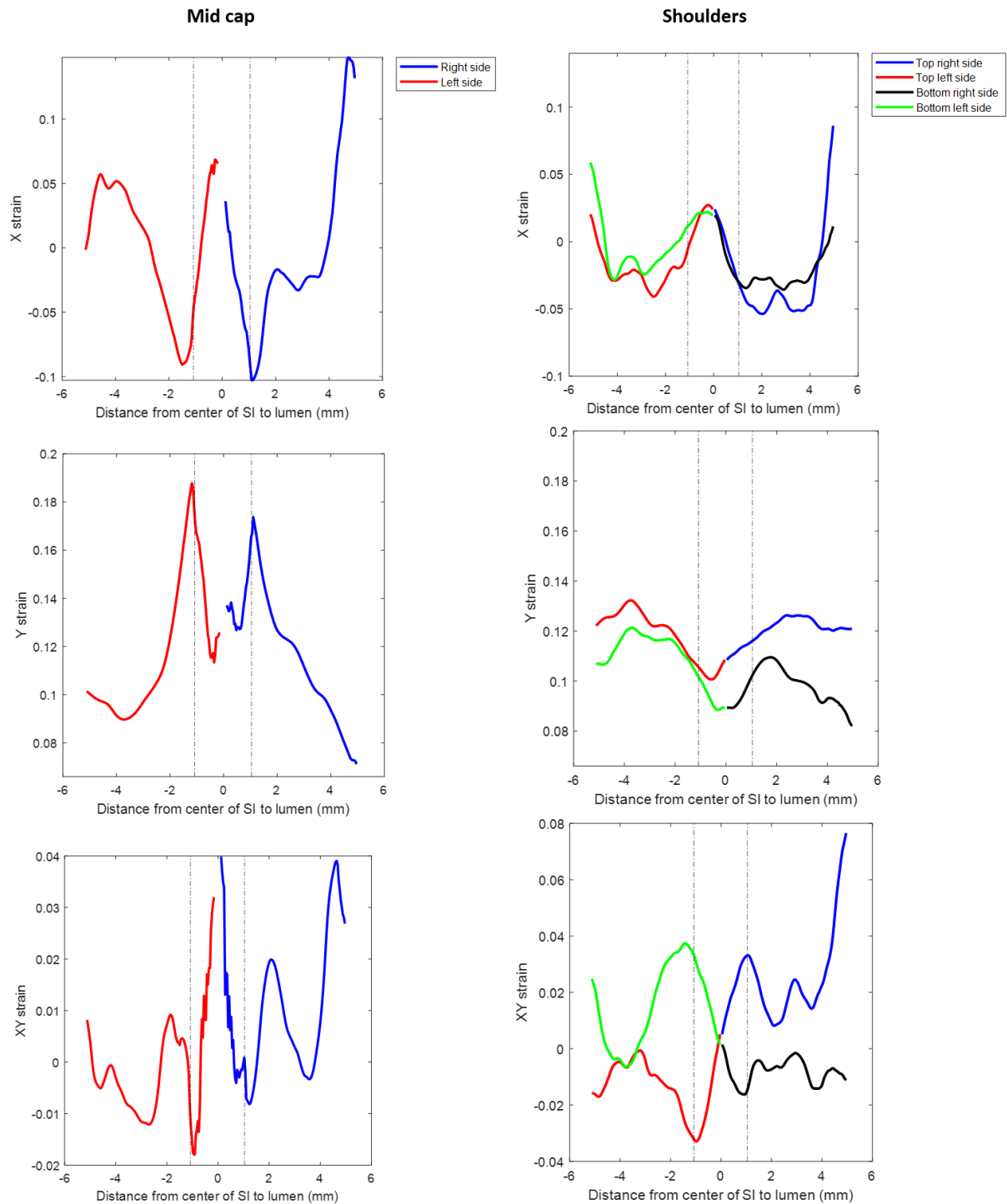


**Figure 3.11:** X and Y average strain plots running along the width of an IS construct, excluding the SI for the mid cap and shoulder regions, subdivided into left/right and top/bottom regions. The normal X and Y strains are presented in the first and second rows, respectively, as well as the XY shear strain in the last row. The grey dotted lines enclose the left and right most side boundaries of the SI region

The IS construct example previously shown was also used to compare the average  $\epsilon_{xx}$  and  $\epsilon_{yy}$  in the different regions of the construct surrounding the SI (Figure 3.12, refer to Figure 2.12 in the methods section for the selected regions). The inverse trend between the left and right sides of the SI and top and bottom of the SI was apparent for the  $\epsilon_{xx}$  and  $\epsilon_{yy}$ . The statistical comparison of these averages grouped for each region are displayed in Figures 3.13-3.15. No statistical difference in average  $\epsilon_{xx}$  between regions and constructs was observed, with one exception. The shoulder regions of the static constructs in redesigned clamps proved to have a statistically higher  $\epsilon_{xx}$  than the static constructs in the commercial clamps ( $p < 0.05$ ), which showed compressive behavior. Similarly, the average  $\epsilon_{yy}$  in the mid cap region of the IS constructs tested in the commercial clamps was statistically higher than the  $\epsilon_{yy}$  in the static constructs in the commercial clamps ( $p < 0.005$ ), showing more  $\epsilon_{yy}$  extension. Also, the average  $\epsilon_{xy}$  was statistically higher in the mid cap region of the static constructs (commercial clamps) when compared to the static constructs (redesigned clamps) ( $p < 0.05$ ).

To summarize, for  $\epsilon_{xx}$ , no statistically significant differences were found for the top/bottom and left/right mid cap regions of the SI between the different groups analyzed. For  $\epsilon_{yy}$  and  $\epsilon_{xy}$ , no statistically significant differences were found for the shoulder regions surrounding the SI between the different groups analyzed. Statistical analysis was not carried out if the total number of samples were too small ( $n < 3$ ), as was the case with the top and bottom regions of the SI for the static constructs in the redesigned clamps, although the plots were still presented.

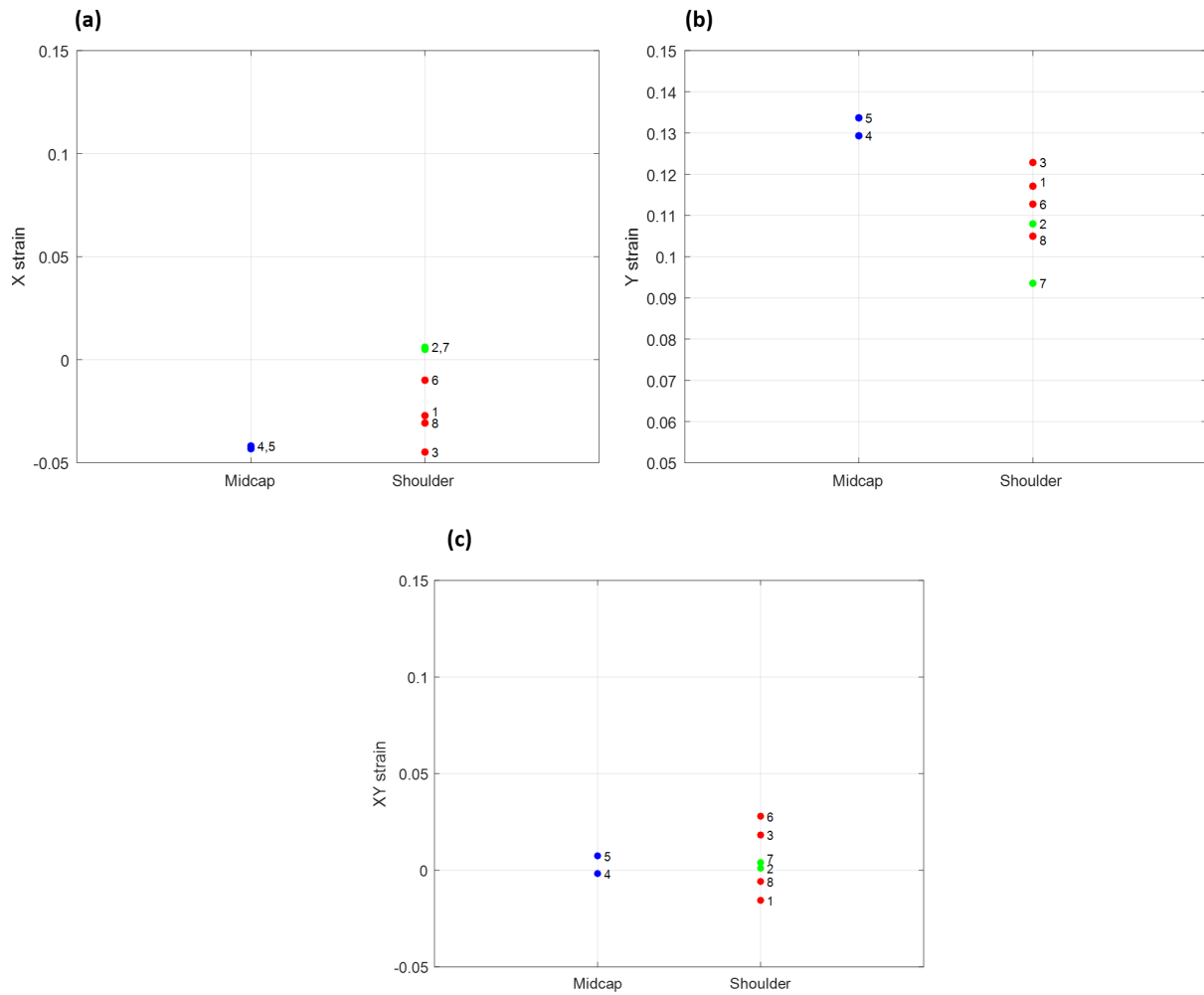


**Figure 3.12:** Average  $\epsilon_{xx}$  (a),  $\epsilon_{yy}$  (b), and  $\epsilon_{xy}$  (c) from different regions of an IS construct (refer to Figure 2.12 for corresponding regions); blue: right and left sides of SI in mid cap region, green: top and bottom sides of SI in shoulder region, red: remaining shoulder regions, excluding edges

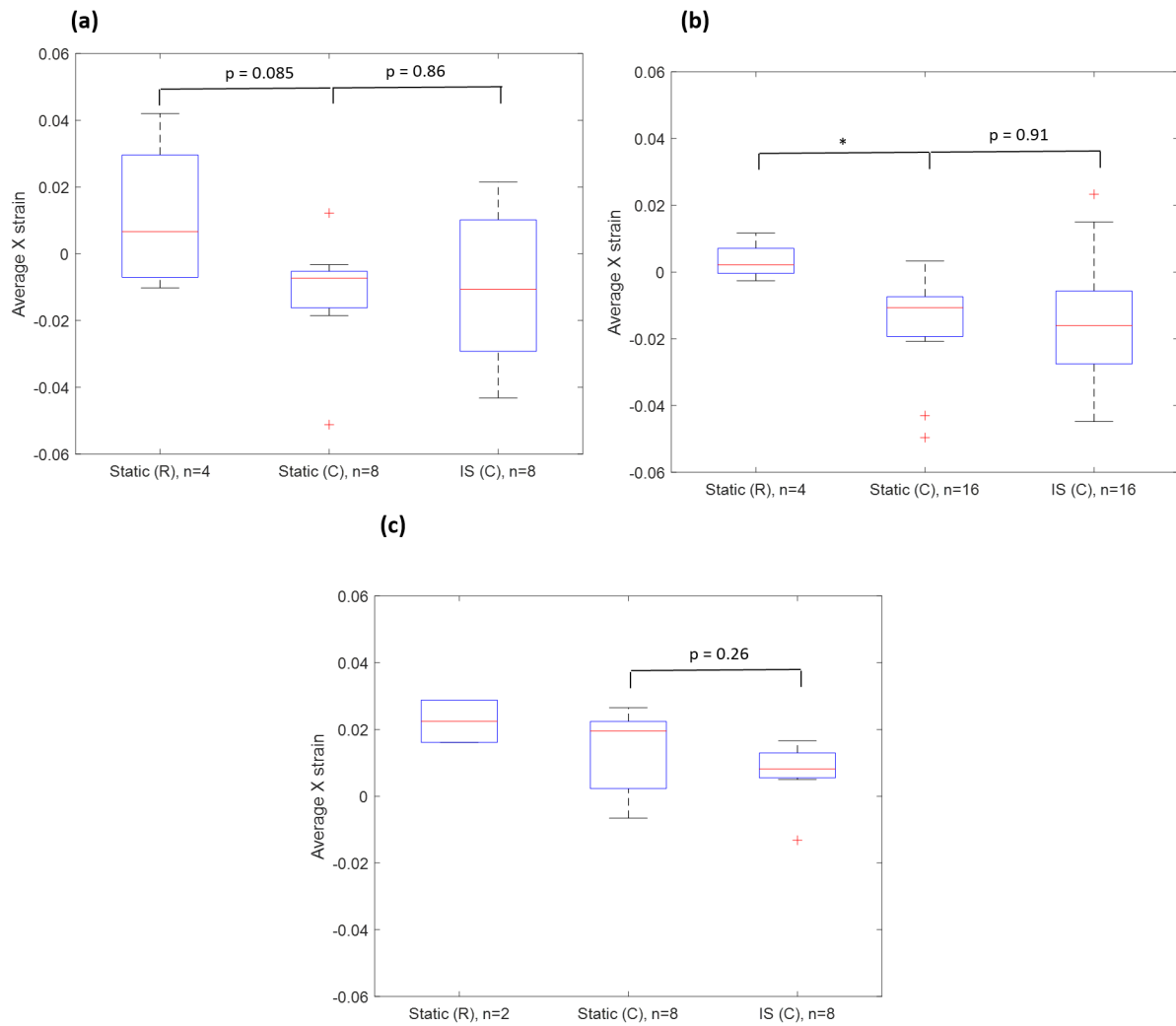


**Figure 3.13:** Comparisons of average  $\epsilon_{xx}$  between construct types and clamps used: a) left/right SI in mid cap region b) shoulder regions, excluding edges c) top/bottom SI in shoulder region; Note: (R) redesigned clamps, (C) commercial clamps \*:  $p < 0.05$ .

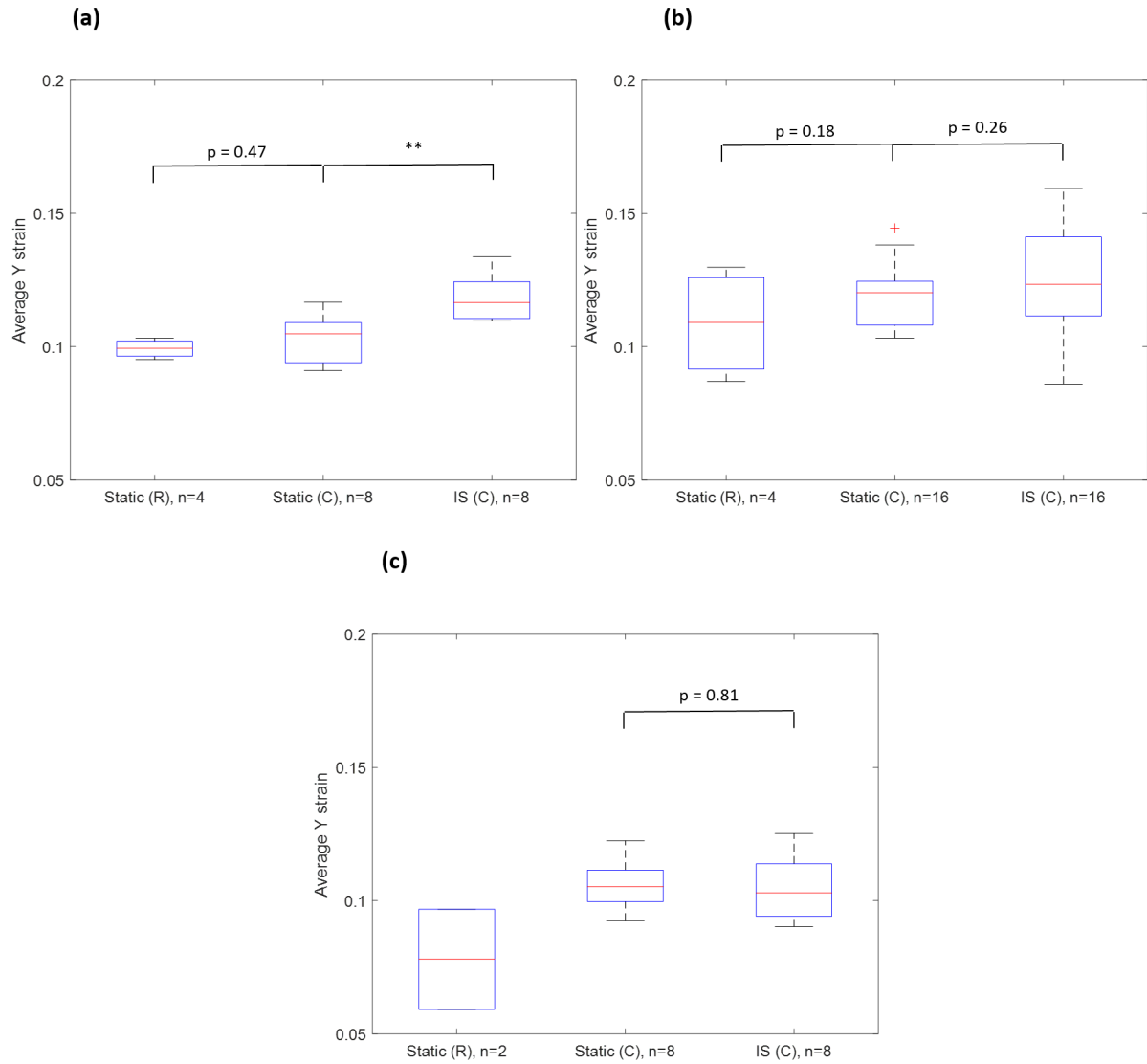


**Figure 3.14:** Comparisons of average  $\epsilon_{yy}$  between construct types and clamps used: a) left/right SI in mid cap region b) shoulder regions, excluding edges c) top/bottom SI in shoulder region; Note: (R) redesigned clamps, (C) commercial clamps \*\*:p<0.005.

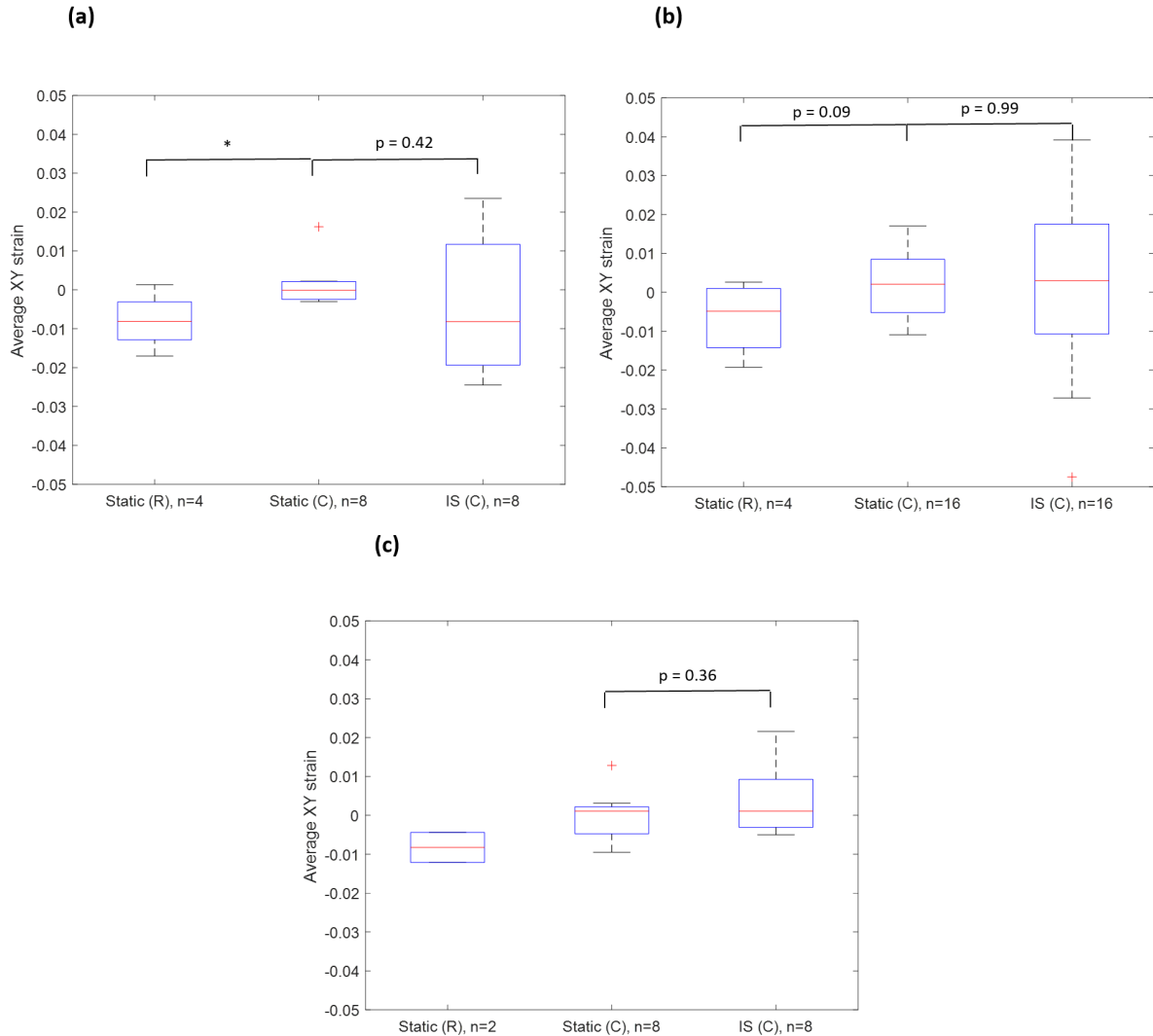


**Figure 3.15:** Comparisons of average  $\epsilon_{xy}$  between construct types and clamps used: a) left/right SI in mid cap region b) shoulder regions, excluding edges c) top/bottom SI in shoulder region; Note: (R) redesigned clamps, (C) commercial clamps \*:  $p < 0.05$ .

### 3.4 Rupture Behavior

The IS constructs tested in the commercial clamps demonstrated a variation in rupture location, either rupturing near the SI (2/4) or at the clamp edge (2/4). The static constructs tested in the commercial clamps all ruptured at the clamp edge (Figure 3.16). It can be seen in the strain maps, that a high  $\epsilon_{yy}$  (extension) on the right and left sides of the SI is apparent in the construct that ruptured near the SI, but does not exist in the constructs that rupture at the clamp edge. The region of highest  $\epsilon_{yy}$  in these constructs is located near the clamp edges. This may be a possible link to how  $\epsilon_{yy}$  may relate to rupture location.

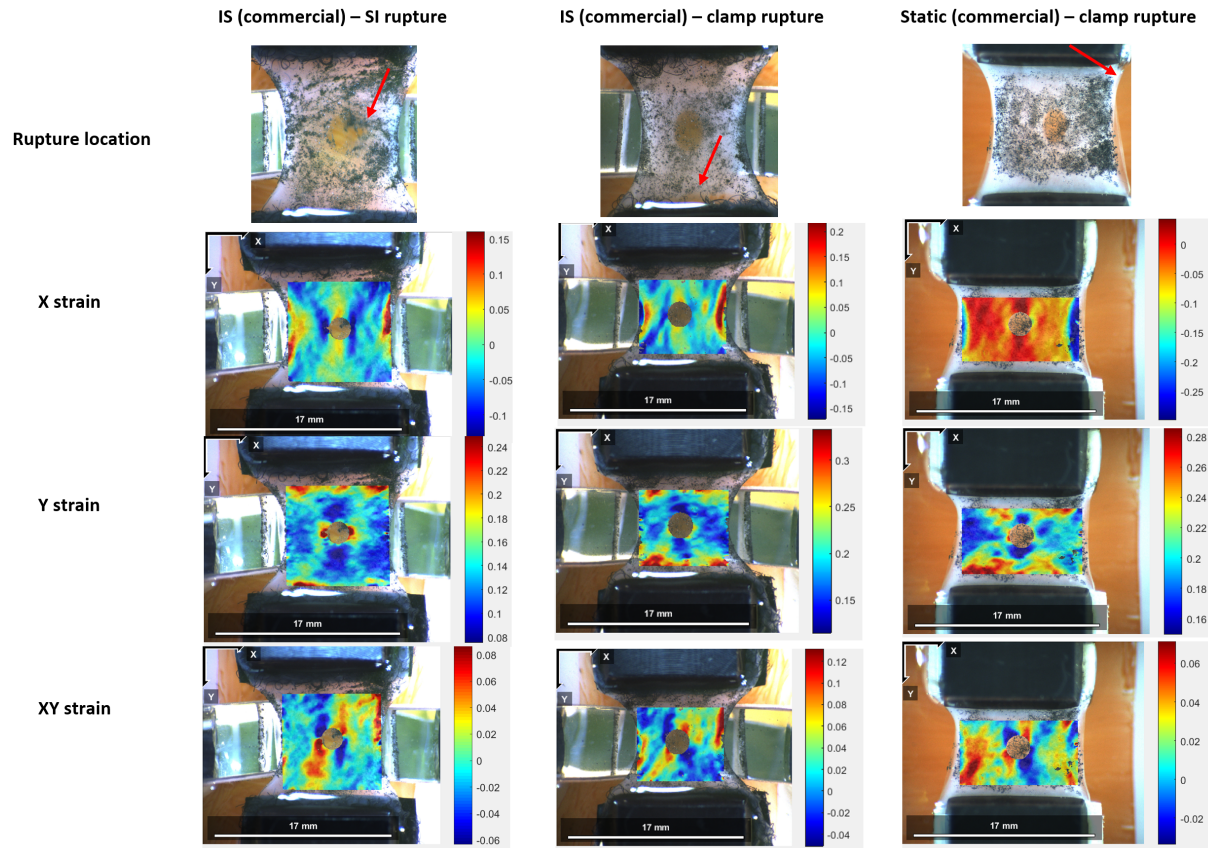


**Figure 3.16:** X and Y strain maps taken immediately before rupture observed during uniaxial tensile testing: IS constructs tested in the commercial clamps show rupture near the clamp edges (2/4) and near the SI (2/4), static construct in commercial clamps show rupture near the clamps only (4/4)

In the static constructs that were tested in the redesigned clamps, rupture was observed near the SI in 2 out of the 3 constructs. A similar trend of maximum  $\epsilon_{yy}$  occurs at the location of rupture when ruptured near the SI (Figure 3.17). Similarly, this maximum  $\epsilon_{yy}$  is seen near the clamp region where the construct ruptured. A significant  $\epsilon_{xx}$  compression behavior was also observed at the location of rupture near the SI, as was also seen in the IS constructs rupturing near the SI.

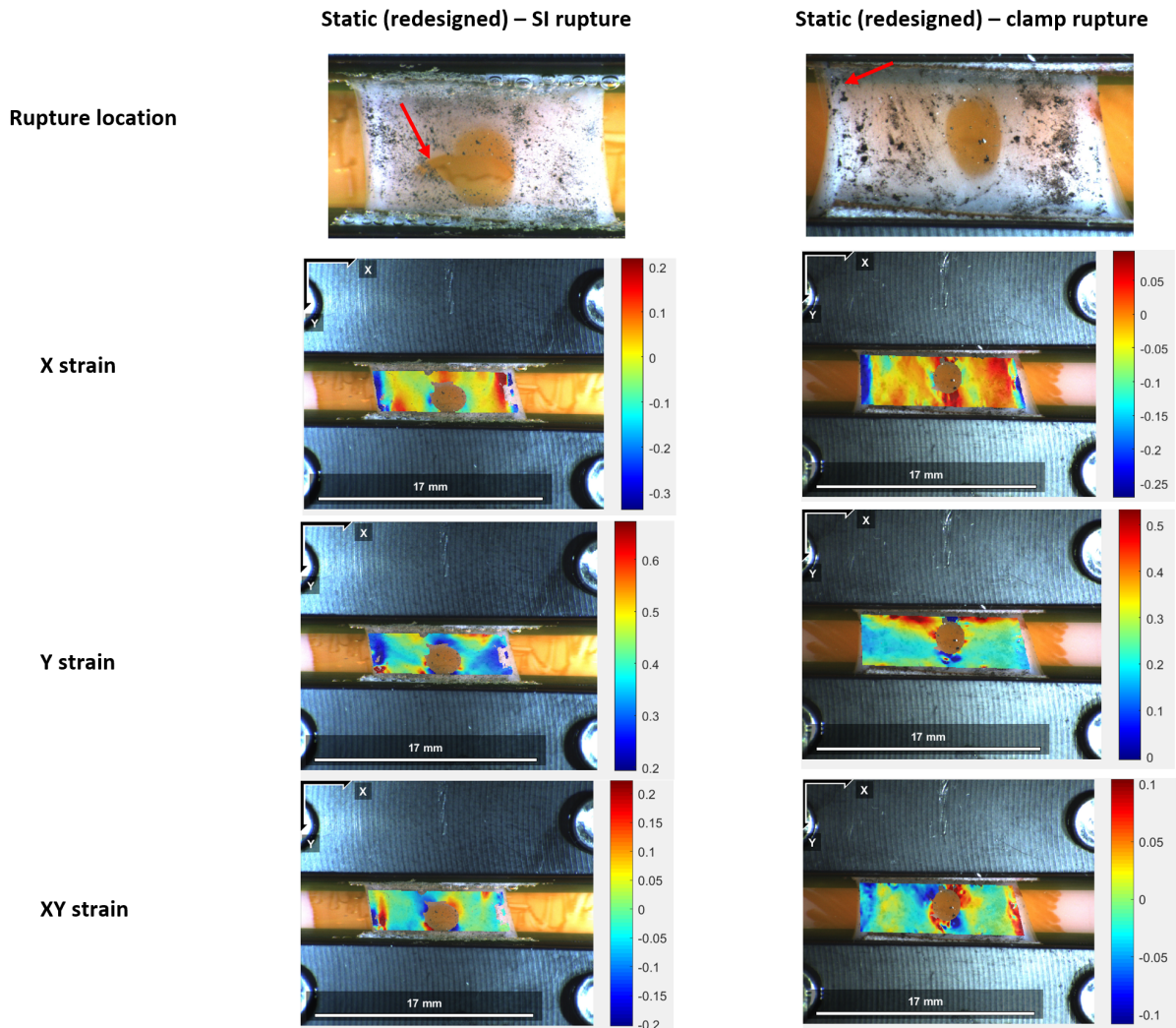


**Figure 3.17:** X and Y strain maps taken immediately before rupture observed during uniaxial tensile testing: static constructs tested in redesigned clamps show rupture near the SI (2/3) and clamp region (1/3)

# 4

## Discussion

The aim of this study was to create collagenous constructs, incorporate a soft inclusion, and mechanically characterize them to aid in the development towards an *in vitro* atherosclerotic fibrous cap model to systematically study plaque rupture mechanics. These constructs were created with a fibrin gel containing HVSCs and either statically cultured or subjected to uniaxial intermittent straining during culture. Uniaxial tensile testing was performed using two different clamp designs to investigate the global mechanical behavior, as well as local strain patterns preceding rupture using DIC.

### 4.1 Tissue Engineered Constructs

In this study, collagenous constructs were created according to previously established static and dynamic (IS) cell culture protocols used for tissue engineered collagen-rich heart valve constructs [8]. The protocol was altered to reflect the environment of an atherosclerotic fibrous cap. Following these altered protocols, tissue engineered constructs without a SI were previously created using static and intermittent straining protocols, as these methods have been reported to improve and accelerate the alignment of collagen fibers in the direction of loading [5]. The previously created constructs were subjected to 7 days of static culture and 14 days of straining. The stiffness values extracted for these constructs ranged between approximately 0.2-5 MPa at 5% stretch, which was within the range found in literature for carotid fibrous caps (approx. 0.5-5 MPa) [24]. However, the ultimate tensile properties of these constructs were substantially higher when compared to the scarce literature evaluating fibrous cap tensile strengths. To compensate for the high strength behavior seen previously, this study altered the straining protocol to 14 days of static culture and 7 days of intermittent straining. Also, in this study, a SI (with

stiffness of approximately 1 kPa) was introduced into the collagenous structure in order to represent the mechanical properties of the lipid pool and to investigate the effect of this substantially less stiff structure on the rupture mechanics of the construct. The SI became well integrated within the collagenous environment, as seen *in vivo*, containing even cell growth on all sides of the SI. Ultimately, this SI incorporated model could aid in discovering the underlying principles behind plaque rupture mechanics. Due to the large variation seen *in vivo* atherosclerotic plaque collagenous structure and the variety of potential rupture mechanisms, future research should focus on better characterizing these constructs and changing culture conditions to embrace the biological variance seen *in vivo*.

Dependent on the loading regime applied, various amounts of construct compaction were observed at day 21. Approximately 50% compaction in the X direction (width) was observed in the IS constructs when compared to the statically cultured constructs which showed approximately 15% compaction (Figure 3.2). Accordingly, there was a large amount of Z compaction (thickness) observed for both the static and IS constructs (approx. 80%). As expected, minimal Y compaction (length) was observed in all constructs as the tissues were constrained in this direction during culture. The significant difference in X compaction could signify a substantial effect of straining on the micro-structure of the constructs. This increase in compaction seen in the IS constructs could possibly be caused by an increase in cell-to-cell interactions and tissue reorganization along the edges of the construct when uniaxial strain was introduced [25]. The similar Z compaction behavior between constructs reveals that the uniaxial straining did not have an impact on the thickness. The large amount of Z compaction observed may be due to the cell matrix forces increasing in time as the fibrin matrix degrades [25].

## 4.2 Global Mechanical Behavior

### 4.2.1 Effect of Straining Protocol: Static vs IS Constructs

Interestingly, no significant difference was observed in global mechanical behavior between the static and IS constructs tested in the commercial clamps (Figure 3.4). The large difference in X compaction (width) between these constructs did not appear to significantly effect their force-stretch curvature behavior, as was observed in previous experiments. Additionally, the maximum Y force before rupture consistently varied in both constructs, ranging from 1000-2500 mN. The similar force-stretch curvature behavior between constructs could be explained by the amount of time that the IS constructs were strained for which may not have been sufficient to create a substantial difference in micro-structure compared to the static constructs. The variation in maximum Y force could indicate variation occurring on the microscopic-scale which could be affecting the global rupture behavior. Also, any variation in micro-structure near the clamp edge, where rupture most often occurred, could have an affect on the global mechanical behavior of both constructs.

### 4.2.2 Effect of Clamp Design: Commercial vs Redesigned Clamps

In order to mechanically characterize the constructs, ideally the clamping technique should have no effect on the mechanical behavior. The static constructs in the commercial clamps displayed consistent rupture behavior near the clamp edge, demonstrating a sudden decrease in Y force, remaining constant, and then dropping in Y force again (Figure 3.5). Due to rupture occurring consistently at the edge of the commercial clamps during testing, redesigned clamps were created in which 2 mm of tissue near the Velcro edges were gripped onto each side to further improve the load transmission from clamp to tissue. Observations showed a consistent two-bump sudden decrease rupture behavior in the static constructs tested in the redesigned clamps, not seen with the commercial clamps. These bumps appeared to be linked to the initial rupture on one side of the SI (first bump) and the second rupture on the other side (second bump), successfully producing consistent rupture at the site of the SI. Additionally, it was observed that the static constructs tested in the redesigned clamps as opposed to the commercial clamps displayed higher Y forces at comparable stretch (Figure 3.5).

The consistent rupture mechanical behavior in the static constructs tested with the commercial clamps could indicate that the fibers in the region near the clamp edge held on for some amount of stretch until a larger rupture occurred. This could be linked to an increase in micro-failure occurring at this region and subsequently a gradual decrease in maximum Y force. Contrarily, the clear and consistent two bump sudden Y force decrease rupture pattern observed in the redesigned clamps could denote a more structured mid cap region with higher maximum strength properties. The two bump behavior was visually linked to rupture occurring on one side of the SI, followed by the other side soon after. This behavior could be related to the collagen composition in the constructs surrounding the SI. The fact that the constructs do not rupture near the clamp edge in the redesigned clamps shows an improvement in load transmission to the tissue. Furthermore, a larger slope in force-stretch was observed with the redesigned clamps when compared to the commercial clamps, therefore clamp redesign may have a large effect on the mechanical behavior observed.

Interestingly, the experimental data of the static constructs tested in the redesigned clamps consistently followed a 2-curvature non-linear curve observed while curve fitting (Figure 2.9), which was unlike the behavior of other constructs tested in the commercial clamps. A consistent strain hardening behavior (increase in force needed to stretch construct) was observed until approximately 5% stretch, after which a gradual strain softening behavior was seen (decrease in force needed to stretch construct). Contrarily, the commercial clamps consistently followed a 1-curvature non-linear curve (solely strain hardening behavior), which also reflects the behavior seen in literature for human plaques. Strain hardening behavior is often observed in biological soft tissue due to cell-matrix stiffening interactions which increase with stretch. This strain softening behavior in the redesigned clamp could possibly be due to an increase in gradual fiber micro-failure

occurring after approximately 5% stretch. This behavior is not seen in human plaques possibly due to a difference in structural fiber strength. Due to the consistency in behavior, further investigation is needed. It can be hypothesized that the redesigned clamps improved the transfer of tissue displacement, leading to more homogeneity and reported the actual stretch occurring in the region of interest (mid cap region), when compared to the commercial clamps. The commercial clamps reported higher stretch values which may not accurately reflect the actual stretch occurring in this region. This could explain why the strain softening behavior was not seen with the commercial clamps, as this effect occurred at 5% stretch in the mid cap region and may not have been captured by the commercial clamps before rupture occurred. Due to this 2-curvature behavior in the static constructs with the redesigned clamps, in order to extract the tangential moduli, the 5-parameter Mooney-Rivlin material model best fit the data.

### 4.2.3 Comparison to human atherosclerotic fibrous caps

In this study, the stiffness values for the constructs tested in the commercial clamps were not reported due to possible artefacts occurring near the clamp region. However, the tangential moduli were extracted from nominal global measurements for the static constructs tested in the redesigned clamps in order to get an idea of their stiffness values (Table 3.1). The stiffness values reported for the static constructs tested in the redesigned clamps were approximately 2 MPa and 4 MPa at 10% stretch. These values are within the wide range found in literature for carotid atherosclerotic fibrous caps ranging from 0.5 to 5 MPa at 10% stretch [24]. This two-fold difference in stiffness from the two constructs can be attributed to the fact that the initial average thickness calculated for the constructs had a two-fold difference, which affected the nominal stress reported, and therefore the tangential moduli as well. This difference could have been caused by measurement error, as the boundaries of the constructs were at times difficult to distinguish, therefore the measuring procedure could be further optimized. These reported values should be read with caution as the sample size was also small due to experimental access limitations. The ultimate tensile strength values were not reported in this study due to possible differences in local tissue thickness which would not accurately reflect the local maximum tissue strength. When converting from global to local scale, a good command of the current cross sectional area is necessary.

## 4.3 Local Strain Patterns

### 4.3.1 Effect of Straining Protocol: Static vs IS Constructs

Using DIC, similar trends were observed in the  $\epsilon_{xx}$  and  $\epsilon_{yy}$  patterns around the SI in both the static and IS constructs tested in the commercial clamps at  $\epsilon_{10\%}$  (Figure 3.8).  $\epsilon_{xx}$  compression was experienced by the SI left and right sides, as well as  $\epsilon_{xx}$  extension at the top and bottom of the SI. An inverse trend for the  $\epsilon_{yy}$  was observed, with high  $\epsilon_{yy}$  extension at the left and right of the SI and low  $\epsilon_{yy}$  extension at the top and bottom.

However, the largest difference between the constructs was that the  $\epsilon_{xx}$  pattern in the IS constructs appeared to follow a symmetric “C” shaped compression trend going from clamp to clamp, and extension occurred at the edges. This differed significantly from the  $\epsilon_{xx}$  pattern seen in the static constructs where homogeneous  $\epsilon_{xx}$  behavior was seen throughout the construct, with compression observed at the edges. Additionally, the IS constructs showed a statistically significant higher  $\epsilon_{yy}$  extension in the mid cap region when compared to the other constructs.

The compressive behavior on the sides of the SI show that there is compaction occurring on the sides of the constructs moving towards the SI, which is the expected behavior shown in the FEA model for a material undergoing uniaxial tensile testing. If incompressibility is assumed and the material is stretched in one direction, compaction is expected in the orthogonal direction. This concept can also explain the interesting inverse trend observed between  $\epsilon_{xx}$  and  $\epsilon_{yy}$  behavior surrounding the SI. The high  $\epsilon_{yy}$  extension at the left and right of the SI could be due to the parallel fiber alignment in the direction of stretch in which the SI elongates. This interface between the SI and tissue is important to investigate as it may exhibit stress/strain concentrations due to the difference in stiffness properties. Furthermore, the difference in  $\epsilon_{xx}$  patterns could be due to the fact that there is more cell-to-cell force interactions occurring in the IS constructs because it is more developed than the static constructs. Accordingly, the IS constructs showed a statistically significant higher  $\epsilon_{yy}$  extension in the mid cap which could also be due to a more structured collagen architecture in this region, leading to stiffer local mechanical properties (Figure 3.14). The unique differences in X displacement and strain behavior observed in two constructs (one static and one IS) could possibly relate to any slack present in the construct before testing due to either how they were loaded into the clamps or their composition (Figure 3.9). Further histology analysis is necessary.

### 4.3.2 Effect of Clamp Design: Commercial vs Redesigned Clamps

The DIC strain patterns for the static constructs tested in the commercial and redesigned clamps were overall comparable and followed a similar pattern, surrounding the SI, to the constructs mentioned in the previous section (Figure 3.10). However, the static constructs in the redesigned clamps showed more homogeneity within the mid cap region, specifically for  $\epsilon_{yy}$ . Furthermore, the  $\epsilon_{xy}$  in the mid cap region for the static constructs in the redesigned clamps demonstrated to be statistically lower than the static constructs in the commercial clamps (Figure 3.15).

The increase in homogeneity displayed in the static constructs with the redesigned clamps indicates better load transmission from the clamp to tissue during testing. The lower  $\epsilon_{xy}$  seen in the mid cap region for the static constructs in the redesigned clamps may also support this notion of improved load transmission as the mid cap region of the construct may be more sensitive to shear strain effects.

The regions of  $\epsilon_{10\%}$  determined by DIC are located on the global mechanical behavior plots for all of the constructs in Appendix E (Figure E.1). The fact that there is a large variation in these locations for all constructs tested in the commercial clamps, especially located at higher stretch than the redesigned clamps, further supports the notion that the commercial clamps could be greatly effecting the actual global mechanical behavior reported for the area of interest (mid cap region). This location on the constructs tested in the redesigned clamps varies less.

## 4.4 Rupture Behavior

In this study, the IS constructs tested in the commercial clamps varied in rupture location, either occurring at the clamp edge or near the SI (Figure 3.16). The static constructs tested in the commercial clamps all ruptured at the clamp edge and 2 out of 3 of the static constructs tested in the redesigned clamps ruptured near the SI (Figure 3.17). Regions of high  $\epsilon_{yy}$  extension near the clamp area were observed in the constructs that ruptured in this region. Similarly, high  $\epsilon_{yy}$  extension and  $\epsilon_{xx}$  compression occurred near the rupture location in the constructs that ruptured near the SI. The increase in the mid cap  $\epsilon_{yy}$  extension showed statistical significance in the IS constructs (commercial clamps) when compared to the static constructs (commercial clamps) (Figure 3.14). Furthermore, the  $\epsilon_{xy}$  seen in all the constructs leading to rupture demonstrated a consistently symmetric pattern surrounding the SI, in which the positive and negative values on each side of the SI equated to approximately zero.

The increase in the mid cap  $\epsilon_{yy}$  extension in the IS constructs (commercial clamps) when compared to the static constructs (commercial clamps) could be due to a more structured mid cap region in the IS constructs, which may contain stronger local mechanical properties than the global behavior reported (affected by the inadequate load transmission). This demonstrates the importance of clamping design on the tissue constructs when performing mechanical testing. The consistent symmetric  $\epsilon_{xy}$  behavior surrounding the SI indicates fairly symmetric collagen composition (i.e. orientation, amount) within the constructs.

Using the strain pattern information discovered in this study surrounding the SI leading to rupture could translate to clinical measurement in order to predict plaque rupture. For example, the increase in  $\epsilon_{yy}$  extension found at the rupture locations near the SI can be representative of the circumferential strain experienced in the fibrous cap. Similarly, the  $\epsilon_{xx}$  compression found at the rupture locations near the SI can be representative of the radial strain. By measuring high circumferential strain and compressive radial strain near the lipid pool of a vulnerable plaque using imaging techniques, such as ultrasound, rupture prediction strain fingerprints can be made. Although this is a step in the right direction, a complete strain fingerprint is necessary. Inflation testing of TE circular cross sections, representative of human plaque cross sections, could also supply additional mechanical property data. This atherosclerotic *in vitro* disease model could be used in pharmaceutical intervention to study drug delivery to suppress inflammation, decreasing rupture risk.

## 4.5 Limitations

Due to the COVID-19 pandemic and limited resources available, this study contained low sample sizes. Additionally, inter-experimental differences might have led to some variation in the analysis, as the data taken from previously tested constructs were used in this study as well, and could have also led to some variation in the analysis. Furthermore, assumptions and estimations were made while measuring the initial and final dimensions which may have an effect on the final results reported, although the measure error is expected to be consistent between all samples.

Many of the observations made with the commercial clamps could be explained due to the fact that the redesigned clamps may be more suitable for gradually transferring the forces from the clamp to the tissue of interest (mid cap region) during testing. It is hypothesized that this region of tissue, located near the clamp edge in the commercial clamps, contains less amount of structured collagen when compared to the center of the construct (mid cap region) due to it being a transition region into the Velcro. However, this hypothesis must be confirmed with collagen histological analysis (i.e. orientation, amount). This potentially less structured region could cause micro-structural slippage to occur in the commercial clamps due to inadequate load transmission, in turn causing more heterogeneity to occur in the mid cap region where the  $\epsilon_{10\%}$  is determined. Contrarily, this  $\epsilon_{10\%}$  region in the redesigned clamps displayed homogeneous behavior, possibly linked to the differences in mechanical behavior observed between clamp designs.

Due to the comparable mechanical behavior observed between the static and IS constructs tested in the commercial clamps, testing the IS constructs in the redesigned clamps and investigating the collagen composition (i.e. fiber orientation, amount, type) between constructs is recommended as the next step before considering adjusting the straining protocol. The global mechanical behavior of the commercial clamps may be reporting behavior that is largely effected by this possible micro-structural slippage occurring near the clamp-tissue interface.

In this study, the nominal engineering stress was calculated in order to report the tangential moduli, however tracking the change in thickness during mechanical testing and reporting Cauchy (true) stress in the future is recommended as tissue exhibits some compressible behavior, although in this study incompressibility is assumed when extracting the tangential moduli. This could be done by using a microscope or mirror which would allow the visualization of the tissue thickness and therefore the true stress could be determined. Furthermore, linking the true stress to the local strain regions determined by DIC analysis could provide a more representative mechanical behavior measure during testing, largely due to the heterogeneity occurring within the construct. However, the two-dimensional DIC used in this study has its own limitations for a three-dimensional construct. It does not account for possible tissue deformation and any micro-structural failure that may be occurring below the surface of the tissue, therefore three-dimensional DIC should be considered.

Regardless of these limitations, the findings found in this study regarding the mechanical behavior and local strain fields of the TE constructs can be used to further investigate how to successfully replicate the mechanical structure of an *in vitro* atherosclerotic fibrous cap model to study plaque rupture mechanics. By successfully and consistently generating rupture at the site of the SI in this study, future tests can be performed to mechanically characterize the constructs with minimal clamping effects.

# 5

## Concluding Remarks

### 5.1 Conclusion

The main findings of this study are further elaborated below based on the aims of this study.

1. Create TE collagenous constructs containing a SI subjected to different straining protocol during culture:  
Fibrin-based gel constructs containing HVSCs were created which successfully began to produce their own collagenous matrix. A soft inclusion was incorporated successfully.
2. Subject the constructs to mechanical testing and investigate their global mechanical behavior leading to rupture:  
The different straining protocol led to different compaction behavior, however, this difference in compaction behavior did not effect the global mechanical behavior of the constructs significantly when tested in the commercial clamps. The redesigned clamps displayed a consistent two bump rupture pattern correlating to rupture near the SI, as well as higher measured force at comparable stretch, not seen with the commercial clamps. Additionally, the redesigned clamps decreased the chance of rupture near the clamp edge as seen in the commercial clamps.
3. Investigate local strain patterns of the constructs undergoing mechanical testing:  
The static and IS constructs tested in the commercial clamps differed in  $\epsilon_{xx}$  patterns, as the static constructs displayed more homogeneity throughout the construct and compressive behavior at the edges, whereas the IS constructs exhibited a symmetric

“C-shaped” compressive pattern and extension at the edges, signifying a possible difference in micro-structure. The redesigned clamps created for mechanical testing demonstrated an improvement in the testing method for the TE constructs when compared to the commercial clamps by exhibiting a better load transmission from clamp to tissue, by creating more homogeneous strain distribution within the region of interest and leading to rupture more often near the SI.

4. Investigate rupture behavior of the constructs:  
DIC analysis demonstrated that high  $\epsilon_{yy}$  values occurred at the rupture location in both the redesigned and commercial clamps, possibly demonstrating a linkage between high  $\epsilon_{yy}$  extension behavior and rupture location.

## 5.2 Future recommendations

The following recommendations are based on the results of this study:

1. Use the redesigned clamps to study all constructs:  
It is recommended to perform more testing with the redesigned clamps in the future, as the sample size was low in this study. However, the redesigned clamps appeared to better transfer the load from the clamps to the tissue and successfully led to rupture near the SI more often. By imaging the region of possible micro-structural slippage in the commercial clamps near the clamp edge, we can get a better understanding of what is happening in that region and why rupture consistently occurred there.
2. Perform collagen histology to link mechanical properties to collagen structure:  
Ultimately, understanding how collagen content (i.e. amount, types) and structure (i.e. orientation) relates to the local and global mechanical properties of the constructs is the overall goal of this project in order to create an *in vitro* atherosclerotic fibrous cap model to study plaque rupture. The original plan of this study was to relate collagen histology and mechanical properties of these constructs, however, due to the pandemic, histology could no longer be performed. It would be interesting to further investigate the region of tissue near the commercial clamp edge, which was assumed to contain less structured collagen when compared to the center of the construct, as it acts a transition region into the Velcro.
3. Increase the number of samples for statistical analysis:  
The number of samples in this study were few and different variables were introduced as well to optimize mechanical testing, therefore the power of the statistical analysis performed was low. By increasing the number of samples and decreasing the number of variables, more reliable statistics can be achieved between the constructs.

4. Include different straining protocol during culture:

This study included statically cultured control constructs as well as intermittently strained constructs, which were subjected to 2 weeks of static culture and 1 week of intermittent uniaxial straining (see Appendix B). This protocol can be modified to also include continuous straining as this has demonstrated to increase collagen synthesis, remodeling, and maturation [26]. The number of weeks of culture can also be increased as this has shown to increase collagen concentration [5]. Additionally, the shape of the loading post where the fibrin-based gel was seeded in the Flexcell system can be altered to introduce a gradient-like straining during culture, which can better reflect the collagen structure and composition found in human atheroma fibrous caps. Also, by including off-centered soft inclusion constructs in future experiments, the effect of distance from the soft inclusion to the lumen edge on rupture behavior can also be investigated.

5. Add other biological factors to the model during culture:

By systematically adding other biological factors that are known to contribute to plaque rupture, such as macrophages, calcifications, etc, the model can become more realistic and complex.

# Bibliography

- [1] O. Ovchinnikova, *Immune mechanisms behind plaque vulnerability : experimental and clinical studies*. 2010.
- [2] P. Libby, J. E. Buring, L. Badimon, G. K. Hansson, J. Deanfield, M. S. Bittencourt, L. Tokgözoğlu, and E. F. Lewis, “Atherosclerosis”, *Nature Reviews Disease Primers*, vol. 5, no. 1, pp. 1–18, 2019.
- [3] G. Holzapfel, *Collagen: Structure and Mechanics, Collagen in Arterial Walls: Biomechanical Aspects*. Springer, 2008, pp. 285–324.
- [4] A. C. Akyildiz, C.-K. Chai, C. W. Oomens, A. van der Lugt, F. P. Baaijens, G. J. Strijkers, and F. J. Gijsen, “3D Fiber Orientation in Atherosclerotic Carotid Plaques”, *Journal of Structural Biology*, vol. 200, no. 1, pp. 28–35, 2017.
- [5] M. P. Rubbens, A. Mol, R. A. Boerboom, R. A. Bank, F. P. T. Baaijens, and C. V. C. Bouten, “Intermittent straining accelerates the development of tissue properties in engineered heart valve tissue”, *Tissue Engineering - Part A*, vol. 15, no. 5, pp. 999–1008, 2009.
- [6] C. Pagiatakis, R. Galaz, J.-C. Tardif, and R. Mongrain, “A comparison between the principal stress direction and collagen fiber orientation in coronary atherosclerotic plaque fibrous caps.”, *Medical & biological engineering & computing*, vol. 53, no. 6, pp. 545–555, Jun. 2015.
- [7] A. M. Schnell, S. P. Hoerstrup, G. Zund, S. Kolb, R. Sodian, J. F. Visjager, J. Grunenfelder, A. Suter, and M. Turina, “Optimal cell source for cardiovascular tissue engineering: venous vs. aortic human myofibroblasts.”, *The Thoracic and cardiovascular surgeon*, vol. 49, no. 4, pp. 221–225, 2001.
- [8] N. de Jonge, F. P. Baaijens, and C. V. Bouten, “Engineering fibrin-based tissue constructs from myofibroblasts and application of constraints and strain to induce cell and collagen reorganization.”, *Journal of visualized experiments : JoVE*, no. 80, 2013.
- [9] N. De Jonge, F. M. W. Kanters, F. P. T. Baaijens, and C. V. C. Bouten, “Strain-induced collagen organization at the micro-level in fibrin-based engineered tissue constructs”, *Annals of Biomedical Engineering*, vol. 41, no. 4, pp. 763–774, 2013.
- [10] K. Phelan and K. M. May, “Mammalian cell tissue culture techniques”, *Current Protocols in Pharmacology*, vol. 2016, pp. 12.1.1–12.1.23, 2016.

- [11] H. Duong, B. Wu, and B. Tawil, “Modulation of 3D fibrin matrix stiffness by intrinsic fibrinogen-thrombin compositions and by extrinsic cellular activity.”, *Tissue engineering. Part A*, vol. 15, no. 7, pp. 1865–1876, 2009.
- [12] E. Maher, A. Creane, S. Sultan, N. Hynes, C. Lally, and D. J. Kelly, “Tensile and compressive properties of fresh human carotid atherosclerotic plaques.”, *Journal of biomechanics*, vol. 42, no. 16, pp. 2760–2767, 2009.
- [13] M. T. Walsh, E. M. Cunnane, J. J. Mulvihill, A. C. Akyildiz, F. J. Gijssen, and G. A. Holzapfel, “Uniaxial tensile testing approaches for characterisation of atherosclerotic plaques”, *Journal of Biomechanics*, pp. 793–804, 2014.
- [14] B. Pan, “Reliability-guided digital image correlation for image deformation measurement”, *Applied Optics*, vol. 48, no. 8, pp. 1535–1542, 2009.
- [15] B. Pan, H. Xie, Z. Guo, and T. Hua, “Full-field strain measurement using a two-dimensional Savitzky-Golay digital differentiator in digital image correlation”, *Optical Engineering*, vol. 46, no. 3, p. 033601, 2007.
- [16] C. A. Schneider, W. S. Rasband, and K. W. Eliceiri, “NIH Image to ImageJ: 25 years of image analysis”, *Nature Methods*, vol. 9, no. 7, pp. 671–675, 2012.
- [17] “Hyperelastic behavior of rubberlike materials”, 2017. [Online]. Available: <https://abaqus-docs.mit.edu/2017/English/SIMACAEMATRefMap/simamat-c-hyperelastic.htm>.
- [18] J. Lee, M. Wong, Q. Smith, and A. B. Baker, “A novel system for studying mechanical strain waveform-dependent responses in vascular smooth muscle cells”, *Lab Chip*, vol. 13, no. 23, pp. 4573–4582, 2013.
- [19] G. Chagnon, J. Ohayon, J.-l. Martiel, D. Favier, G. Chagnon, J. Ohayon, J.-l. Martiel, D. Favier, and H. Modeling, “Hyperelasticity Modeling for Incompressible Passive Biological Tissues To cite this version : HAL Id : hal-01974109”, 2019.
- [20] “Fitting of rubber test data”, 2017. [Online]. Available: <https://abaqus-docs.mit.edu/2017/English/SIMACAEBMKRefMap/simabmk-c-rubberfit.htm>.
- [21] M. Latorre and F. J. Montáns, “On the interpretation of the logarithmic strain tensor in an arbitrary system of representation”, *International Journal of Solids and Structures*, vol. 51, no. 7-8, pp. 1507–1515, 2014.
- [22] A. BenSaïda, “Shapiro-Wilk and Shapiro-Francia normality tests”, 2020. [Online]. Available: <https://www.mathworks.com/matlabcentral/fileexchange/13964-shapiro-wilk-and-shapiro-francia-normality-tests>.
- [23] A. Trujillo-Ortiz, “Levenetest”, 2020. [Online]. Available: <https://www.mathworks.com/matlabcentral/fileexchange/3375-levenetest>.
- [24] A. C. Akyildiz, L. Speelman, and F. J. Gijssen, “Mechanical properties of human atherosclerotic intima tissue”, *Journal of Biomechanics*, vol. 47, no. 4, pp. 773–783, 2014.

- 
- [25] D. Seliktar, R. M. Nerem, and Z. S. Galis, “Mechanical strain-stimulated remodeling of tissue-engineered blood vessel constructs”, *Tissue Engineering*, vol. 9, no. 4, pp. 657–666, 2003.
- [26] D. van Geemen, A. Driessen-Mol, F. P. T. Baaijens, and C. V. C. Bouten, “Understanding strain-induced collagen matrix development in engineered cardiovascular tissues from gene expression profiles”, *Cell and Tissue Research*, vol. 352, no. 3, pp. 727–737, 2013.
- [27] J. Blaber, B. Adair, and A. Antoniou, “Ncorr: Open-Source 2D Digital Image Correlation Matlab Software”, *Experimental Mechanics*, vol. 55, no. 6, pp. 1105–1122, 2015.
- [28] H. Akoglu, “User’s guide to correlation coefficients.”, *Turkish journal of emergency medicine*, vol. 18, no. 3, pp. 91–93, 2018.
- [29] P. Ferraiuoli, B. Kappler, S. van Tuijl, M. Stijnen, B. A. J. M. de Mol, J. W. Fenner, and A. J. Narracott, “Full-field analysis of epicardial strain in an in vitro porcine heart platform”, *Journal of the Mechanical Behavior of Biomedical Materials*, vol. 91, pp. 294–300, 2019.
- [30] G. Cahn, A. Barrios, S. Graham, J. Meth, A. Antoniou, and O. Pierron, “The role of strain localization on the electrical behavior of flexible and stretchable screen printed silver inks on polymer substrates”, *Materialia*, vol. 10, p. 100642, 2020.
- [31] C. Lane, R. L. Burguete, and A. Shterenlikht, “An objective criterion for the selection of an optimum DIC pattern and subset size”, *Society for Experimental Mechanics - 11th International Congress and Exhibition on Experimental and Applied Mechanics 2008*, vol. 2, pp. 900–908, 2008.



# Protocols

Appendix A.1 includes the protocol used to create the fibrin-based TE constructs and Appendix A.2 includes the mechanical testing protocol used.

## A.1 Creating Fibrin-based TE Constructs

TU Eindhoven (Gemini-Zuid 4.105), 06.03.2020, Sheila & Tamar

### Materials

- Fibrinogen
- 0.05% TRYPSIN/EDTA
- Medium (previously made)
- PBS (sterile)
- 2x tweezer (sterile)
- Big petri dishes (sterile)
- Big beaker glass
- Culture plates (sterile)
- Eppendorf tubes and holder (sterile)
- 200  $\mu$ l / 1000  $\mu$ l pipets and tips
- 50 ml tubes
- T75 flasks
- Thrombin (100 u/ml)

- Ice
- 3x syringe
- 3x needle
- 3x 0.2  $\mu\text{m}$  filter
- Pipet boy
- Eppendorf holder
- Extra needles
- $\epsilon$ -amino caproic acid (10 mg/ml)
- Vitamin C (0.25 mg/ml)
- Nucleometer
- Solution A and B (near nucleometer)

## Methods

### Step 1. Preparations

1. Obtain the culture plates with the pasted Velcros
2. Obtain the sterilized PDMS bars created
3. Obtain the fibrinogen, 0.05% TRYPSIN/EDTA, and medium and allow them to adapt to room temperature

### Step 2. Cell Counting

1. Wash each of the four T150 flasks with 10 ml PBS (2x) to remove the proteins that inactivate the TRIS/EDTA using a vacuum pipette
2. Add 7 ml TRYPSIN-EDTA per flask in a vertical position
3. Incubate flasks in horizontal position at 37 degrees in the incubator for 7 minutes (make sure cell side is covered properly with the TRYPSIN-EDTA solution)
4. Remove the flasks and hit them from the sides to loosen all cells
5. Check under the microscope to verify that the cells appear rounded (loosened)
6. Add 14 ml of medium per flask, mix well by pipetting up and down, and transfer to a sterile T75 flask
7. Divide the contents in the T75 over 50 ml tubes
8. Take about 200  $\mu$ l for cell counting using the nucleometer (follow the protocol of the nucleometer):
  - (a) Transfer 50  $\mu$ l of the cell suspension to a new Eppendorf tube to count the cells
  - (b) Add 50  $\mu$ l of solution A and vortex for 2 seconds (permeabilizing the cell membrane)
  - (c) Add 50  $\mu$ l of solution B and vortex for 2 seconds (stabilizing the permeabilized cells)
  - (d) Take a cassette, suck the solution up, and place the cassette into the nucleometer. This will count both dead and alive cells by binding propodium iodide to the cell's DNA. To make sure the number of dead cells are less than  $5 \times 10^3$ , repeat without adding solutions A and B. If this holds true, proceed with the next step.
  - (e) Record the total number of cells counted with the first measurement (cells/ml), factoring in the diluted solution (ml)
  - (f) Calculate how many constructs can be created with the amount of cells counted ( $N = \text{cells}/675,000$ ), where 675,000 cells/construct
9. Centrifuge the 50 ml tubes at 1200 rpm for 5 minutes (acceleration and braking speed 4)

10. Remove the medium with a vacuum pipette
11. Add 1-3 ml of medium and loosen the cell pallet with a 1 ml pipette
12. Transfer all cell suspensions to one tube and wash the remaining tubes with 5ml medium per tube to collect all cells that are left
13. Centrifuge the tube at 1200 rpm for 5 minutes (acceleration and braking speed 4) and place it on ice

### Step 3. Prepare Thrombin and Fibrinogen Solution

1. Obtain the thrombin solution (100 u/ml) and dilute to 10 u/ml
2. Calculate how much thrombin (10 u/ml) solution is necessary ( $N * 225 \mu\text{l} = \text{ml thrombin}$ ), make slightly more always
3. Put the thrombin solution on ice
4. Remove the supernatant of the cells after centrifuging (previous step 13)
5. Add 1 ml of thrombin solution, tilt the 50 ml tube, and carefully loosen the cell pallet with a 1 ml pipette
6. Calculate the cell pallet volume, make sure you add the correct amount of thrombin
  - (a) Transfer with the 1 ml pipette, the cell suspension into a clean 50 l tube
  - (b) Measure how much volume you have more (cell pallet volume)
7. Add the rest of the necessary thrombin solution (minus the 1 ml), mix the cell suspension properly, and place it on ice
8. Calculate the volume of thrombin ( $\mu\text{l}$ ) per construct ( $225 \mu\text{l} * N + \text{cell pallet volume} = \text{total volume } (\mu\text{l})$ ), divide this total volume by N)
9. Calculate the total volume for each construct (thrombin volume +  $225 \mu\text{l} = \text{total volume per construct}$ )
10. Obtain the room temperature fibrinogen (12.65 mg/ml)
11. Measure the amount of fibrinogen (mg) needed by taking the same amount of fibrinogen as the thrombin (ml), but adding at least 1 ml extra ( $\text{ml} * 12.65 \text{ mg/ml} = \text{mg fibrinogen}$ ). Dissolve the fibrinogen (mg) into the appropriate volume of medium, calculated above, under warm water
12. Immediately filter the solution through a  $0.2 \mu\text{m}$  filter with a syringe (renew filter after 1.5 ml) and place it on ice

### Step 4. Make the Fibrin-based Gels and Seeding

1. Add the PDMS pieces to a clean large Petri dish and use a sterile tweezer to place two on both sides of the Velcro's (make sure they are stuck so that no fibrin will go underneath it)
2. Pipette out remaining water (PBS) to make the PDMS bars stick better

3. Take a clean Eppendorf tube per construct. Add the correct amount of the thrombin-cell solution (previous step 8- volume of thrombin per construct) and place it in the Eppendorf tube
4. Get a 100-1000  $\mu\text{l}$  pipette and pipette 225  $\mu\text{l}$  of fibrinogen in the pipette tip. Switch the volume to 492.9  $\mu\text{l}$  (previous step 8- total volume per construct) and press out the air before mixing it into the thrombin-cell suspension to prevent air-bubble formation
5. Pipette 2x up and down without introducing bubbles and divide the solution over the half of the Velcro, the middle compartment, and the other half of the Velcro (make sure everything is well divided and there are no bubbles. Do this fast as everything clots really easily. Use a sterile needle to remove bubbles)
6. Repeat this for the other constructs and place them in the incubator for at least 30 minutes
7. Make medium with fresh Vit C and  $\epsilon$ -ACA ( $N * 5 \text{ ml} = \text{total volume of medium (ml)}$ , always make a little extra)
8. Weigh the appropriate amount of Vit C ( $0.25 \text{ mg/ml Vit C} * \text{total volume of medium (ml)} = \text{mg Vit C}$ )
9. Dilute Vit C to 25 mg/ml ( $\text{mg Vit C} / 25 \text{ mg/ml} = \text{ml medium}$ )
10. Filter the diluted Vit C using a 0.2  $\mu\text{m}$  filter
11. Calculate the amount of  $\epsilon$ -ACA needed ( $1 \text{ mg/ml} * \text{total volume of medium (ml)} = \text{mg of } \epsilon\text{-ACA}$ )
12. Weigh some amount of  $\epsilon$ -ACA and record the value
13. Dilute the  $\epsilon$ -ACA in 3 ml (record mg/ml of  $\epsilon$ -ACA)
14. Calculate the ml of  $\epsilon$ -ACA needed for the mg calculated above
15. Combine the calculated amounts of Vit C,  $\epsilon$ -ACA, and normal medium (total volume of medium - Vit C -  $\epsilon$ -ACA)
16. Make a photo of your constructs and add the medium to the wells and refresh medium every 2-3 days (remove the PDMS pieces with the second medium change)

## A.2 Mechanical Testing

TU Eindhoven (Gemini-Zuid 4.105), 27.03.2020, Sheila & Tamar

### Materials

- BioTester, Biaxial test system from CellScale
- Calibration spring (5 N)
- Two 5 N load cells
- Tweezers
- Well plate filled with PBS
- Large beaker filled with PBS
- Ice
- Coarse graphite sandpaper
- Cotton swabs
- Two clamps (redesigned)
- 1mm thick double sided foam tape
- Double sided tape
- Screwdriver for M2.5 screws
- Fine sandpaper (P400)
- Cutting plate
- Microtome blades
- Scissors
- Microscope (Keyence)
- Hard drive to collect data

## Methods

### Step 1. Preparations

1. Pour PBS into the black fluid chamber to fill it up
2. Turn on the tensile tester machine and the temperature with the two black switches on the machine
3. Turn on the PC and start the LabJoy program
4. Reset the actuators
5. Create a new protocol for testing by selecting “Collect New” under “File”
6. Set parameters to the following:

#### **For pre-conditioning at 10% stretch:**

- (a) Set “Control Mode” to “Displacement” for both X and Y Axis
- (b) Set “Control Function” to “Ramp” for both X and Y Axis
- (c) Set “Stretch Magnitude” to “0%” for X Axis and “10%” for Y Axis
- (d) Set “Preload” to “Not Applied” for both X and Y Axis
- (e) Set “Stretch Duration” to “3 S” and “Recovery Duration” to “3 S”
- (f) Set “Repetitions” to “10”, “Data Output Frequency” to “15 Hz”, and “Image Output Frequency” to “15 Hz”

#### **For stretch until failure at 100%/min:**

- (a) Set “Control Mode” to “Displacement” for both X and Y Axis
  - (b) Set “Control Function” to “Ramp” for both X and Y Axis
  - (c) Set “Stretch Magnitude” to “0%” for X Axis and “300%” for Y Axis
  - (d) Set “Preload” to “Not Applied” for both X and Y Axis
  - (e) Set “Stretch Duration” to “180 S” and “Recovery Duration” to “10 S”
  - (f) Set “Repetitions” to “1”, “Data Output Frequency” to “15 Hz”, and “Image Output Frequency” to “15 Hz”
7. Zero the load cells
  8. Calibrate the load cells:
    - (a) Click on *Tools>Advanced>Load cell calibration*
    - (b) Enter the correct spring K value under the “Spring K” field (found on selected spring package)
    - (c) Lower the PBS chamber and put the calibration springs into place
    - (d) Zero the load cell

- (e) Move the actuators (with the jog buttons) until they are spaced so that the calibration spring can be set onto the posts without applying any significant load (approx 25000  $\mu\text{m}$  x 25000  $\mu\text{m}$ )
  - (f) Set the calibration spring on the posts so that they are in a stable, horizontal position
  - (g) Click on *Tools>Advanced>Load cell calibration* and preload the spring with the preload specified on the box (by moving actuators)
  - (h) Click on “Run” and wait for calibration to complete
  - (i) The number “A” which shows in the main dialogue box after calibration is finished is the ratio of the current calibration value to the previous one. “A” should be between 0.99 and 1.01, if not, restart the system and calibrate again
9. Define new zero point of the actuators (for redesigned clamps):
- (a) Click on *Tools>Advanced>Centre Position Calibration*
  - (b) A dialogue box will show that states “The Operation will Define The Current Position as the Center for the X and Y axes. Do you want to Continue?” Select “Yes”
  - (c) Reset the actuators
  - (d) Select “Advanced then move to Centre” from the tools menu. The dialogue box will say “This Operation Requires The BioRakes to be removed. Do you want to Continue?” Select “Yes”
  - (e) When the actuators stopped, place 2 clamps on the Y-axis
  - (f) Move the actuators (using the jog buttons) until the clamps almost touch each other (with the “mirror matching” button selected, not the “independent” button)
  - (g) Select *Tools>Advanced>Centre Position Calibration*. This is the last “Centre Position Calibration”. The dialogue box will state “The Operation will Define The Current Position as the Center for the X and Y axes. Do you want to Continue?” Press “Yes”
  - (h) Reset the actuators
10. Clamp preparations:
- (a) Use the microtome blade to cut the double sided foam tape, double sided tape, and sandpaper (P400) with the following dimensions per construct: 4x (15 mm x 1.5 mm) sandpaper and double sided tape, 4x (15 mm x 5 mm) sandpaper and double sided foam tape
  - (b) Refer to Figure A.1 to properly prepare the clamps. Stick the foam tape pieces on the center edges of the bottom and top clamps. Stick the smaller pieces of sandpaper directly on top of the foam tape. Stick the larger double sided tape next to the foam tape on the clamps. Stick the larger sandpaper pieces directly on top of the tape.

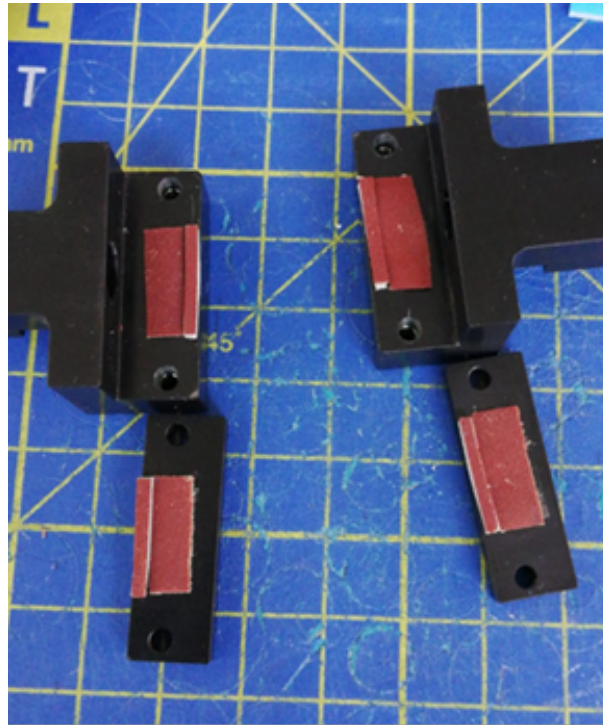


**Figure A.1:** How to properly paste the sandpaper onto the clamps for gripping the constructs during tensile testing \*Image courtesy of Tamar Wissing

11. Placing the constructs into the clamps:

- (a) Use a tweezer with a pointy tip to carefully loosen the Velcro from the bottom of the well plate. Make sure that you do not damage your sample (only touch the Velcro) and place it in a well plate with PBS on ice (keep the samples as much as possible on ice before the test to prevent that they deteriorate)
- (b) Place the construct on the sterilized blue cutting plate and make an image above to measure the starting size in an unconstrained configuration (make sure you record which construct each image corresponds to)
- (c) Place the sample on a clean tissue to dry it a bit and apply graphite particles using the coarse sandpaper and cotton swabs
- (d) Place the sample on the clamp and place the other part of the clamp on top (the Velcro should be positioned after the foam tape so that only the tissue comes into contact with the thicker part of the sand paper, as seen in Figure A.2)

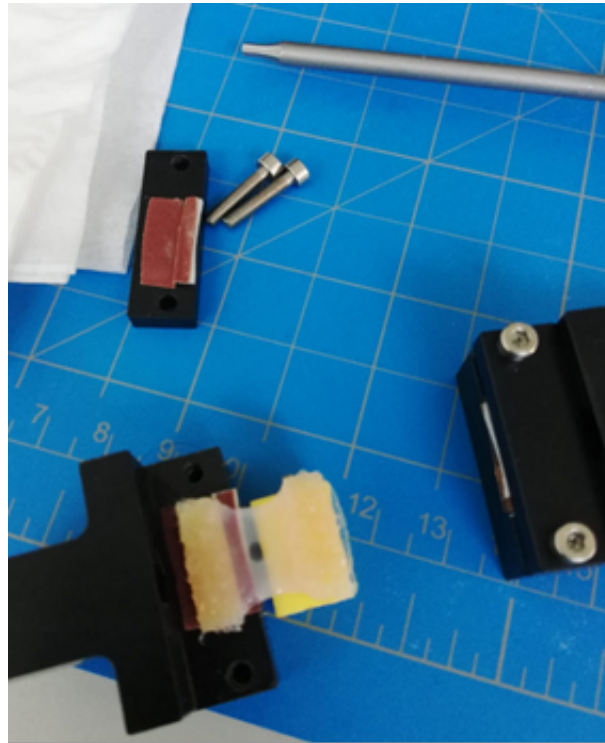


**Figure A.2:** Proper positioning of the construct in the redesigned clamps. The soft inclusion should still be visible. The Velcro should fit snugly into the groove. \*Image courtesy of Tamar Wissing

- (e) When the constructs are placed properly (the soft inclusion is visible), screw the clamps with a torque screwdriver set to 10cNm until it clicks

12. Measure and record the construct thickness:

- (a) Shift the microscope to a horizontal position by removing the pin in the back of the microscope and carefully lowering it to the side. Pull on the handle on the back to be able to move the microscope the last couple of degrees to a 90 degrees angle.
- (b) Change the magnification of the microscope to 20 or 30x.
- (c) Place the loaded clamps in front of the camera and focus on the construct side.
- (d) Measure the thickness (go to measure in the menu and draw measurement lines, approximately 10 over the full length of the construct, as seen in Figure A.3)

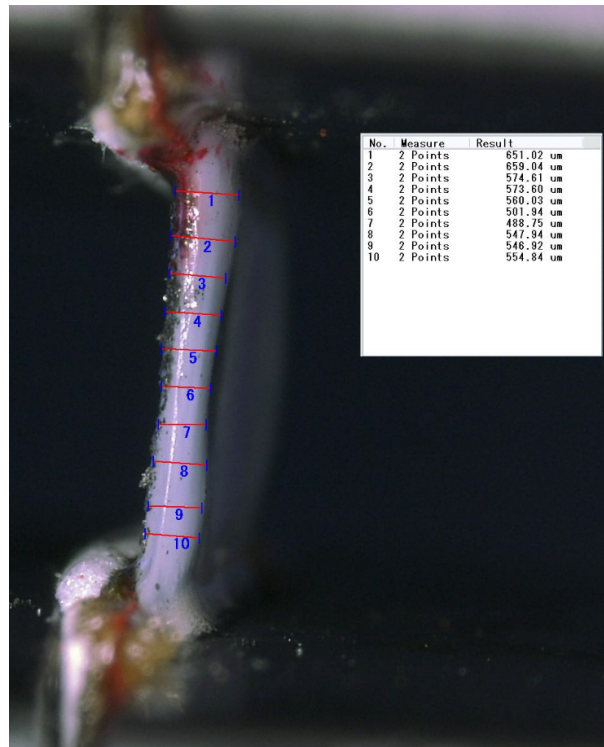


**Figure A.3:** Measure and save 10 thickness values across the construct on both sides \*Image courtesy of Tamar Wissing

- (e) Save the images with the measurements (.jpg) and the CSV file
- (f) Remove the images from the computer with an USB stick
- (g) Turn the sample with the clamps 180 to measure the other side (side 2) in the same way

## Step 2. Execute the Uniaxial Tensile Testing

1. Mount the construct into the tensile tester:
  - (a) Restart the program and click on *File>Collect new*
  - (b) Select the “Starting Point” template if done previously
  - (c) Move actuators to specified size
  - (d) Carefully place on each Y axis actuator, one clamp with the construct in the middle
  - (e) Zero load the cells
  - (f) Use the jog buttons to unfold the sample without stretching it. If the Y force is going up to 5 mN or above you should stop as you start stretching the sample. Go back to 0 mN force.
  - (g) Fully raise the chamber to submerge the sample in the warm PBS

- (h) Unfold the sample once more with the jog buttons until the Y-force goes up. Go back to 0 (Make sure that you focus on the construct. The graphite particles should be clear and the lighting should be good. You want to prevent bright spots of the lighting in the picture)
- (i) Zero load the cells

2. Perform the uniaxial tensile testing:

- (a) When both  $F_x$  and  $F_y$  are approx 0, execute the test by pressing the “Play” button
- (b) Stop when the Y-force exceeds 100 mN
- (c) Go to the data excel sheet of the starting point regimen just run and select one column of the data sheet. Go to *data, text to columns, delimited, comma, next, finish* to get all data in separate columns.
- (d) Note the Y-distance where the specimen exceeded the 40 mN and start a new regimen via *File-Collect new*
- (e) This time you need to run a different template: real measurement (if previously created)
- (f) Specify the Y-distance where 40 mN was reached
- (g) Write down what Y-force you are still measuring (should be approx 12 mN)
- (h) Start the regimen
- (i) Begin with the preconditioning, and proceed to stretch until failure
- (j) The test results can be reviewed and displayed by selecting *Analyse and Review Images* from the file menu and the test file (.tst)

# B

## Clamp Redesign Specifications

Appendix B includes the dimensions (mm) of the redesigned clamp at different view angles. A redesign was necessary due the inadequate clamping technique of the commercial clamps. Michiel Manten, from the Instrumentation department at Erasmus MC, created the SolidWorks model shown below and manufactured the clamps based on the sketch design I provided him.

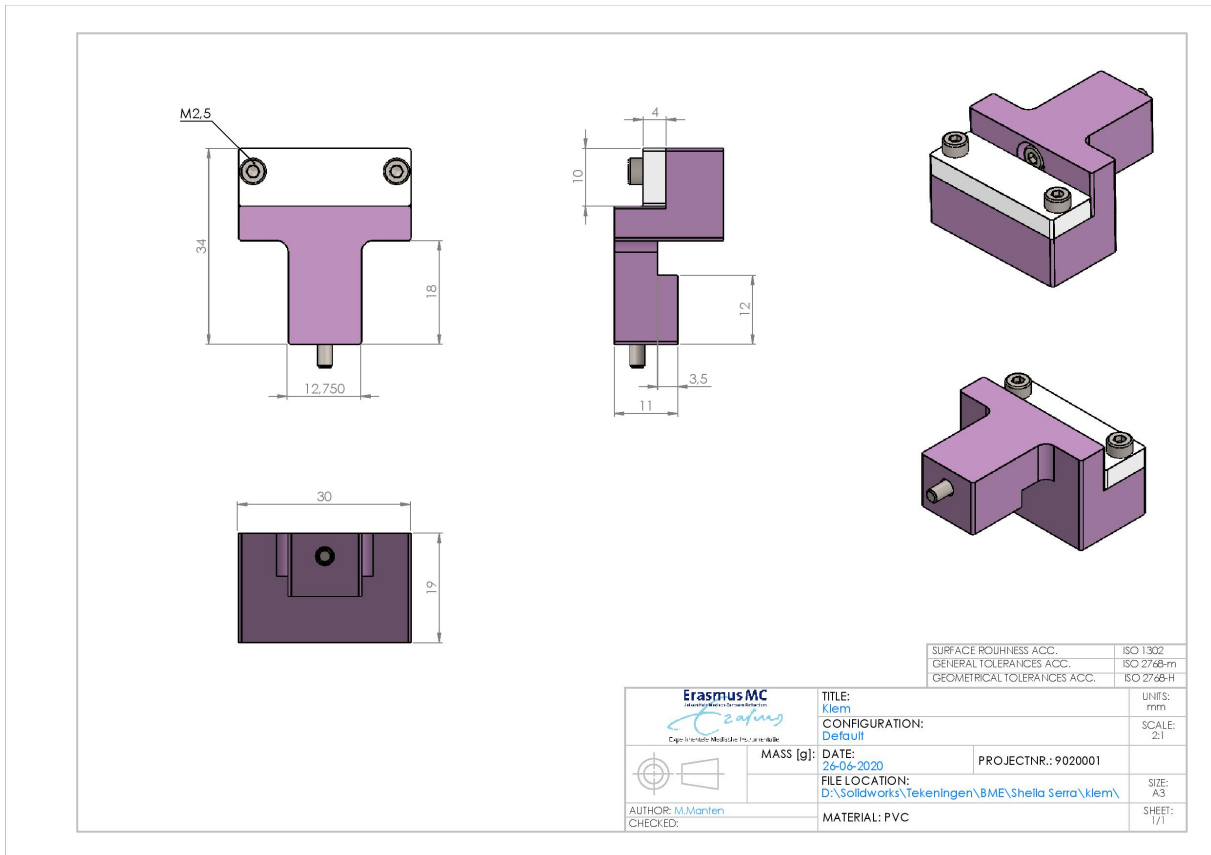


**Figure B.1:** Schematic drawing of clamp redesign with dimensions (mm). Top, side, back, and orthogonal views. Material used: PVC plastic



# Ncorr Software

Ncorr was the DIC software used in this study. Appendix C provides a tutorial of how to use Ncorr using a construct mounted in the redesigned clamps as an example. Furthermore, this appendix explains more about the mathematical algorithms used behind the software.

## C.1 Introduction

Ncorr is an open source 2D digital image correlation software, developed in the MATLAB environment using C++/MEX by a Master's student at the Georgia Institute of Technology. This software allows the user to interact through the graphical user interface (GUI) or through the MATLAB terminal. The Ncorr software and manual can be downloaded at [www.ncorr.com](http://www.ncorr.com). The mathematical algorithms used in Ncorr and the program's work flow are described below.

## C.2 Mathematical Algorithm

Ncorr uses a novel DIC algorithm technique developed by Pan known as reliability-guided DIC (RG-DIC) [14]. This technique uses the Inverse Compositional Gauss-Newton (ICGN) method as the iterative solver, described later. RG-DIC begins with selecting a seed point which determines the middle of the reference (undeformed) subset. The reference subset consists of grayscale values per pixel with the corresponding coordinates. These reference subset coordinates are transformed so that the grayscale values of the reference and deformed subsets match (Figure C.1). Equations C.1-C.3 demonstrate this subset transformation, where  $x_{cur}$  and  $y_{cur}$ , and  $x_{ref}$  and  $y_{ref}$  are the  $x$  and  $y$  coordinates for the

current and reference image;  $i$  and  $j$  represent the position of a point  $(x, y)$  with respect to the subset center  $(c)$  where  $S$  is a set that contains all subset points;  $p$  denotes the components of the vector for the transform (linear, first order at low strain) [27].

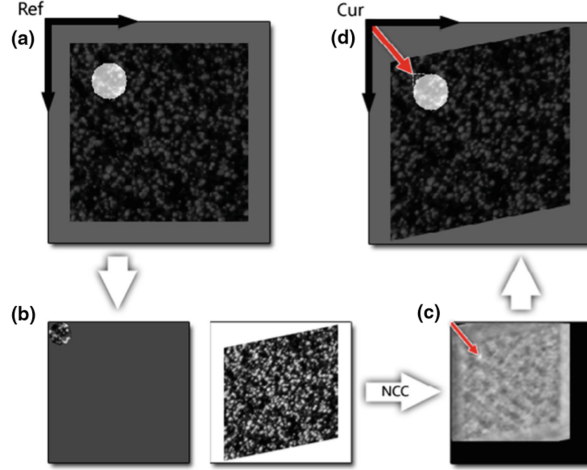


**Figure C.1:** Finding initial guess process: a) reference subset selected b) convolution with the current image to find the normalized cross correlation c) array of correlation coefficient values are output, maximum value is located d) subset location is recovered with respect to the first image [27]

$$\tilde{x}_{cur_i} = x_{ref_i} + u_{rc} + \frac{\partial u}{\partial x_{rc}}(x_{ref_i} - x_{ref_c}) + \frac{\partial u}{\partial y_{rc}}(y_{ref_j} - y_{ref_c}) \quad (i, j) \in S \quad (C.1)$$

$$\tilde{y}_{cur_j} = y_{ref_j} + v_{rc} + \frac{\partial v}{\partial x_{rc}}(x_{ref_i} - x_{ref_c}) + \frac{\partial v}{\partial y_{rc}}(y_{ref_j} - y_{ref_c}) \quad (i, j) \in S \quad (C.2)$$

$$p = \left\{ u \quad v \quad \frac{\partial u}{\partial x} \quad \frac{\partial u}{\partial y} \quad \frac{\partial v}{\partial x} \quad \frac{\partial v}{\partial y} \right\}^T \quad (C.3)$$

To quantitatively determine the quality of the match between the reference and deformed image, the correlation criterion is used. The initial guess for the displacement is found by computing the highest zero mean normalized cross correlation coefficient ( $C_{CC}$ ) around the center point of the seeded subset. Normalizing and including the zero mean allows the results to be invariant to affine shifts in grayscale values (by subtracting the average grayscale values). The  $C_{CC}$  method for initial guess determines the translation values of the reference subset to the deformed image, but an iterative optimization method is necessary to determine the rotations and strains. Using the IG-GN nonlinear optimizer, the search path follows the minimum least squares criteria ( $C_{LS}$ ) in the surrounding subsets and then converts the  $C_{LS}$  to output  $C_{CC}$  values due to its more intuitive range of  $[-1 \ 1]$  for the user. Equations C.4-C.6 represent the correlation criterion used in the

RG-DIC method, where  $f$  and  $g$  are the grayscale values at a subset point in the reference and deformed images;  $f_m$  and  $g_m$  denotes the average grayscale values for the reference and deformed subsets;  $S$  is the set with all of the subset points; and  $n(S)$  represents the amount of subset points in  $S$ . The  $C_{LS}$  criteria is related to the  $C_{CC}$  criteria according to equation C.5, where the normal degree of correlation would be flipped in this case due to subtracting  $C_{LS}$  by 1 to obtain  $C_{CC}$ . For example, 0-0.5 ordinarily signifies a weak correlation, but in this case these values would signify a strong correlation, where 0 represents a perfect match (commonly represented by 1) [28]. The displacement data from the previous point is used as the initial guess for successive surrounding points, as this prevents the use of bad data points (with high  $C_{LS}$ ) [14]. The RG-DIC approach can be seen in Figure C.2.

$$C_{LS} = \sum_{(i,j) \in S} \left[ \frac{f(\tilde{x}_{ref_i}, \tilde{y}_{ref_j}) - f_m}{\sqrt{\sum_{(i,j) \in S} [f(\tilde{x}_{ref_i}, \tilde{y}_{ref_j}) - f_m]^2}} - \frac{g(\tilde{x}_{cur_i}, \tilde{y}_{cur_j}) - g_m}{\sqrt{\sum_{(i,j) \in S} [g(\tilde{x}_{cur_i}, \tilde{y}_{cur_j}) - g_m]^2}} \right]^2 \quad (C.4)$$

$$C_{CC} = \frac{\sum_{(i,j) \in S} (f(\tilde{x}_{ref_i}, \tilde{y}_{ref_j}) - f_m)(g(\tilde{x}_{cur_i}, \tilde{y}_{cur_j}) - g_m)}{\sqrt{\sum_{(i,j) \in S} [f(\tilde{x}_{ref_i}, \tilde{y}_{ref_j}) - f_m]^2 \sum_{(i,j) \in S} [g(\tilde{x}_{cur_i}, \tilde{y}_{cur_j}) - g_m]^2}} = 1 - 0.5 \times C_{LS} \quad (C.5)$$

$$f_m = \frac{\sum_{(i,j) \in S} f(\tilde{x}_{ref_i}, \tilde{y}_{ref_j})}{n(S)} \quad g_m = \frac{\sum_{(i,j) \in S} g(\tilde{x}_{cur_i}, \tilde{y}_{cur_j})}{n(S)} \quad (C.6)$$

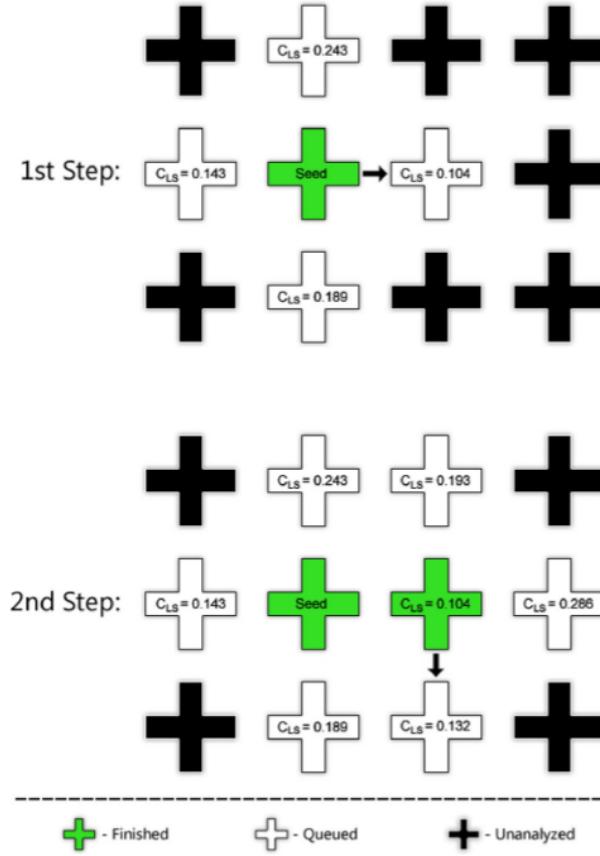


**Figure C.2:** Approach used by the RG-DIC algorithm in Ncorr. The path flows from the seeding point in the direction of the lowest  $C_{LS}$  for each step. [27]

To compute the Lagrangian strains, the four plane displacement gradients seen in C.7-C.9 were obtained by using a least squares plane fit on a subset of displacement data [27]. This was applied to the entire displacement field to obtain the strain field.

$$\epsilon_{xx} = \frac{1}{2} \left( 2 \frac{\partial u}{\partial x} + \left( \frac{\partial u}{\partial x} \right)^2 + \left( \frac{\partial v}{\partial x} \right)^2 \right) \quad (\text{C.7})$$

$$\epsilon_{yy} = \frac{1}{2} \left( 2 \frac{\partial v}{\partial y} + \left( \frac{\partial u}{\partial y} \right)^2 + \left( \frac{\partial v}{\partial y} \right)^2 \right) \quad (\text{C.8})$$

$$\epsilon_{xy} = \frac{1}{2} \left( \frac{\partial u}{\partial y} + \frac{\partial v}{\partial x} + \frac{\partial u \partial u}{\partial x \partial y} + \frac{\partial v \partial v}{\partial x \partial y} \right) \quad (\text{C.9})$$

## C.3 Program Work Flow

The work flow of Ncorr is described in the steps below and further discussed in the subsequent sections:

1. *Starting Ncorr and Using Multithreading*
2. *Set Reference Image*
3. *Set Current Image(s)*
4. *Set Region of Interest*
5. *Set DIC Parameters*
6. *RG-DIC Analysis*
7. *Format Displacements*
8. *Calculate Strains*

### C.3.1 Starting Ncorr and using multithreading

Open the directory of Ncorr in MATLAB, and type “handles\_ncorr = ncorr” into the command window. To use parallel processing, make sure a compiler is installed in MATLAB. Check the “OpenMP Multithreading” box and input the number of cores on the system being used (check this using task manager). Figure C.3 displays the start GUI that should appear if the files were compiled correctly.

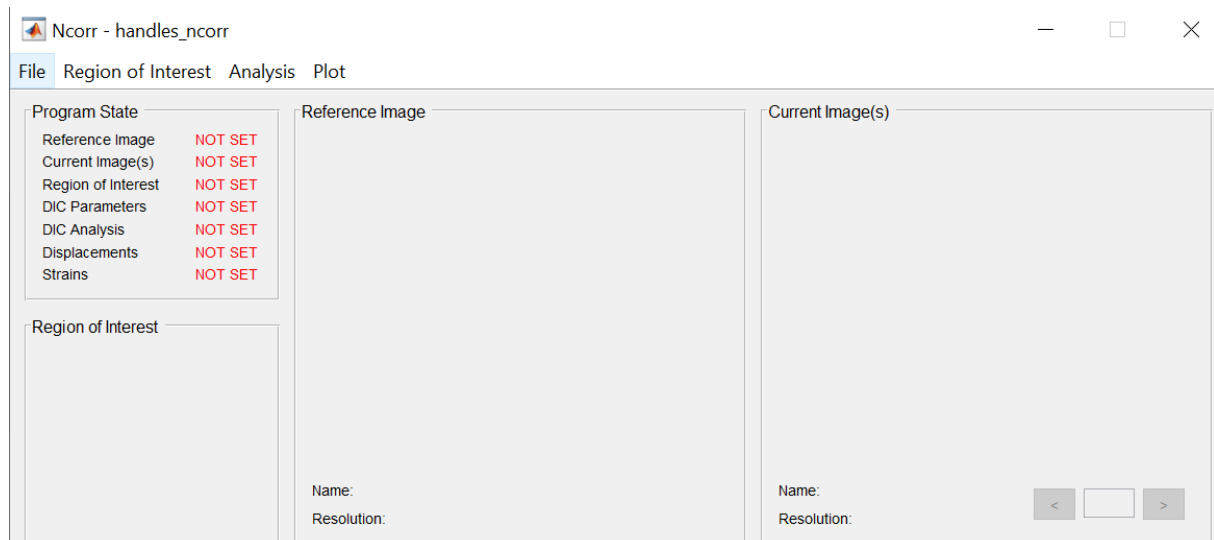


**Figure C.3:** Main start window of the Ncorr GUI

### C.3.2 Setting the reference and current image(s)

The first step is to load the reference image (undeformed), by selecting *File>Load Reference Image*. Next, load the current image(s) in which deformation will be calculated by selecting *File>Load Current Image(s)*. If loading multiple images, the images must follow the format below:

name\_#.ext

This program allows the image extensions including .jpg, .tif, .png, or .bmp. There is an option to choose either to load and store all of the images in the workplace (*Load All*) or to pull each image individually from its stored location (*Load Lazy*). The “*Load Lazy*” option was used in this project and is advised to use when many images will be loaded to save memory. The reference image and current images will display in the window, as seen in Figure C.4 and the “Program State” will display “SET” for these completed steps.

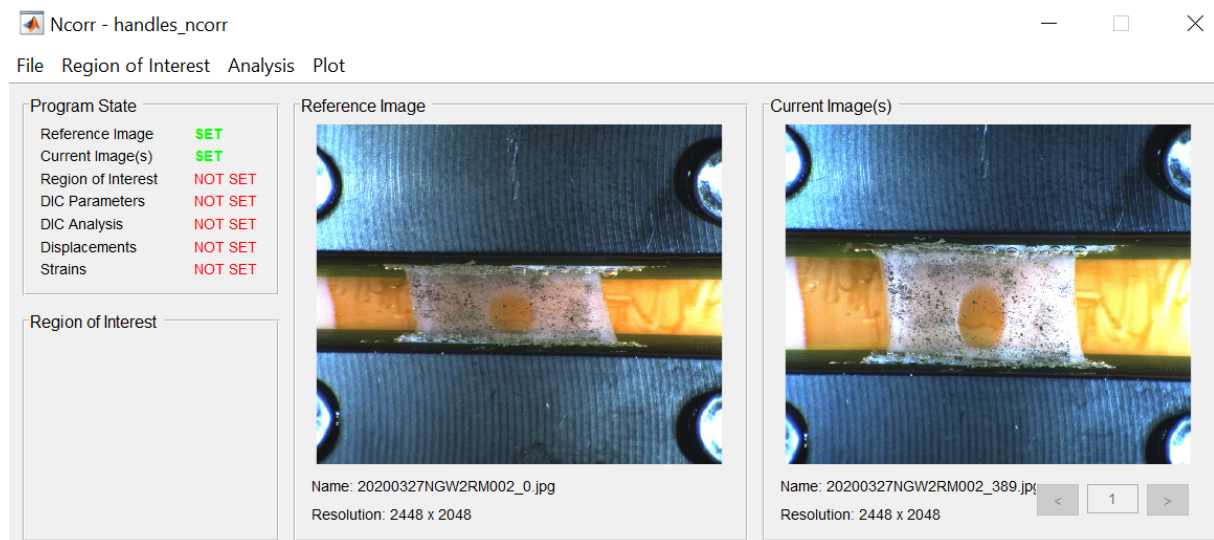


**Figure C.4:** Reference and current images are set as seen under Program State

### C.3.3 Setting the region of interest

The region of interest (ROI) can be loaded from a file, the user can draw it using the provided features in the program, or thresholding can be used with high contrast images. To load a pre-made ROI mask, the image must be the same size as the reference image. The ROI must be colored white, whereas everything else in the image must be colored black (Figure C.5). A simple image editor will be able to create this mask by loading the reference image and drawing on it. Photopea online image editor was used for this study. Drawing the ROI can be done by using the various shapes provided (rectangle, ellipse, and freeform) which can be added or subtracted. The thresholding option can be used as well, but may provide an inaccurate ROI selection with low contrasted images.

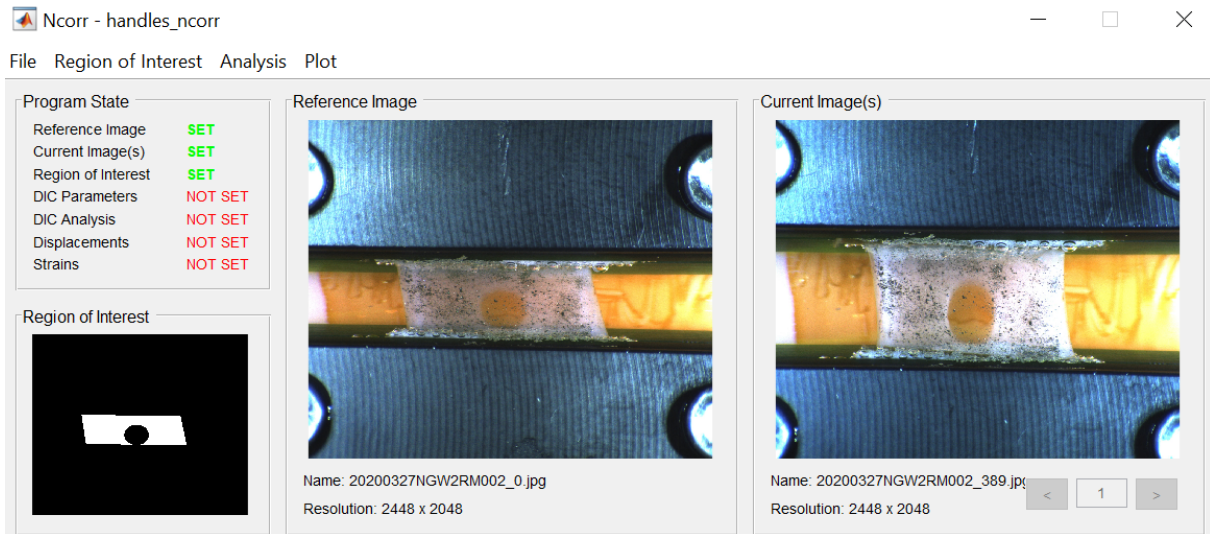


**Figure C.5:** Uploaded .jpg file of ROI is set as seen under Program State

### C.3.4 Selecting parameters and performing RG-DIC analysis

In order to perform the DIC analysis, the parameters must be set first by selecting *Analysis>Set DIC Parameters*. The user can select the subset radius and subset spacing and the preview will display on the right hand side of the window (Figure C.6). The appropriate subset size is dependent on the image and speckle pattern quality. Too large of a subset size can oversmooth the data, whereas too small of a subset size can introduce noise. The subset spacing defines the number of points used in a subset and is linked to the resolution of the image, where a smaller value will have higher resolution and a larger value will have lower resolution. The key is to find the optimal balance for each of these parameters based on the images.

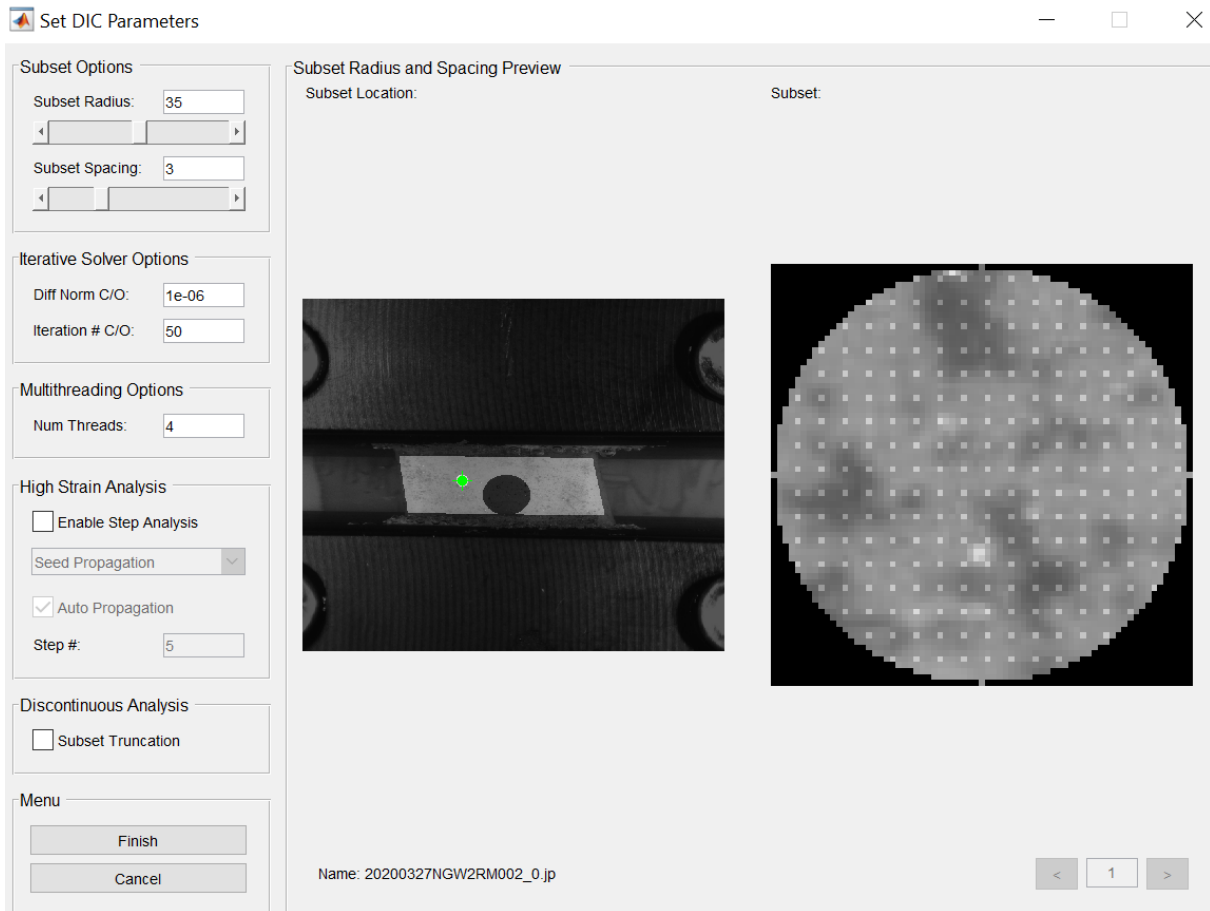


**Figure C.6:** Selecting the subset size and subset spacing in the RG-DIC Parameters window

The default options for the iterative solver were used in this analysis as it is recommended to not adjust. In order to speed up the computational processing time, 4 cores were used in the “Multithreading” option to run analysis on each construct in parallel. Due to the low strain experienced in the constructs before rupture and the continuity of the samples, the “High Strain Analysis” and “Discontinuous Analysis” options were not used.

When the DIC parameters have been set, select *Analysis>Perform DIC Analysis* and the “Select Region” window will appear. Select the ROI and then select “Set Seeds”. The number of seeds you must place on the ROI will match the number of cores you selected to use. Seed placement provides initial guesses for the RG-DIC analysis and partitions the ROI so that each region can be processed in parallel. When using multiple seeds, make sure they are placed so that the regions are somewhat symmetric (Figure C.7). It is also important to choose a seed point region that contains continuous displacement for all images. After seeding has been processed, a window will appear of the seed subset to verify the correct seeding placement has been performed and remains unique enough through all of the images and that the images appropriately match the reference image (Figure C.8). If the “Correlation Coefficient” and “# of Gauss Newton Iterations” are

too high or reach the cutoff value specified, another seeding location should be chosen. The seed can also travel outside of the seeding location in certain images (especially with the highest deformations), therefore it is important to check this before running analysis.



**Figure C.7:** The selected seeding points, which equal to number of cores selected under RG-DIC Parameters (4). It is important that the seeds are placed so that the regions are subdivided somewhat symmetrically as seen in this figure

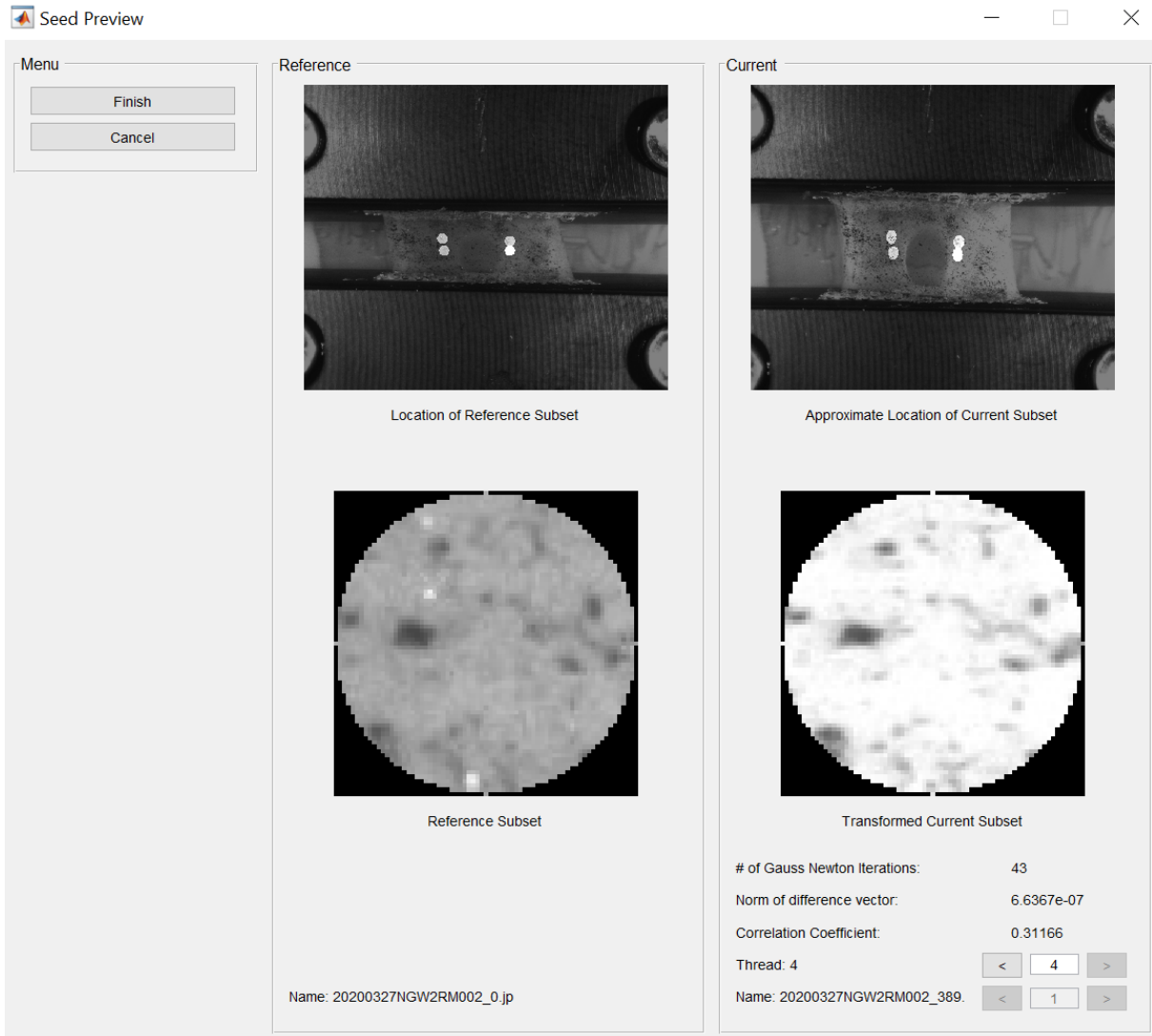


**Figure C.8:** Seed placement preview window. The user must make sure that the seeds do not travel outside the current image as the sample deforms and that they converge properly by checking that the correlation coefficient remains low and the number of iterations remain below the cutoff

### C.3.5 Formatting displacements

Once analysis is complete, the user must appropriately format the displacements to exclude points with a high  $C_{LS}$  by selecting *Analysis > Format Displacements*. The user can apply a scale by drawing a line on the reference image with a known distance. The scale used in this study was 0.0093 mm/pixel. Next, a correlation coefficient cutoff (maximum) value must be chosen and applied to all images. A value of 0.7 was selected as the correlation coefficient cutoff in this project (which included data where  $C_{LS} \leq 0.7$ ) as it excluded the weakly correlated values and the “bad data” points (Figure C.9).

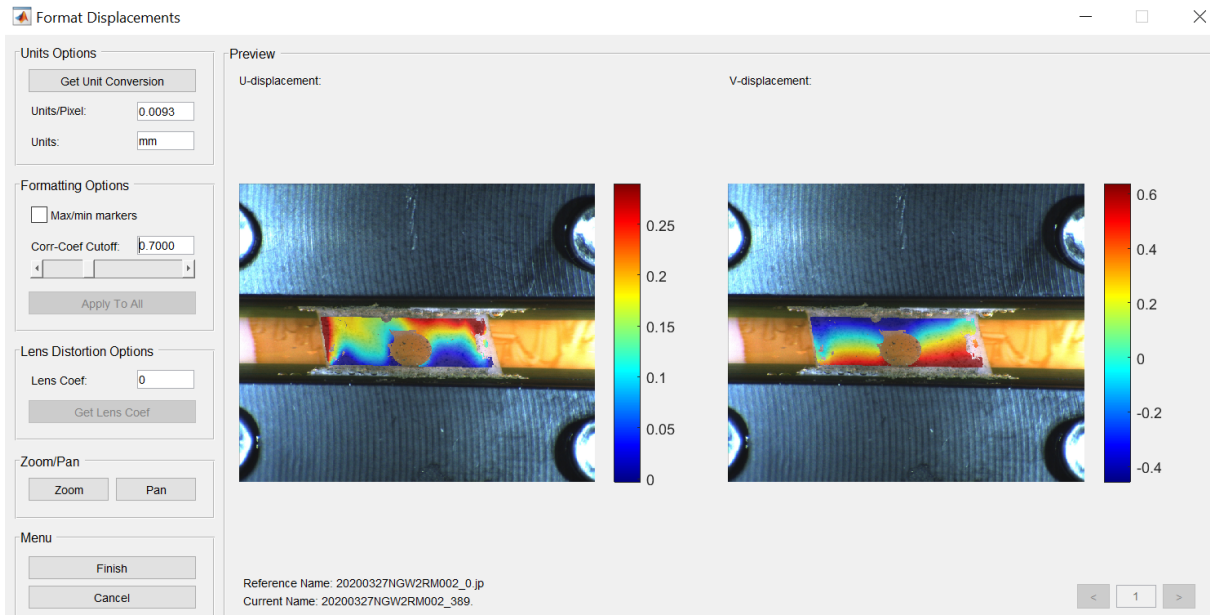


**Figure C.9:** Selection of scaling to 0.0093 mm/pixel and correlation coefficient cutoff,  $C_{LS} \leq 0.7$

### C.3.6 Strain analysis

After formatting the displacements correctly, select the *Analysis > Calculate Strains* option. The strain radius must be chosen which determines the amount of displacement values used in order to determine the strain at each point using a least squares plane fit based on the work of Bing Pan [14], as mentioned in Chapter 2. The type of strain output can be set to Lagrangian or Eulerian (Lagrangian strain was selected for this project) and the U or V displacements can be viewed as well. The window to the right allows the user to view the plane fit of the selected region, which is draggable. It is recommended to drag this point to high deformation regions and see if the curve fit is still appropriate (Figure C.10).

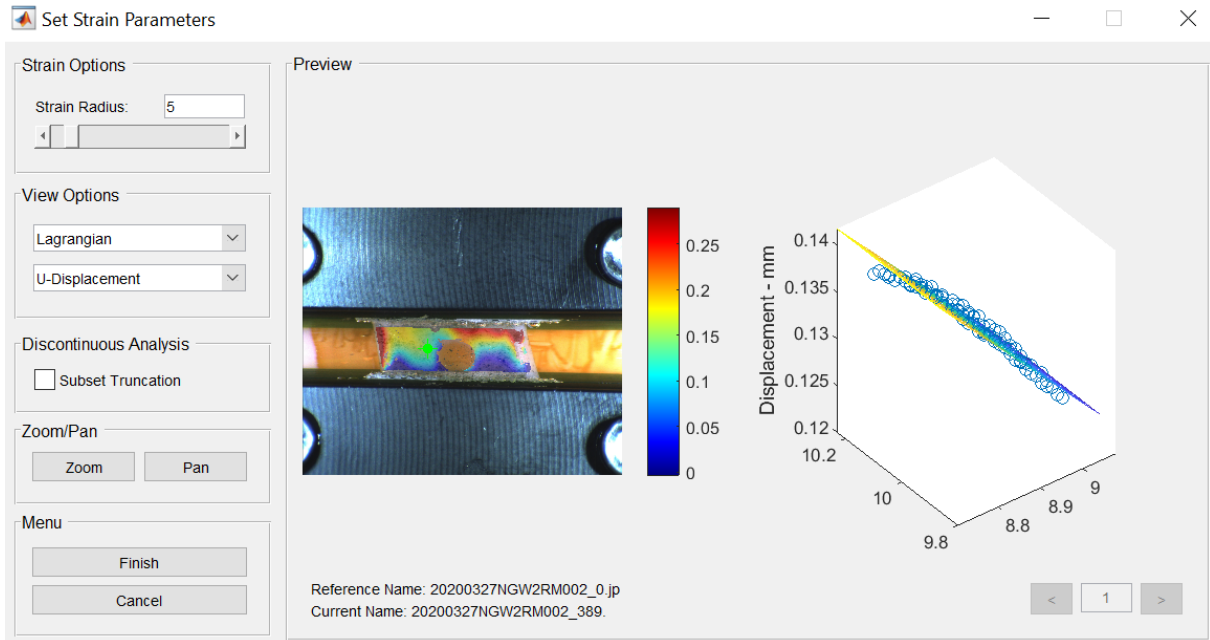


**Figure C.10:** Selection of strain radius=5. The least squares plane fit is shown in the right window

### C.3.7 Plotting and obtaining data

The user is able to plot the displacements and strains calculated by selecting *Plot>View Displacement Plots* or *Plot>View Strain Plots*. The upper and lower bounds of each plot can be altered by the user. Figure C.11 displays an example plot of the Lagrangian strain in the X direction. These images can be save by going to *File>Save Image* within the plot window.

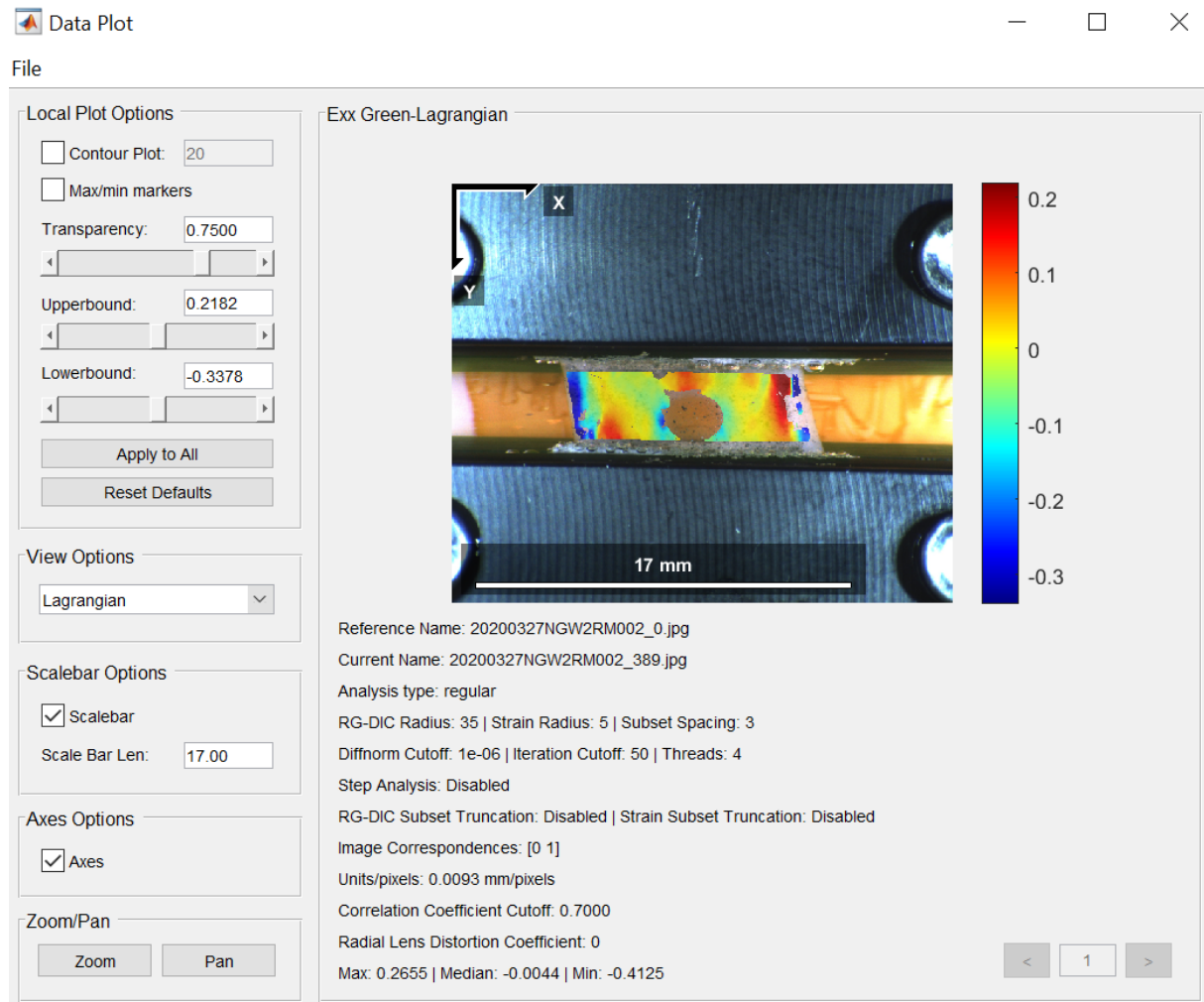


**Figure C.11:** Lagrangian strain plot in the x direction

All of the data calculated by the analysis can be saved by selecting *File>Save Data*. This data will then be accessible in the MATLAB working directory and can be easily loaded into the workspace.

# D

## DIC Parameter Analysis

Appendix D includes the method used in order to select the appropriate parameters per construct for DIC analysis.

### D.1 Subset Size and Strain Radius Selection

The first step in DIC is selecting the appropriate parameters for each construct. In order to do this, a quantitative technique was created to relatively compare parameters in MATLAB. Using this relative comparison between subset sizes and strain radii, allows the user to avoid values which include too much noise (depicted by holes in the strain maps of D.1) as well as oversmoothing of the data. Only the first (reference) and last image before rupture was used in the parameter analyses, as the algorithm is independent of how many images were included.

Multiple analyses were ran on each construct where different subset sizes were applied, ranging from 15-55 pixels with 10 pixel increments. X displacement plots were generated for a horizontal section of the construct in order to compare subset sizes. The average difference between each curve was calculated in MATLAB. The lowest average difference was then selected as the most optimal, and subsequently the lower bound subset size was selected. This same method was applied to select the appropriate strain radius per construct (with 3, 5, 7, 15 pixels chosen to compare).

The parameter selection values can qualitatively be assessed by creating strain maps in Ncorr with the different parameters applied to the construct, as shown in Figure D.1. Figure D.2 shows a quantitative parameter selection example of a construct comparing

the parameter output values for the X displacement and strain. A subset size of 35 pixels was applied to all constructs except for two, in which 45 pixels was a better option due to the sub-optimal speckle pattern (sparsity in some regions). A strain radius of 5 pixels was chosen as the most optimal value for all constructs. A subset spacing of 3 pixels was chosen for all constructs, as this value proved to output the best resolution without losing data.

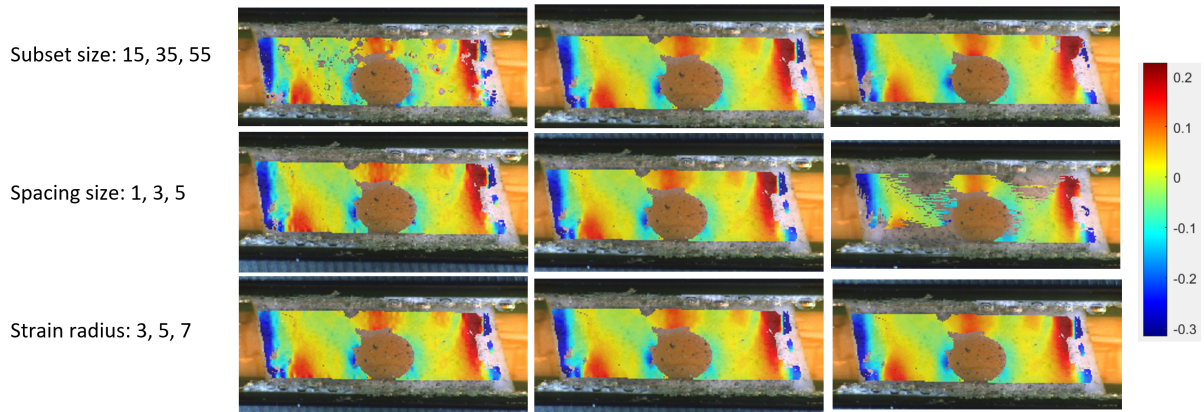


**Figure D.1:** Green-Lagrangian strain maps in the X direction derived from Ncorr allow a visual comparison of the different parameter sizes. The parameter values of the middle column were chosen for this construct, as it contained the least amount of noise and smoothing effect, which was quantitatively verified with the parameter analysis method mentioned and shown in Figure 3.9

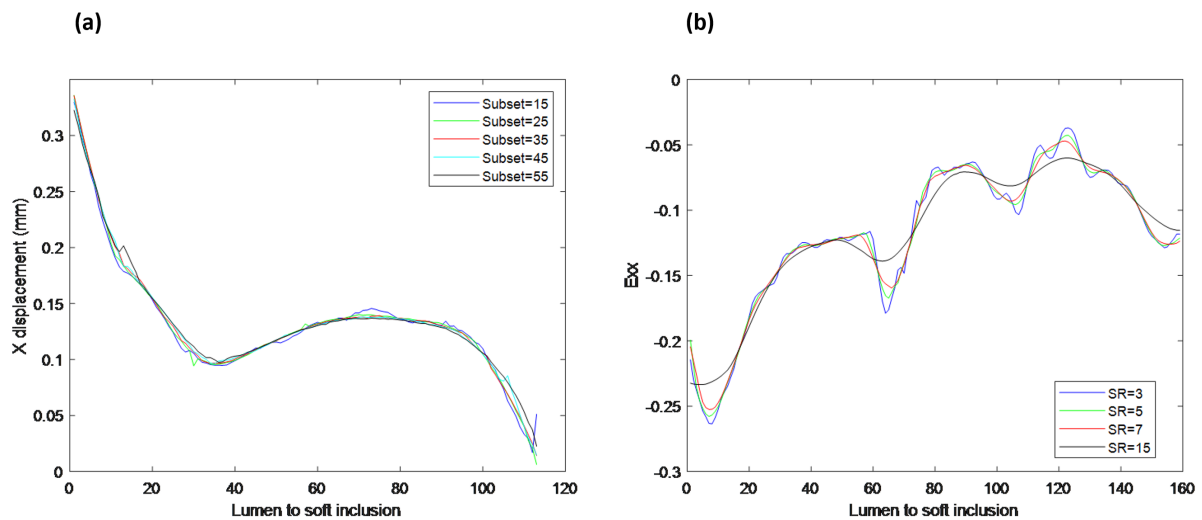


**Figure D.2:** X displacement and strain plots across half a construct from the lumen area to the SI comparing a) subset sizes and b) strain radii sizes. A subset size of 35 pixels and strain radius of 5 were chosen for this construct, as these values demonstrated the most optimal balance between noise and oversmoothing when analyzing the average relative differences between each parameter curve

## D.2 2D Correlation Coefficient Maps

To verify the appropriate parameter selection from the previous section, 2D correlation coefficient maps were generated in MATLAB using the stored correlation coefficient data from the parameter analyses (Figure D.3). An overall strong-moderately strong correlation ( $C_{LS} \leq 0.7$ ) was observed throughout most of the constructs when comparing the first (reference) image to the last image before rupture. This is also apparent near the SI which is of particular interest for this study, therefore a cutoff value of 0.7 was applied for final analyses using all images. One construct seen in D.3 did not contain a speckle pattern around the SI and did not have very good correlation in general, which is apparent in its correlation coefficient map (c), therefore it was excluded from DIC analysis when investigating the region surrounding the SI. DIC was performed on the right side of this construct as it showed a moderately good correlation.

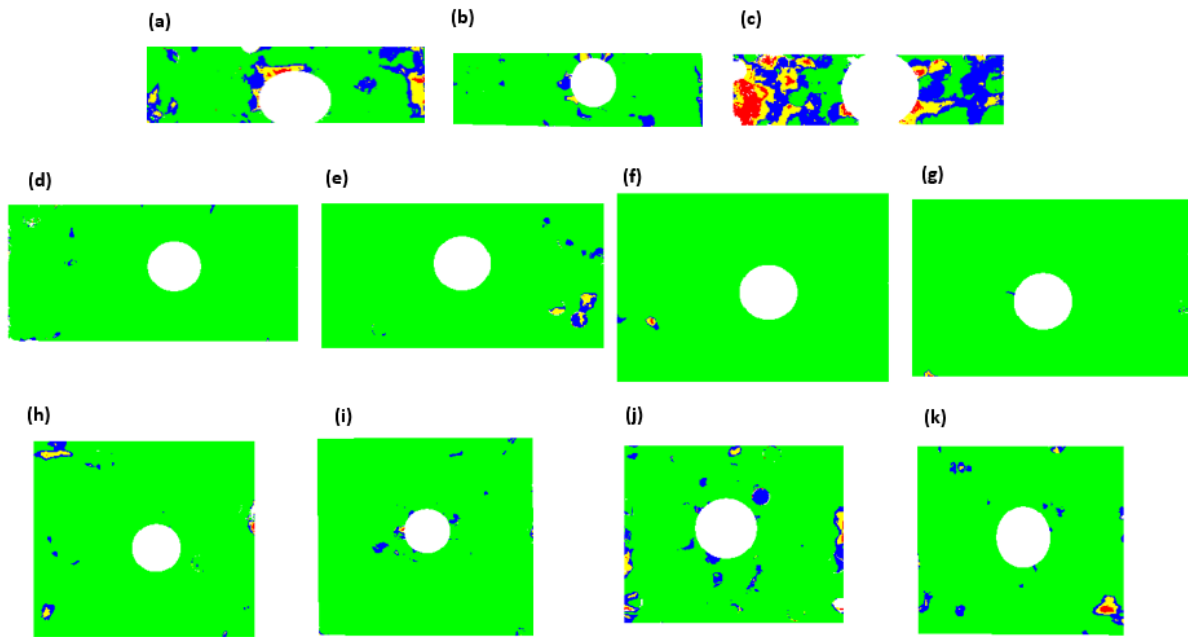


**Figure D.3:** 2D correlation coefficient maps generated in MATLAB: static constructs tested in redesigned clamps (a-c), static constructs tested in commercial clamps (d-g) and IS constructs tested in commercial clamps (h-k). SI was not analyzed due to weak correlation in this region for most constructs. green: strong correlation  $0 < C_{LS} \leq 0.5$ , blue: moderately strong correlation  $0.5 < C_{LS} \leq 0.7$ , yellow: weak correlation  $0.7 < C_{LS} < 1.0$ , red: bad data  $1.0 \leq C_{LS}$ . The green and blue regions were included in the analysis (moderately strong to strong correlation)

## D.3 Optimizing Speckle Pattern

The graphite speckle patterns applied on each construct was assessed in the DIC software and 2D correlation coefficient maps were made from the exported data. It was seen from these correlation coefficient maps (Figure D.3) that most of the constructs contained

good correlation data (defined as  $< 0.7$ ) with respect to the reference image, however a few regions displayed a bad correlation (defined as  $> 0.7$ ), specifically near the SI or edges, therefore there is room for improving the DIC speckle pattern application for future experiments. By using a dabbing technique to apply the graphite, clusters of particles as well as regions of sparsity were created, which are not optimal for DIC analysis.

In order to optimize the speckle pattern application for future DIC analysis, an unique even speckle pattern is recommended. A better method to achieve this could be to apply a dark paint via airbrush for the background creating appropriate contrast and then apply a white paint via airbrush, making sure the paint does not detach when submerged into PBS [29]. Also, outlining the soft inclusion would be recommended if using the above method, in order to trace the boundary for DIC analysis more accurately. In this study, the SI boundary was difficult to locate and had to be estimated through the speckle pattern.

## D.4 Optimizing Parameter Selection

In order to perform DIC analysis, the user must select the appropriate parameters for the sample including subset size, spacing size, and strain radius. In this study, a relative error approach was used to select the parameters, although establishing a ground truth is the usual recommended method, which was discovered after testing was already performed. There are a few methods used to choose these values by establishing the ground truth. One way would be to perform rigid body translation analysis before mechanical testing. For this method, an image of the initial position of the construct must be taken and then the construct should be moved a known distance in one direction and another image should be taken at this location. With this rigid body translation approach, the uncertainty in the displacement and strain under uniform stretch can be determined in  $N_{corr}$  (deviation from zero). Therefore, the minimum error can be calculated for different sizes of subset sizes and strain radii values, and give a more systematic method for parameter selection [30]. It is recommended for future experiments, before the mechanical testing is performed, to carry out rigid body translation analysis to obtain appropriate parameter values.

Another method known as grey level co-occurrence matrix (GLCM) could also be used to choose an appropriate subset size for each construct [31]. GLCM uses offsets between pixels of grayscale values and contrast to quantify the variation of spatial intensity. An optimal DIC speckle pattern contains a low critical offset, in which the contrast values saturate at a certain point. This method could not work in this study due to the sub-optimal speckle pattern on the constructs. The images never saturated to a certain contrast value, but rather continued to increase.

# E

## Supplementary Results

### E.1 Linking local strain patterns to global behavior

Figure E.1 displays the global mechanical behavior of all of the tested constructs as shown in the Results section, however black dots have been added to this plot to depict the location of  $\epsilon_{10\%}$  as determined by DIC analysis. This graph supports the speculation that the commercial clamps could be causing micro-structural slippage within the tissue near the clamp region due to the high amount of stretch variation at this location. Also, these locations are at higher stretch overall in the commercial clamps when compared to the redesigned clamps. This micro-structural slippage region could therefore be greatly effecting the global mechanical properties reported for the entire construct.

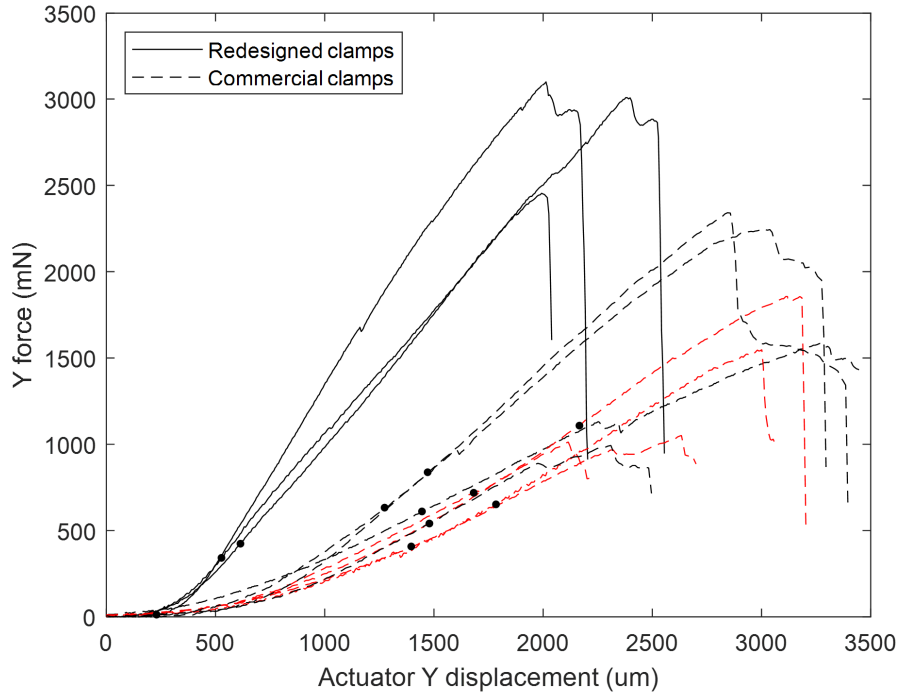


**Figure E.1:** Y force vs actuator Y displacement plots of all static (black) and all IS (red) constructs until rupture: solid lines represent the new clamps, dotted lines represent the commercial clamps. This plot is proportional to the nominal engineering stress vs strain plot. Black dots depict the location of  $\epsilon_{10\%}$  as determined by DIC analysis

## E.2 X-Y displacement/strain maps for all constructs

X and Y displacement and X and Y Lagrangian strain maps at the image of  $\epsilon_{10\%}$  and at the image immediately before rupture are presented below for each of the constructs (excluding the SI). The results section of this report focused on the  $\epsilon_{10\%}$  location in order to normalize the disparities that may be occurring near the clamp region with the commercial clamps and to allow a more direct comparison between clamp designs. The image immediately before rupture show similar trends to this image, but with a higher magnitude.

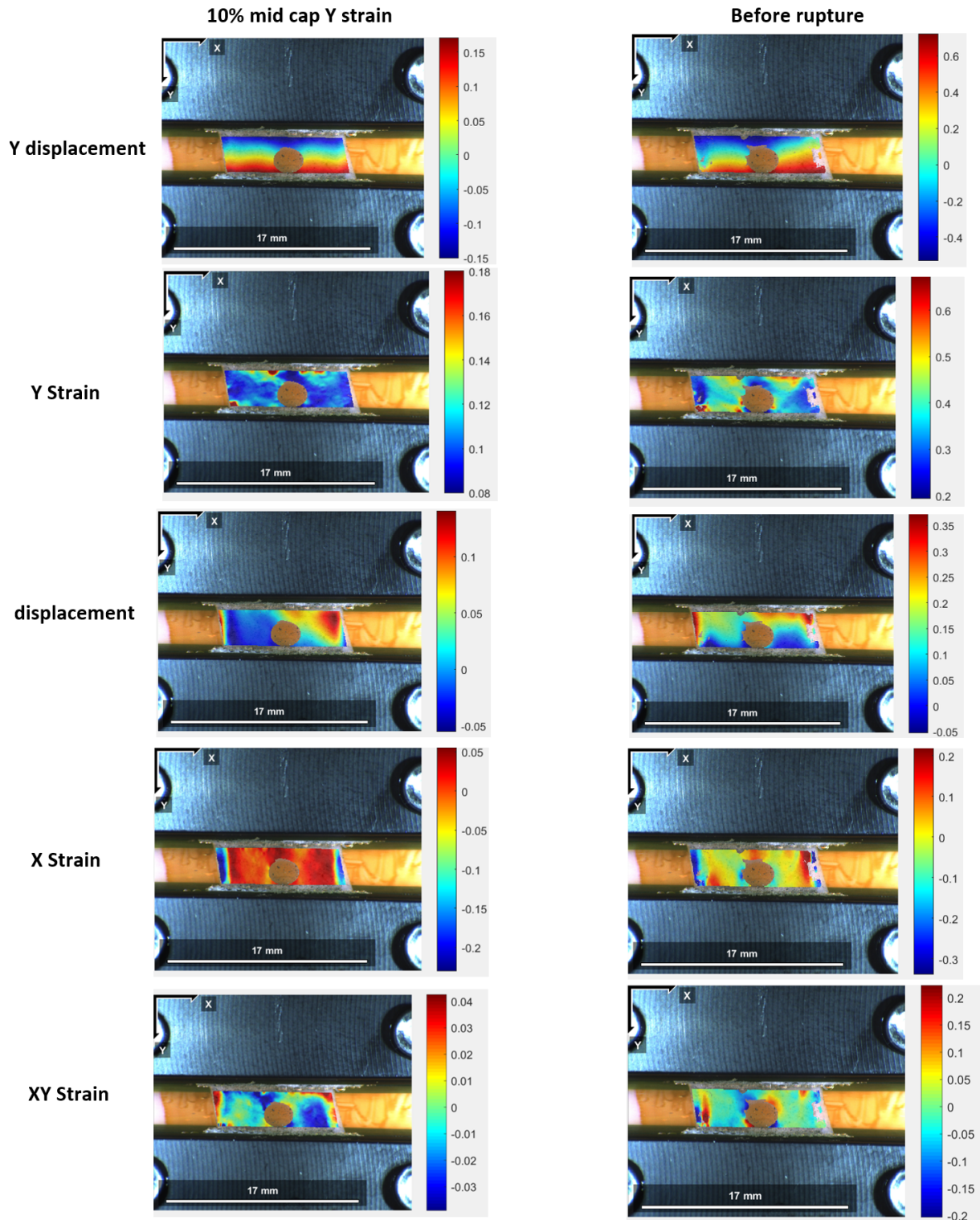


Figure E.2: Static construct tested in redesigned clamps (1/3)

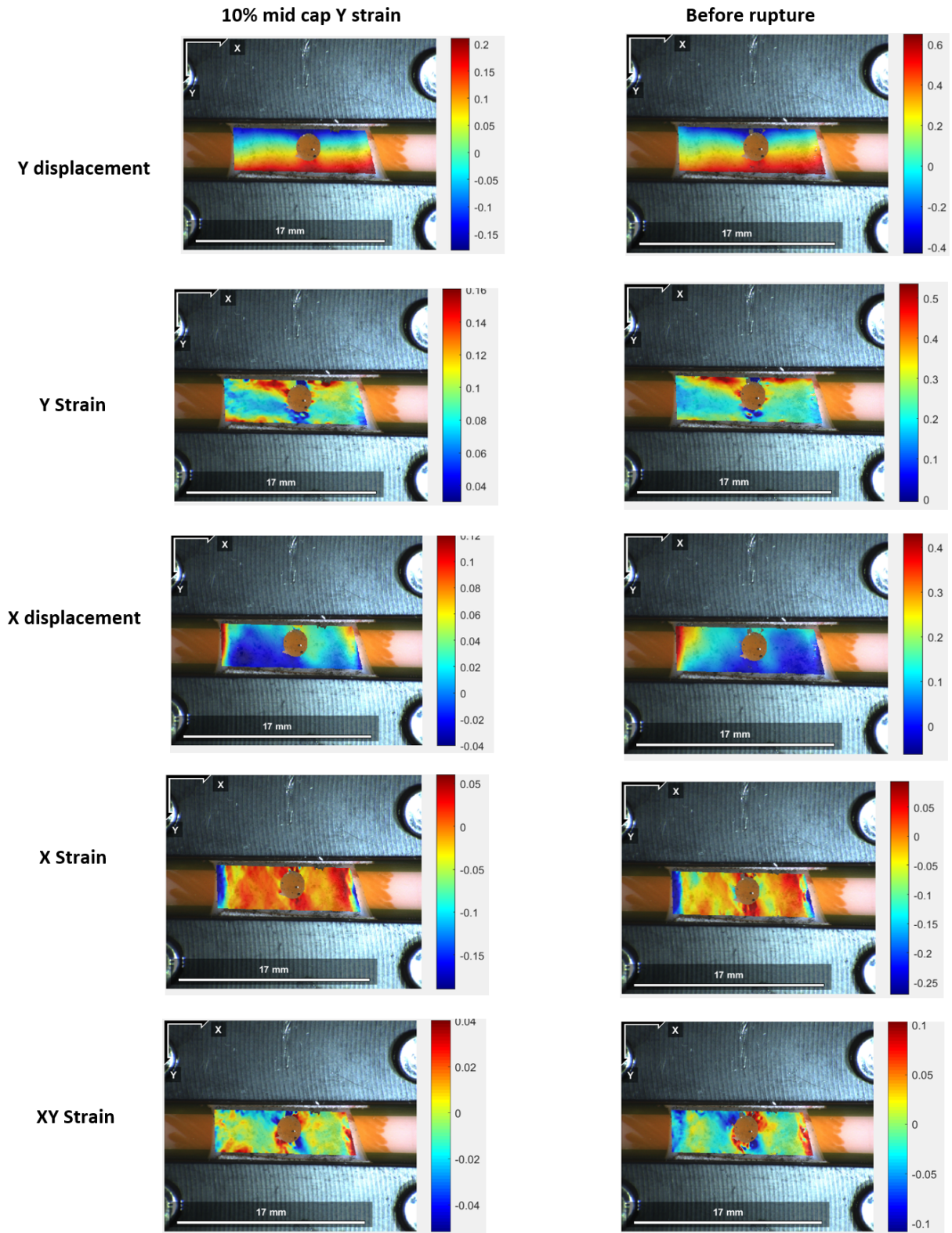
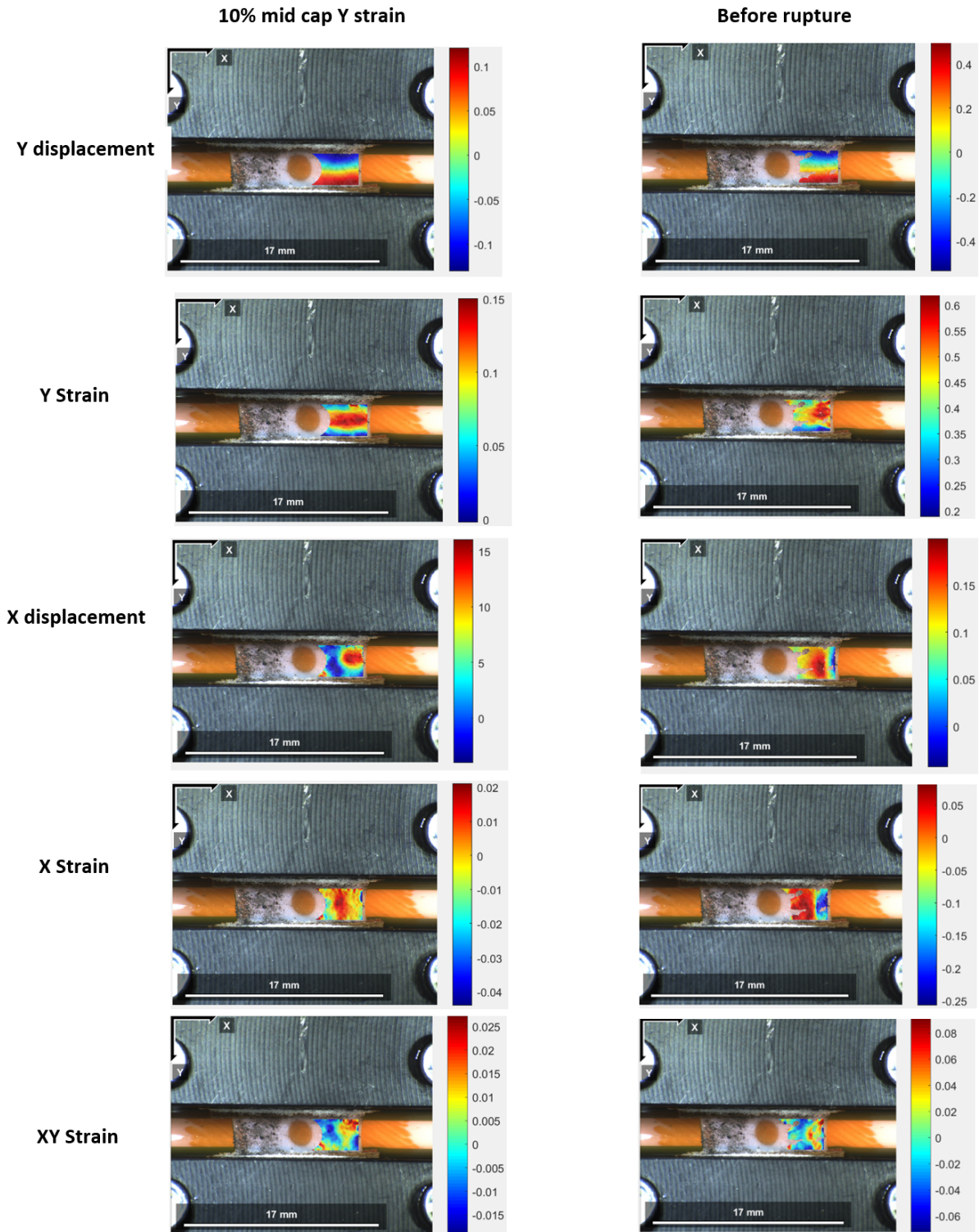


Figure E.3: Static construct tested in redesigned clamps (2/3)



**Figure E.4:** Static construct tested in redesigned clamps (3/3). Inadequate speckle pattern was applied therefore DIC was not comprehensive

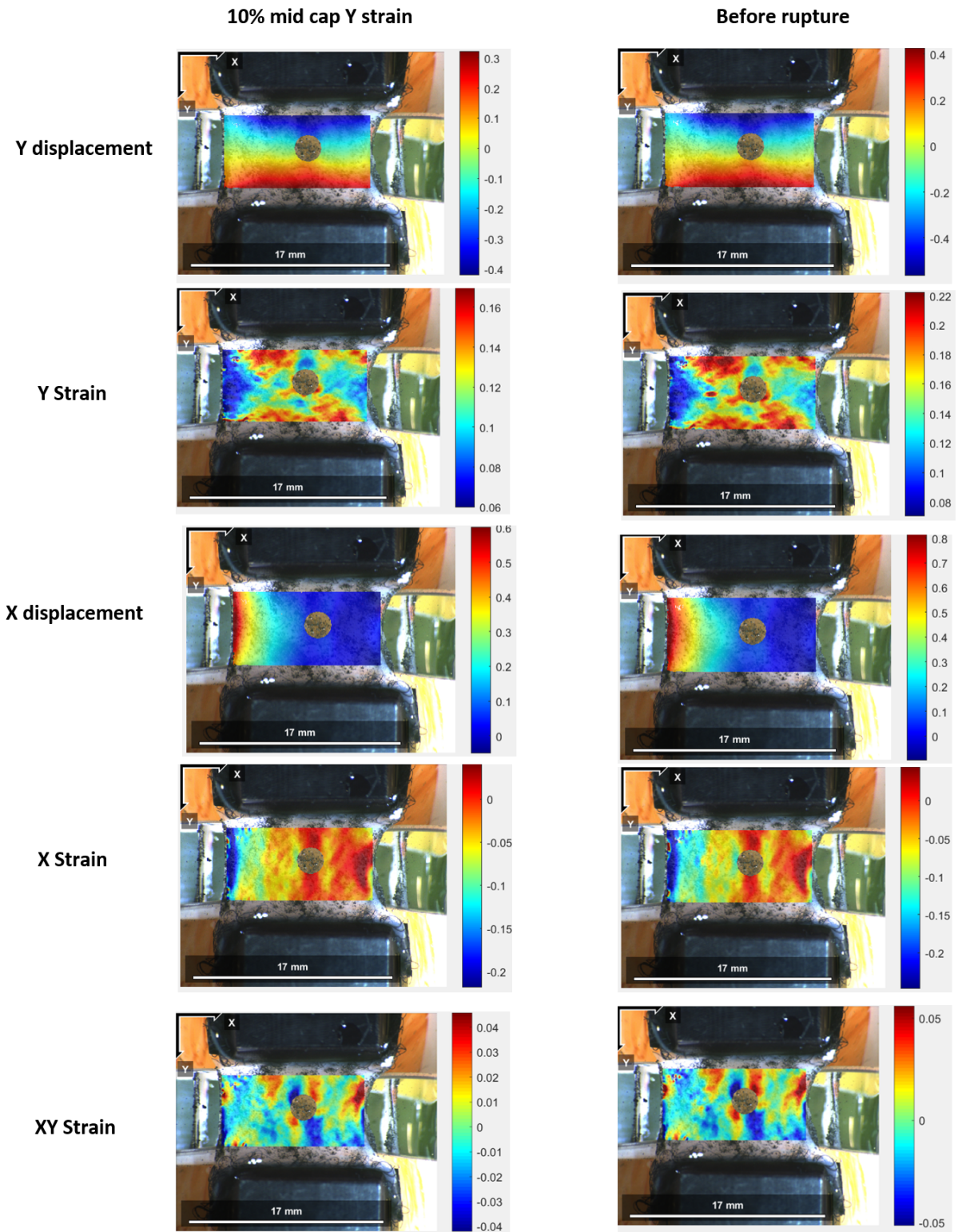


Figure E.5: Static construct tested in commercial clamps (1/4)

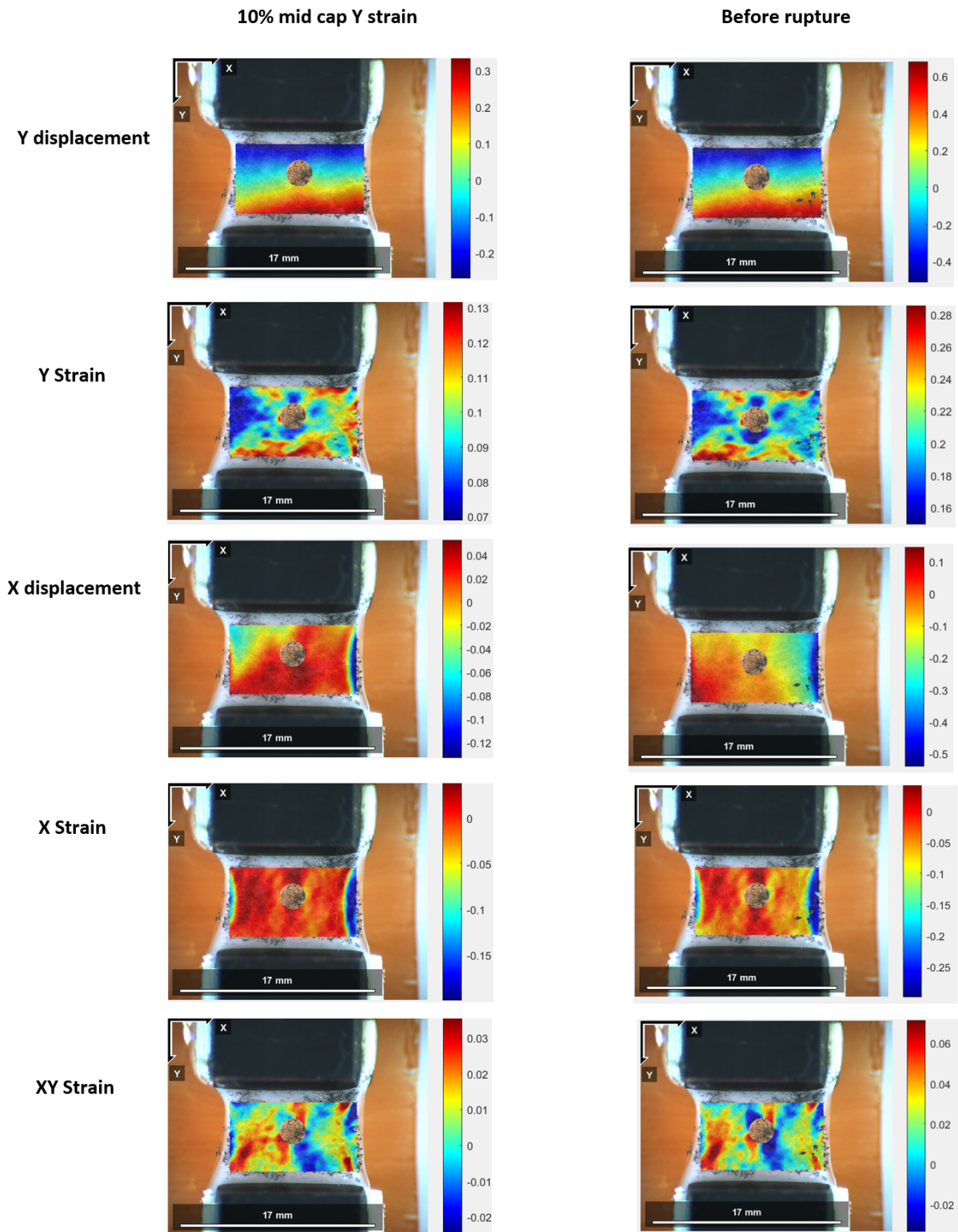


Figure E.6: Static construct tested in commercial clamps (2/4)

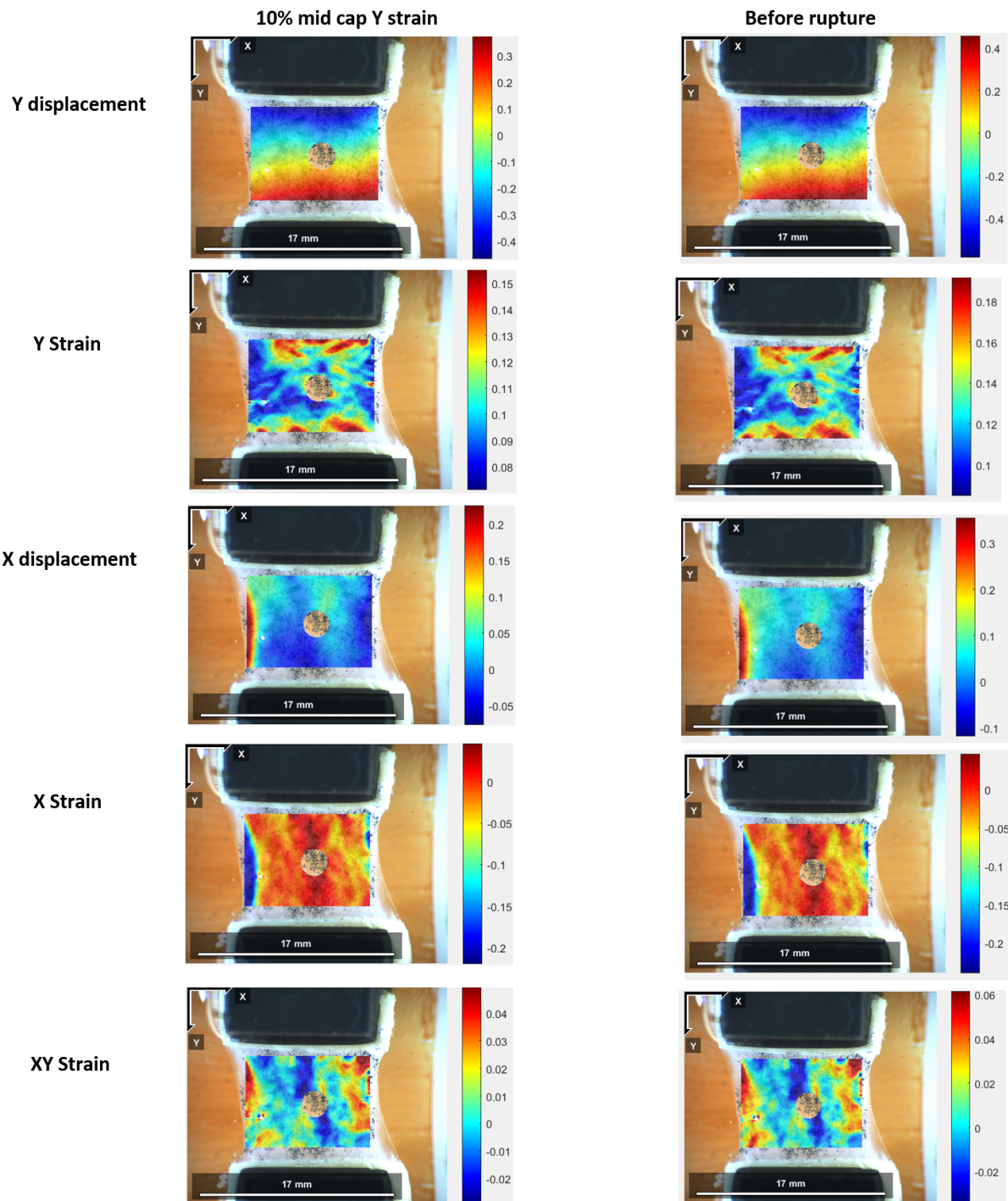


Figure E.7: Static construct tested in commercial clamps (3/4)

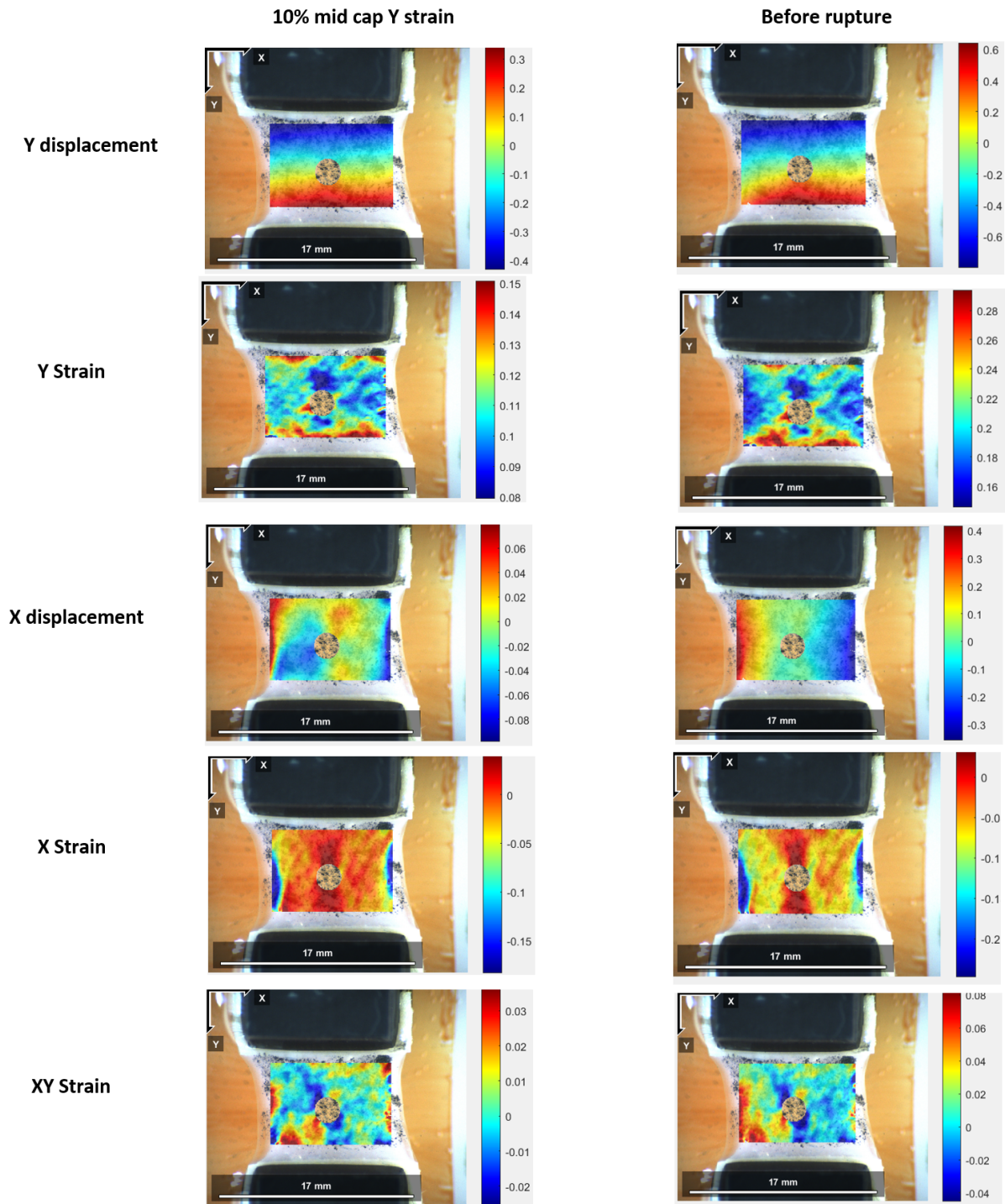


Figure E.8: Static construct tested in commercial clamps (4/4)

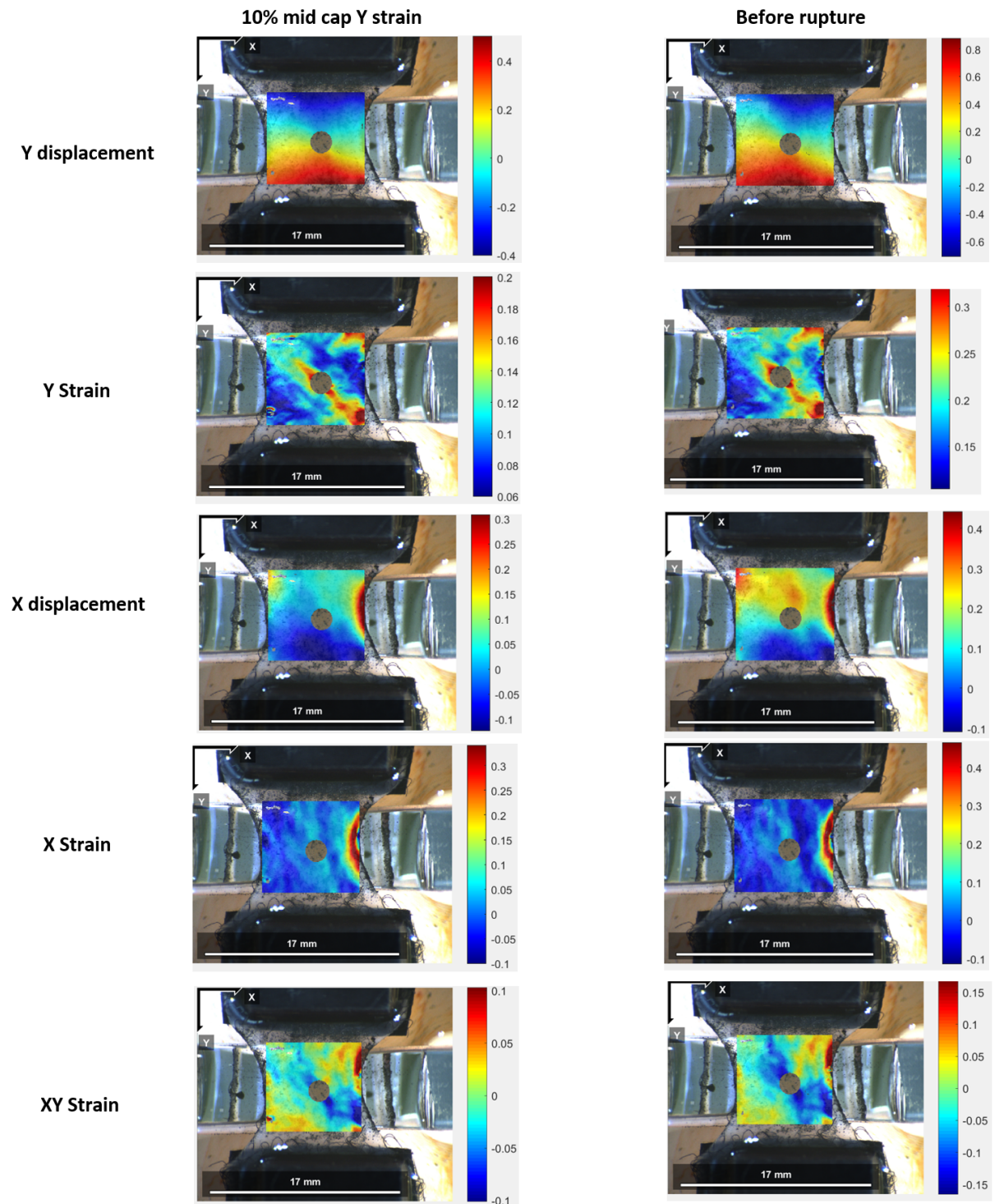


Figure E.9: IS construct tested in commercial clamps (1/4)

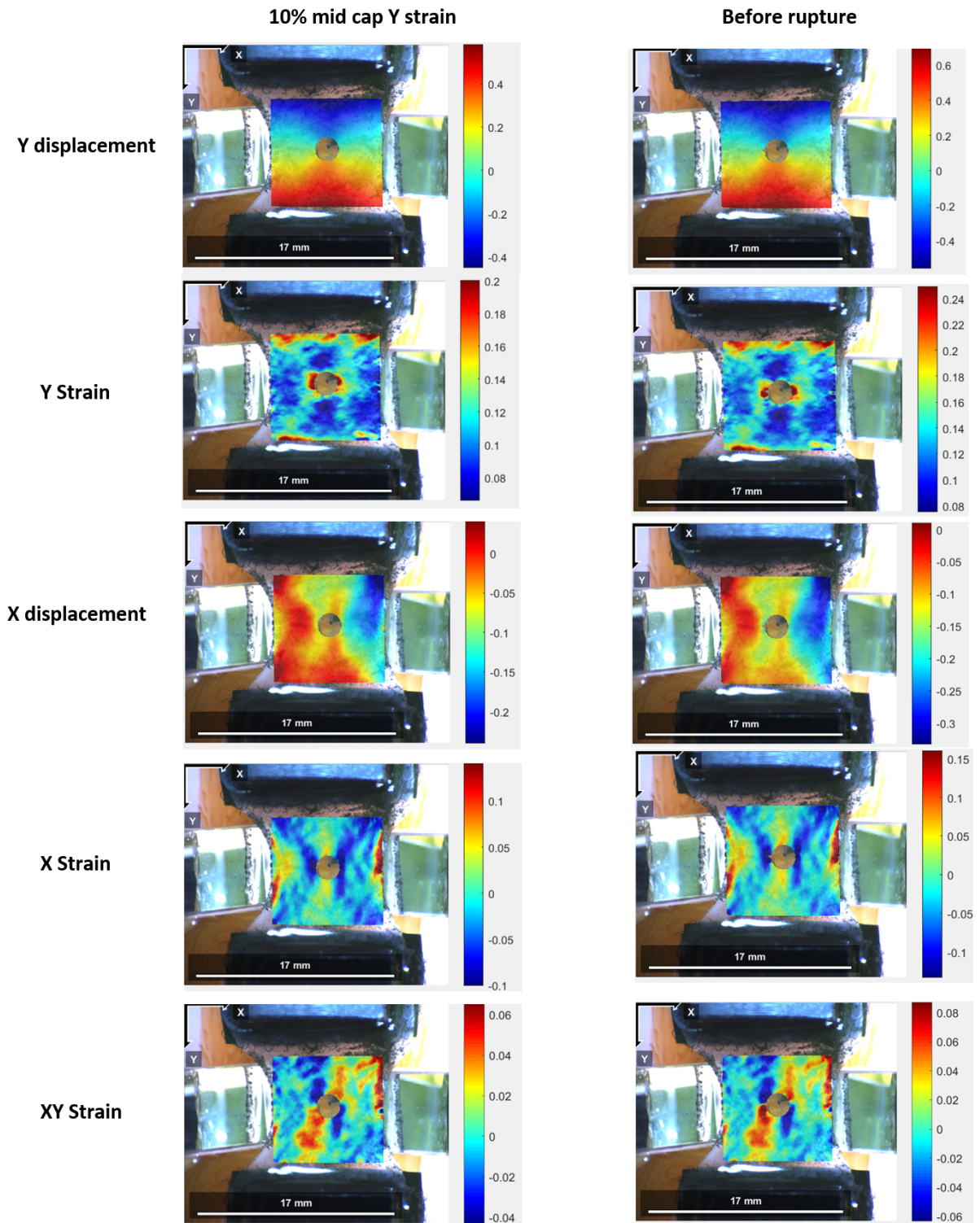


Figure E.10: IS construct tested in commercial clamps (2/4)

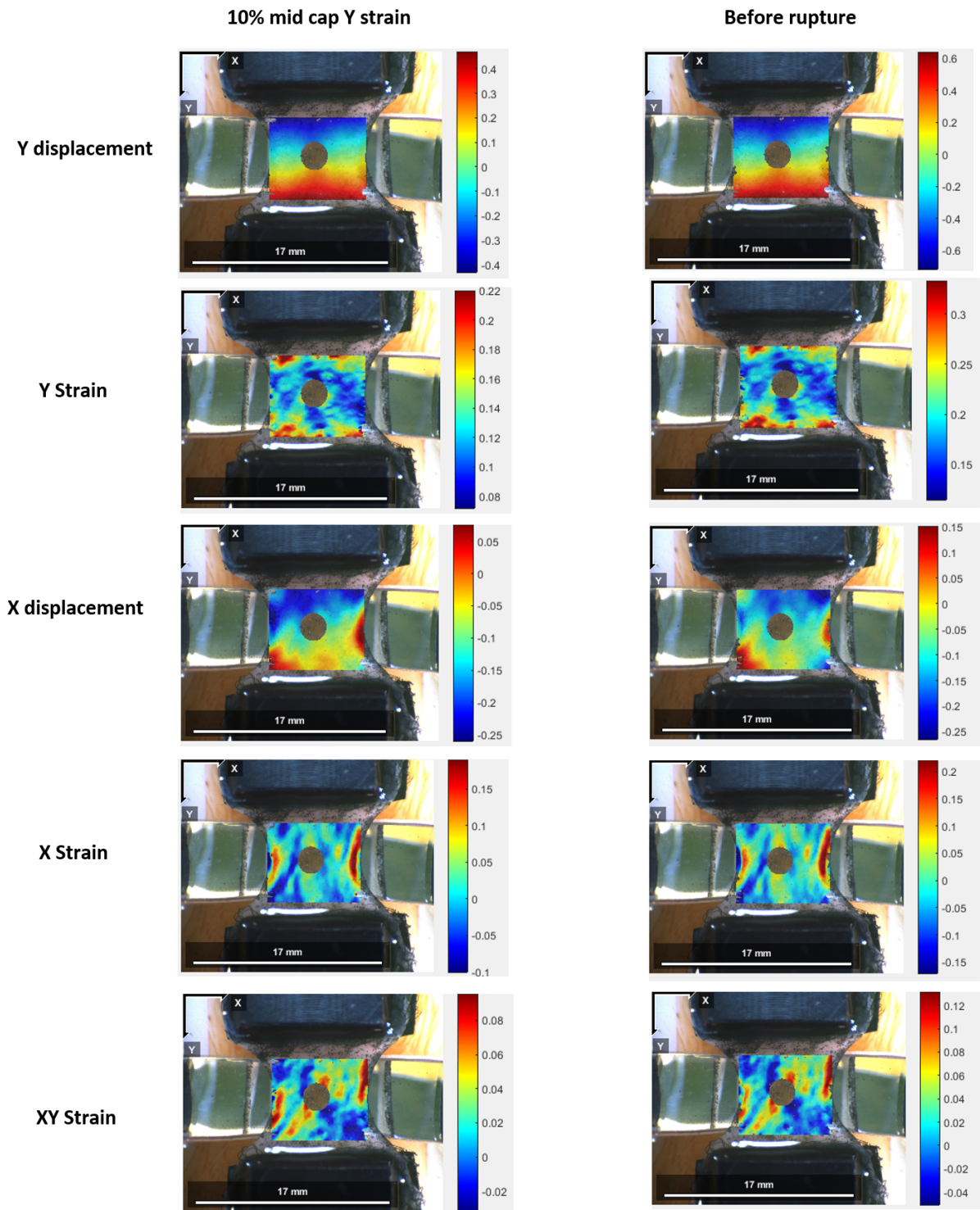


Figure E.11: IS construct tested in commercial clamps (3/4)

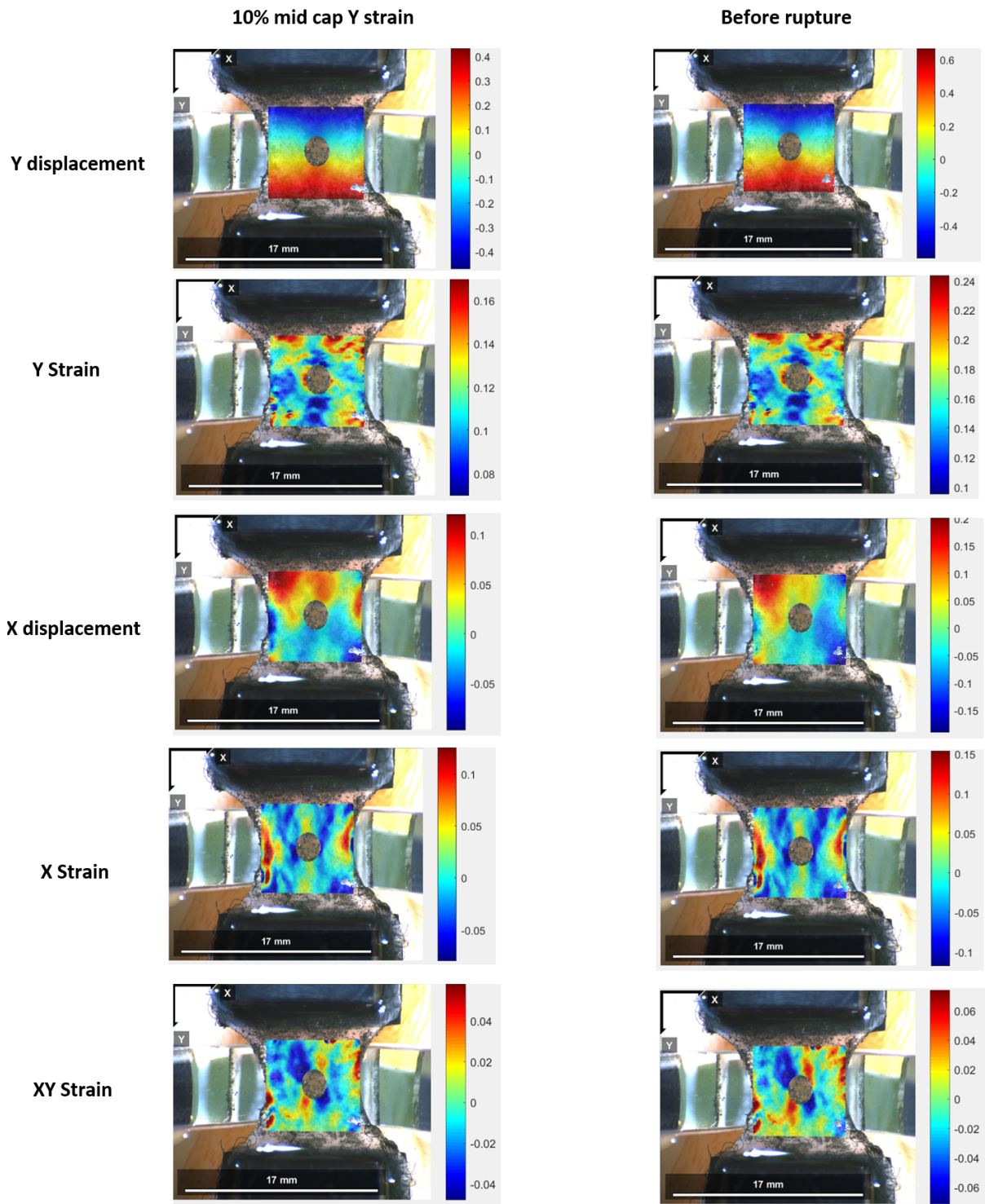


Figure E.12: IS construct tested in commercial clamps (4/4)

### **E.3 Average X-Y strain plots across all constructs**

The average  $\epsilon_{xx}$  and  $\epsilon_{yy}$  values across the constructs divided into the shoulder and mid cap regions are plotted below (excluding the SI). The data presented is located at the image where  $\epsilon_{10\%}$ . The grey dotted lines represent the right and left most point of the SI. Some constructs do not contain all regions specified in the methods section.

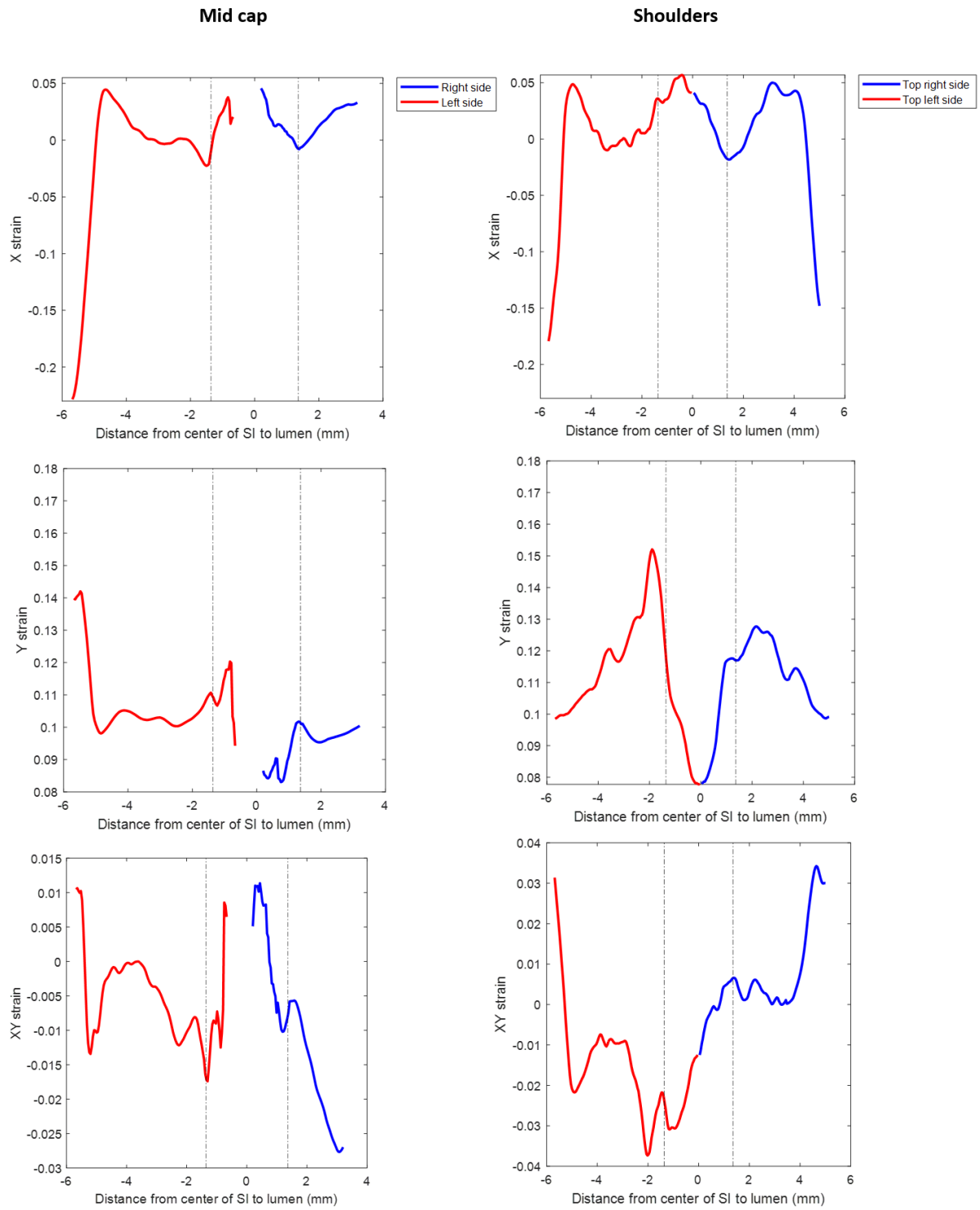


Figure E.13: Static construct tested in redesigned clamps (1/3)

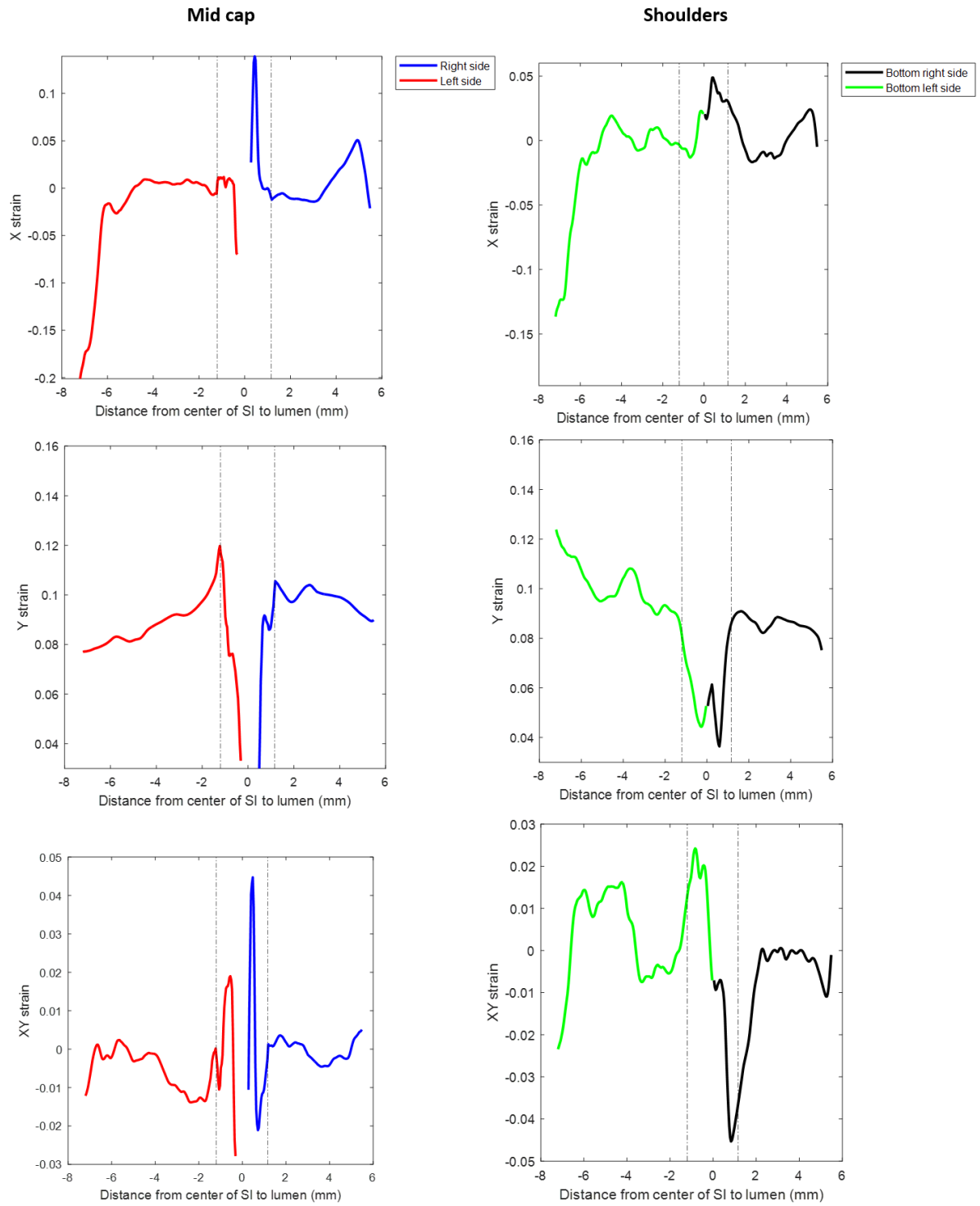
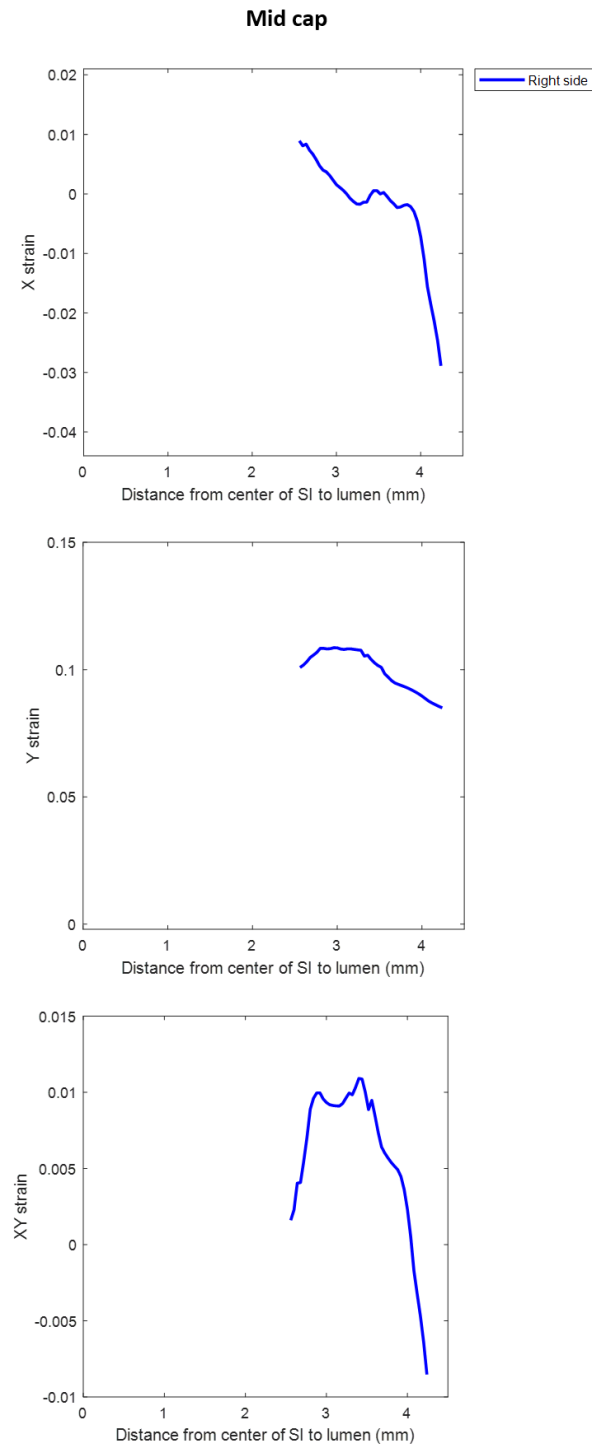
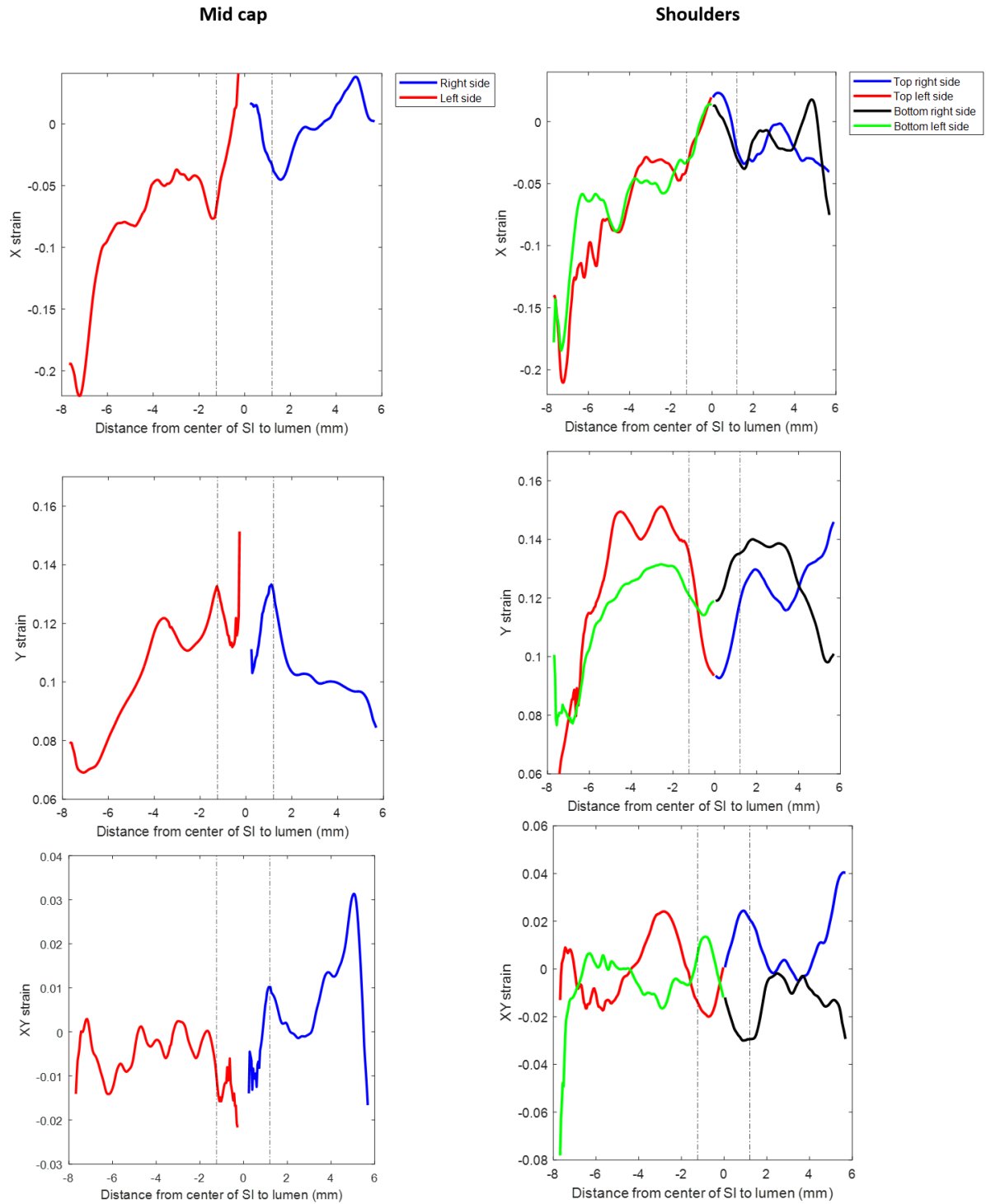


Figure E.14: Static construct tested in redesigned clamps (2/3)



**Figure E.15:** Static construct tested in redesigned clamps (3/3)



**Figure E.16:** Static construct tested in commercial clamps (1/4)

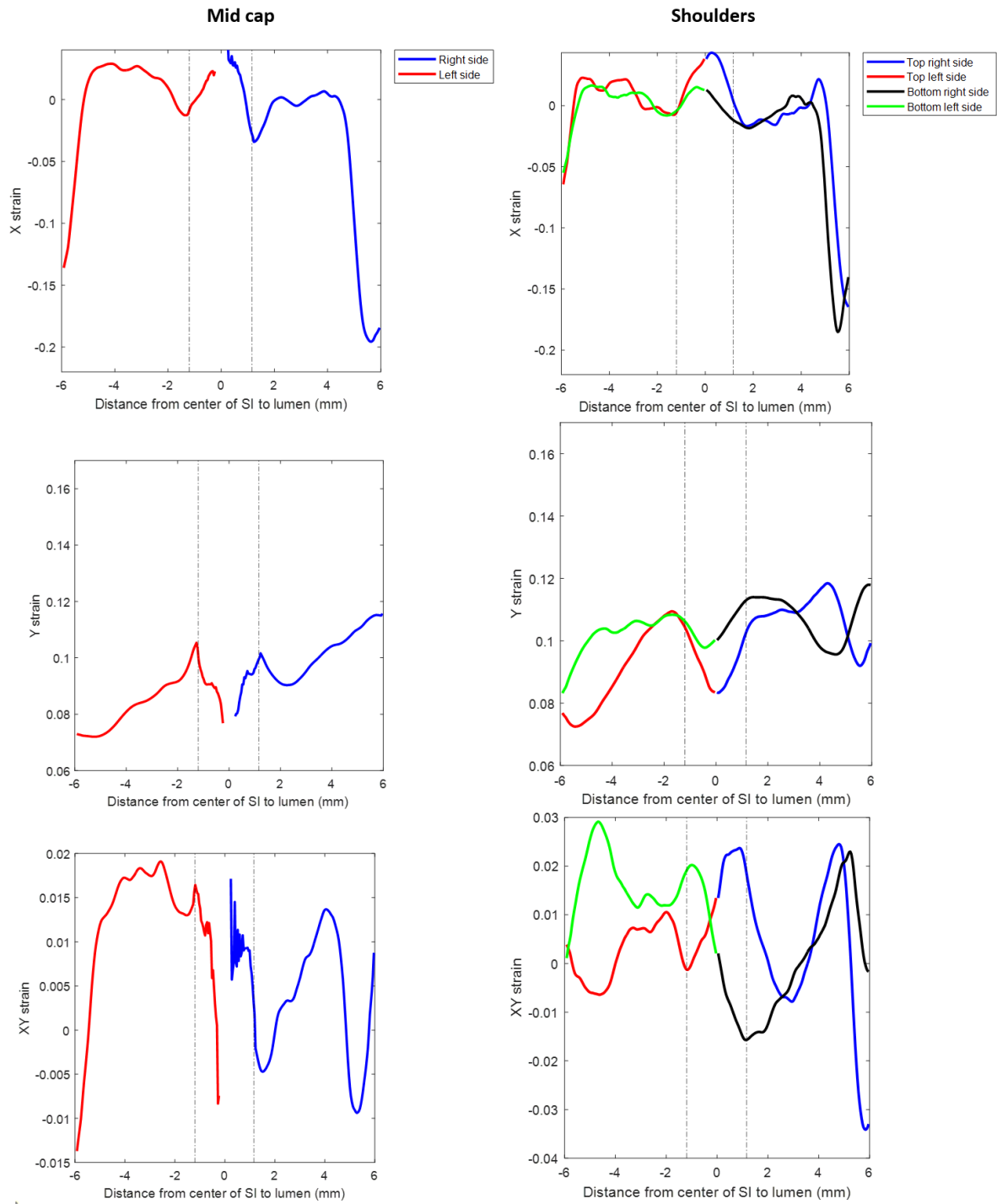


Figure E.17: Static construct tested in commercial clamps (2/4)

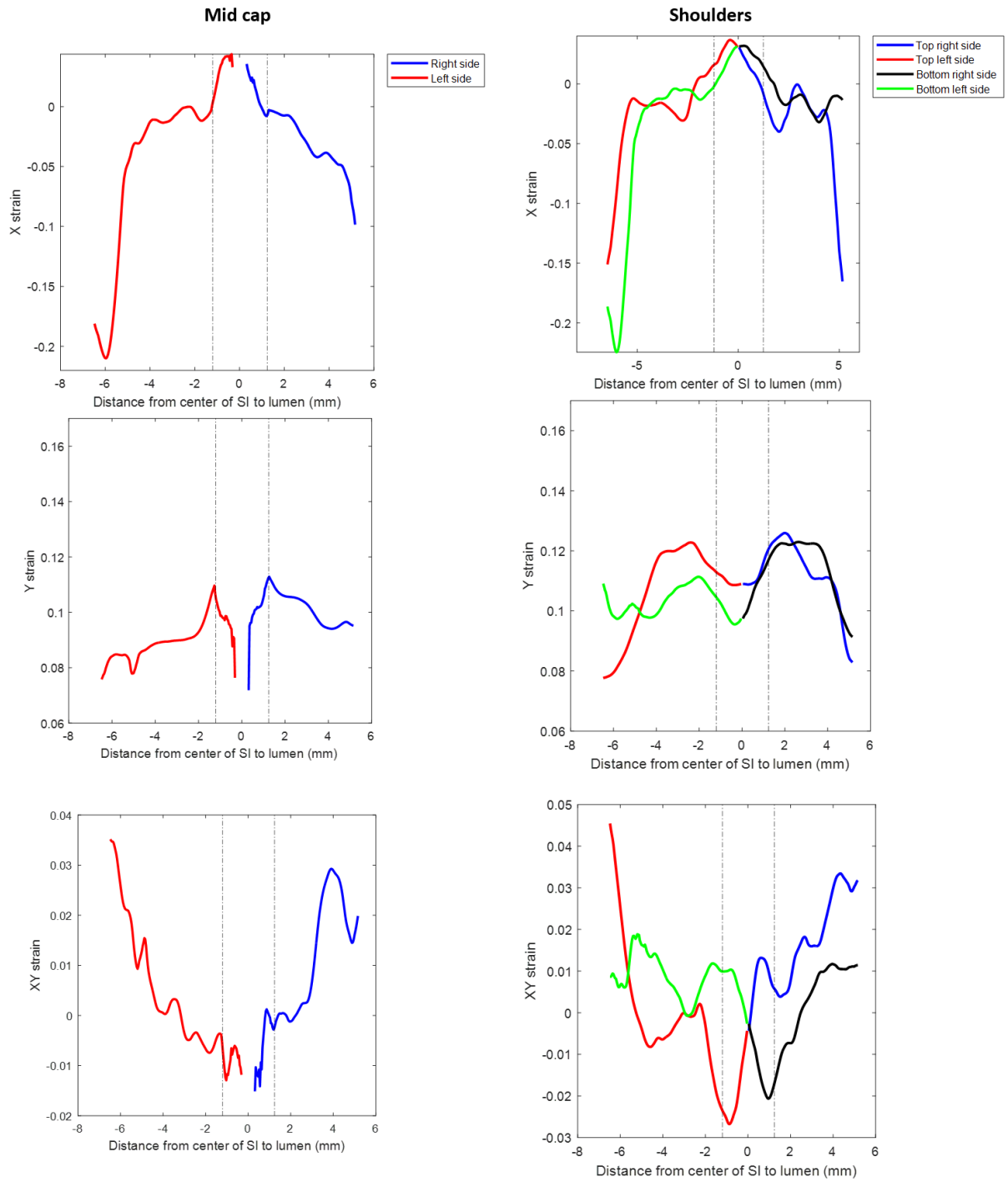
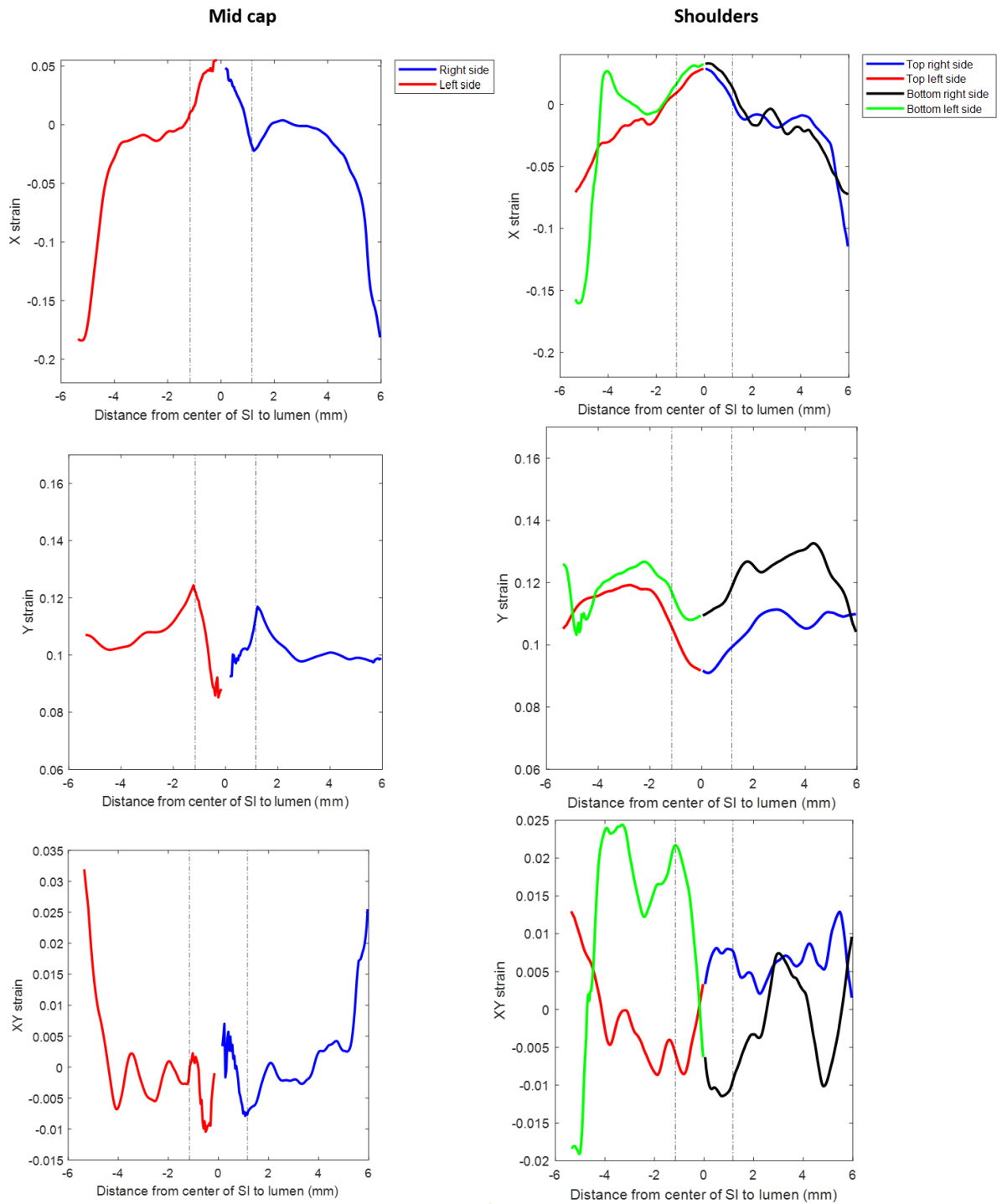


Figure E.18: Static construct tested in commercial clamps (3/4)



**Figure E.19:** Static construct tested in commercial clamps (4/4)

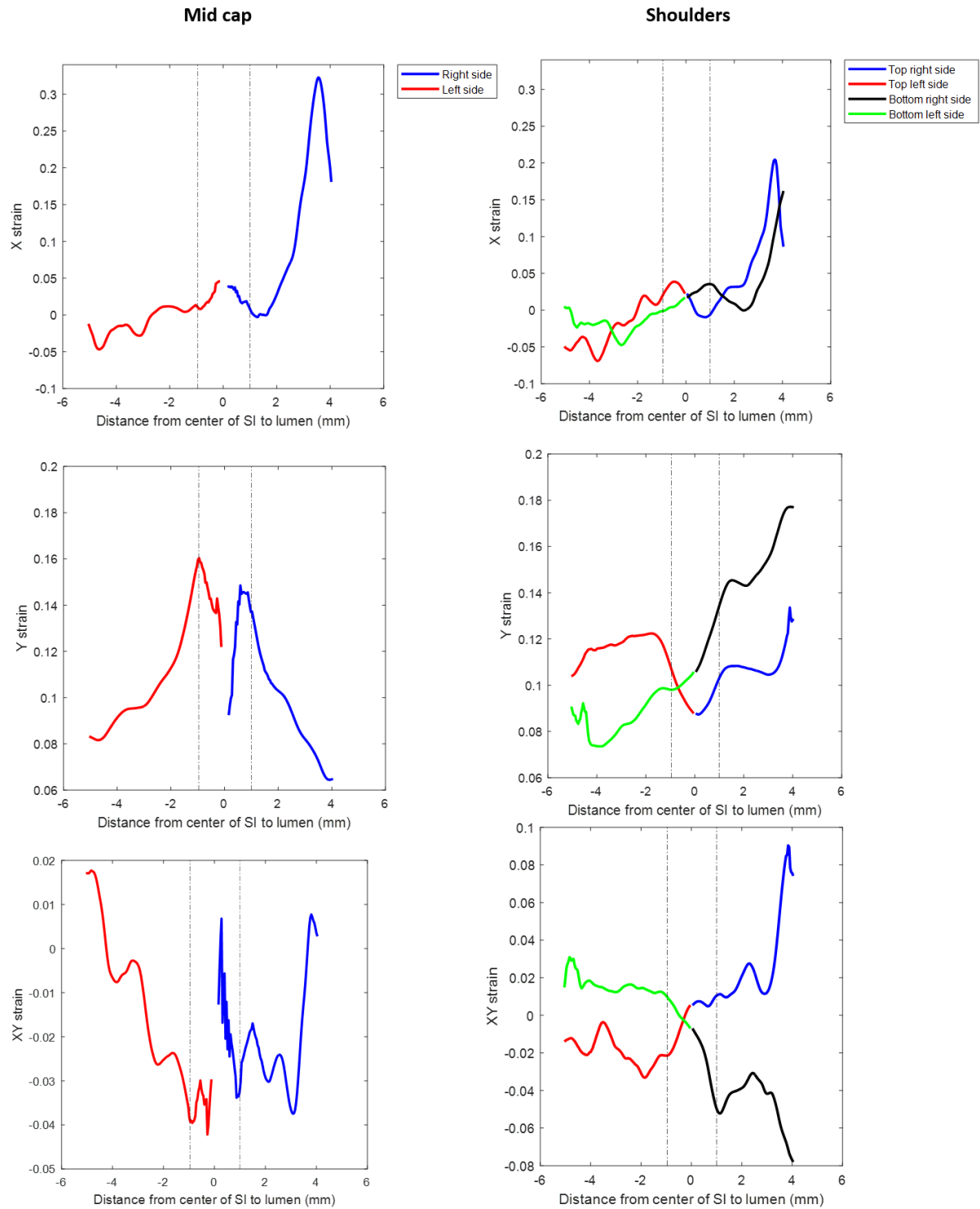


Figure E.20: IS construct tested in commercial clamps (1/4)

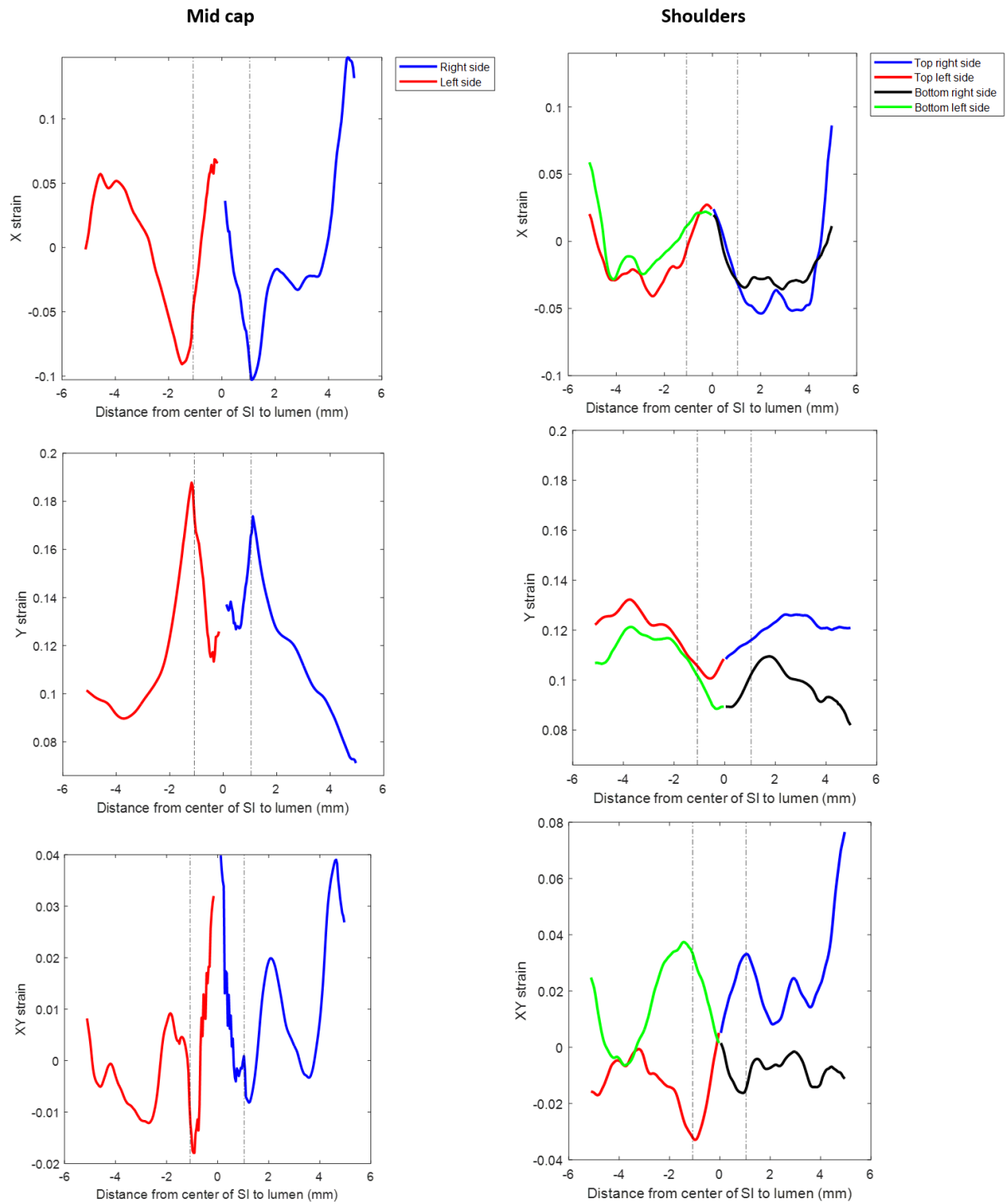


Figure E.21: IS construct tested in commercial clamps (2/4)

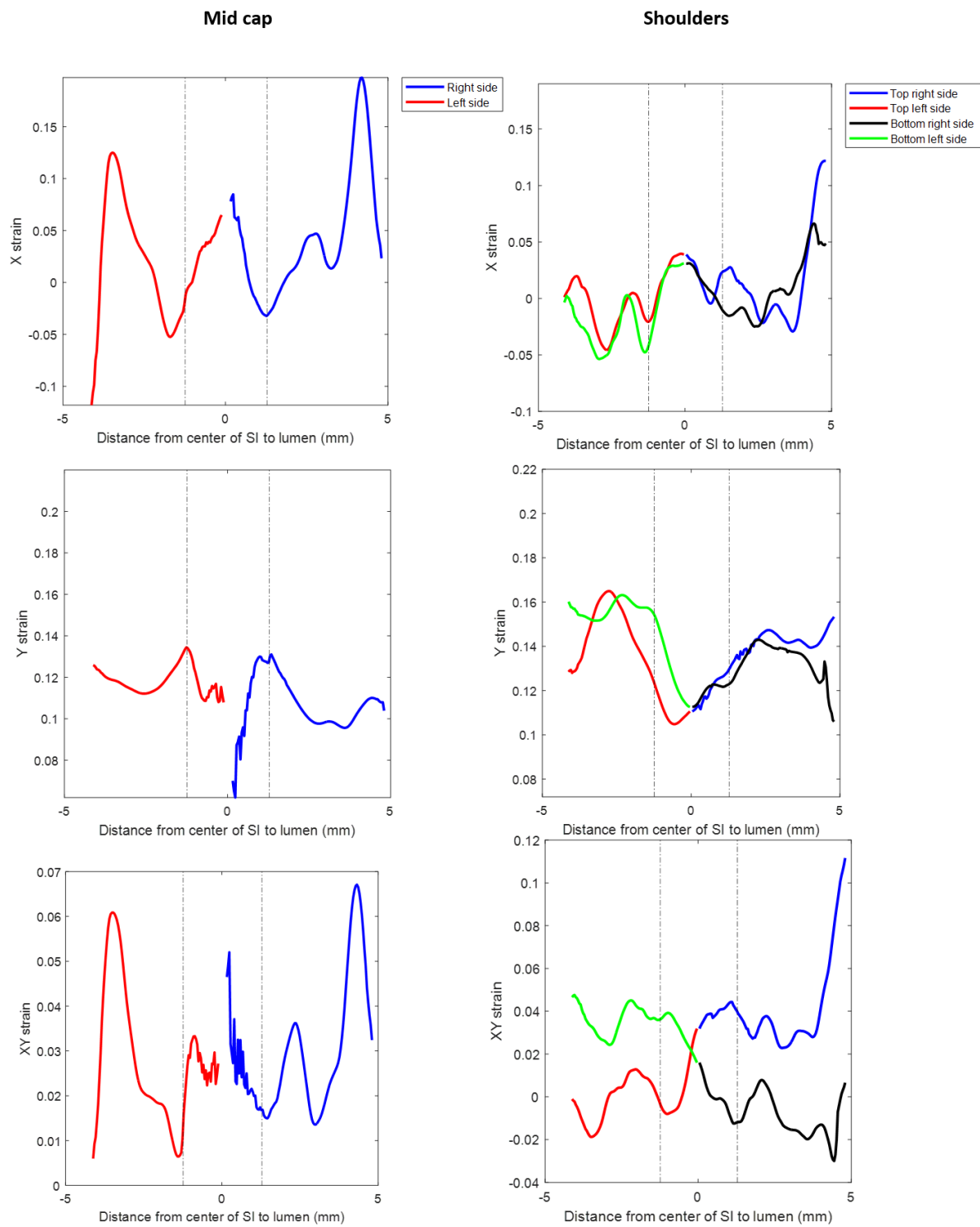


Figure E.22: IS construct tested in commercial clamps (3/4)

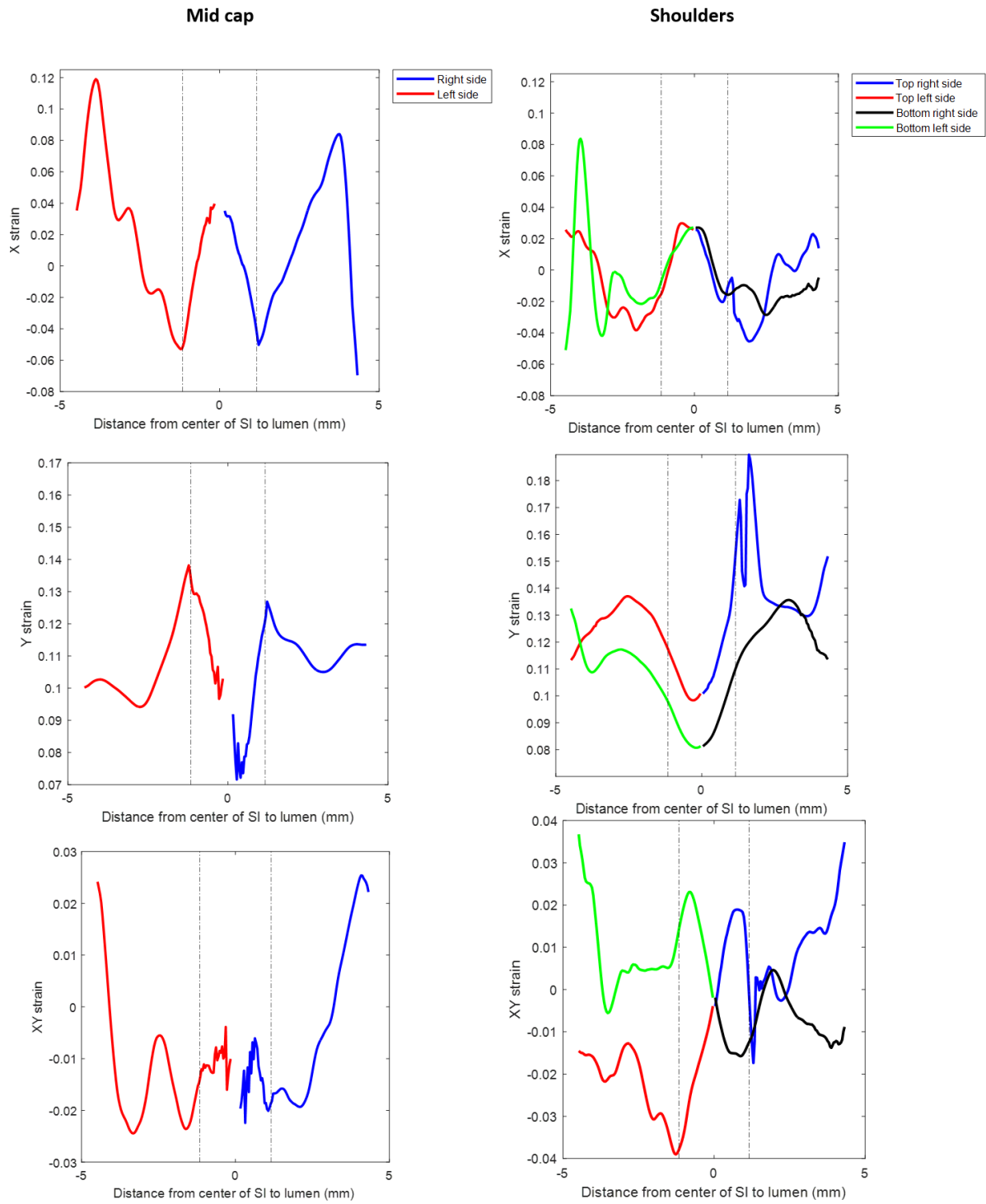


Figure E.23: IS construct tested in commercial clamps (4/4)

## E.4 X-Y strain variation example

The shaded plots below represent the variation in  $\epsilon_{xx}$  and  $\epsilon_{yy}$  values within the shoulder and mid cap regions going across the static construct tested in the commercial clamps. The red and blue lines represent the top and bottom most values for each region, with the grey signifying the range of values in between. It was observed that most variation occurred towards the edges of the construct where compaction occurred.

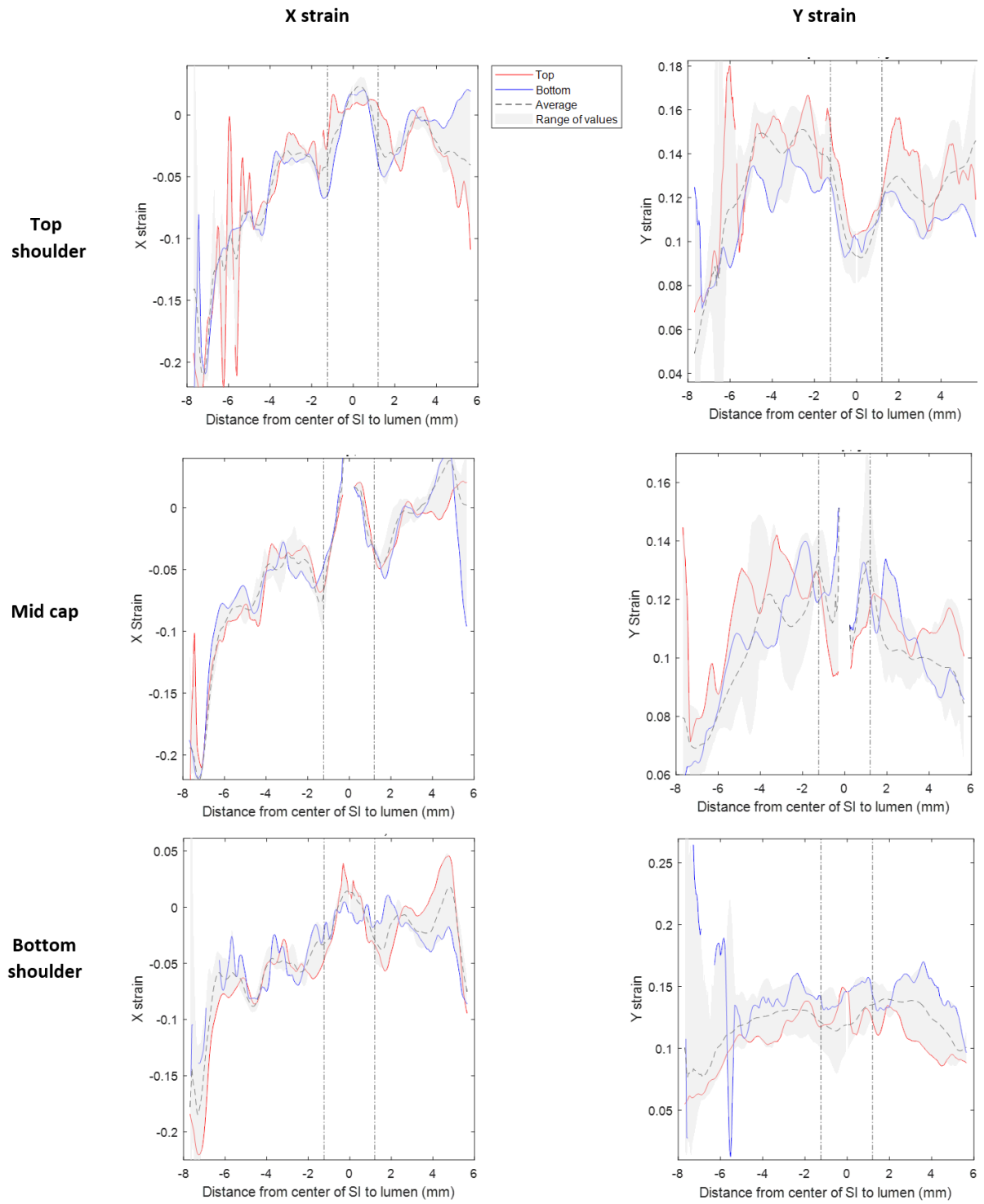


Figure E.24: Static construct tested in commercial clamps (1/1)

## E.5 Scatter plots: average X-Y regional strain

The scatter plots displayed below represent the average  $\epsilon_{xx}$  and  $\epsilon_{yy}$  values in each of the 8 regions for each construct.

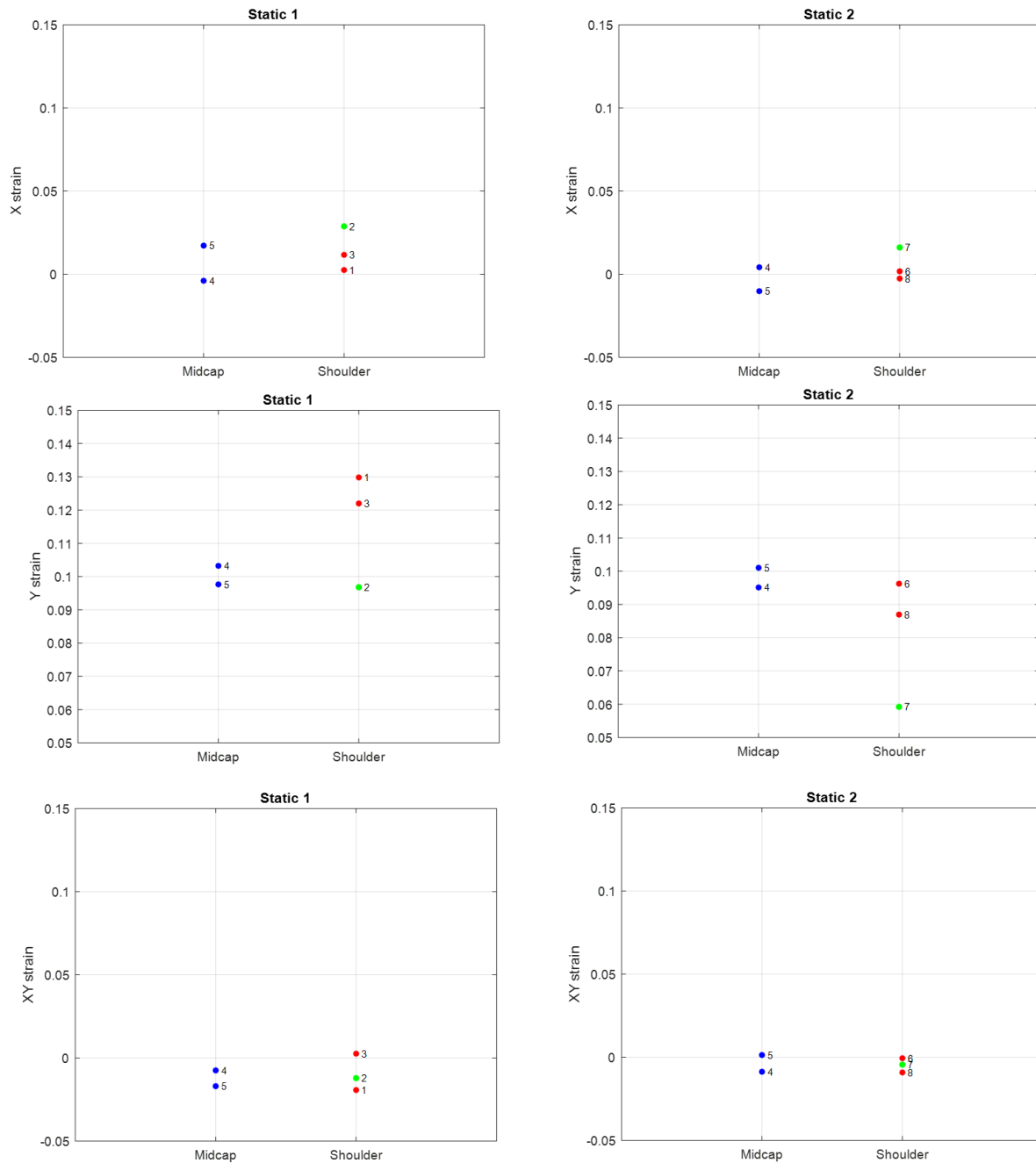


Figure E.25: Static constructs

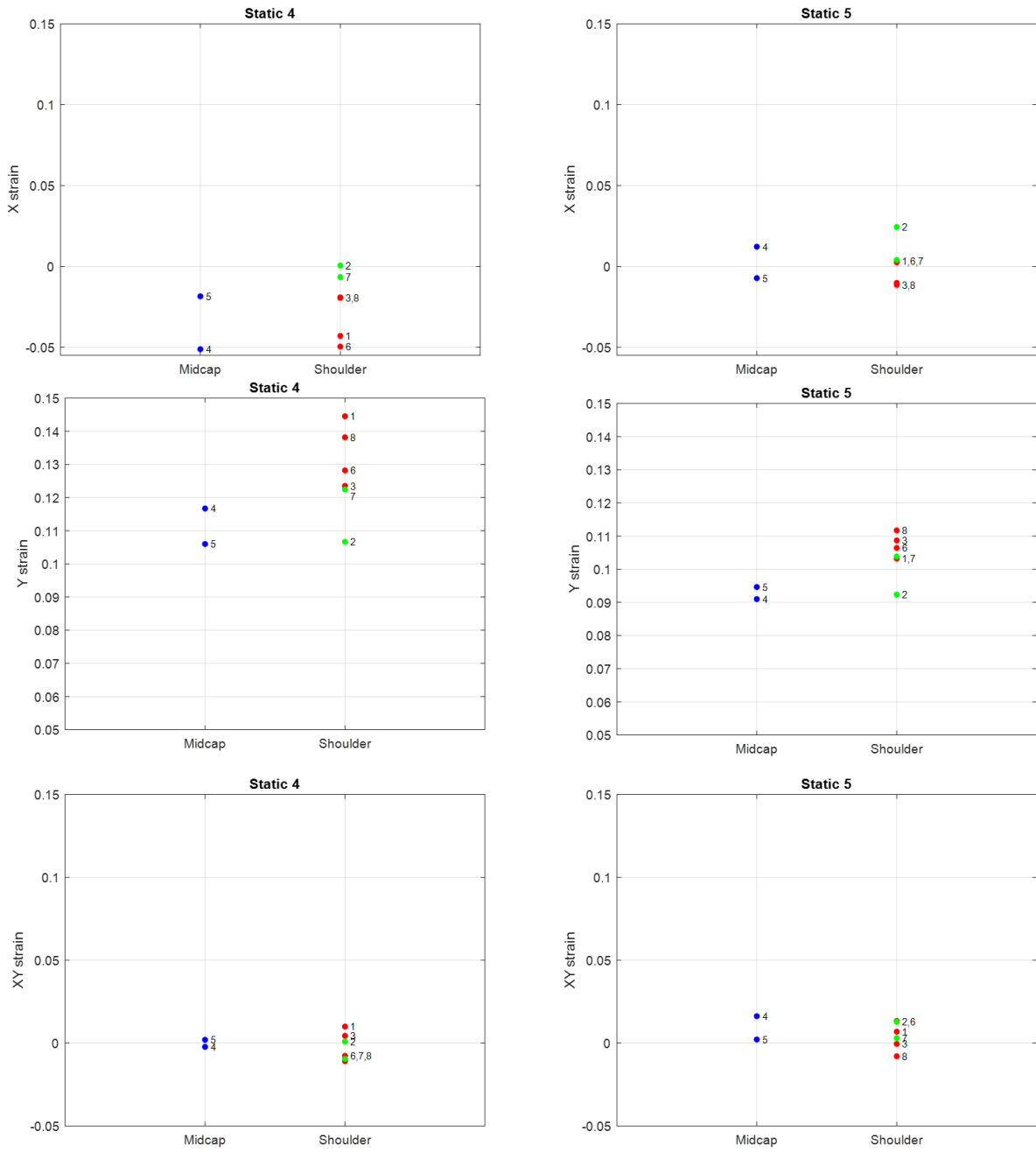


Figure E.26: Static constructs

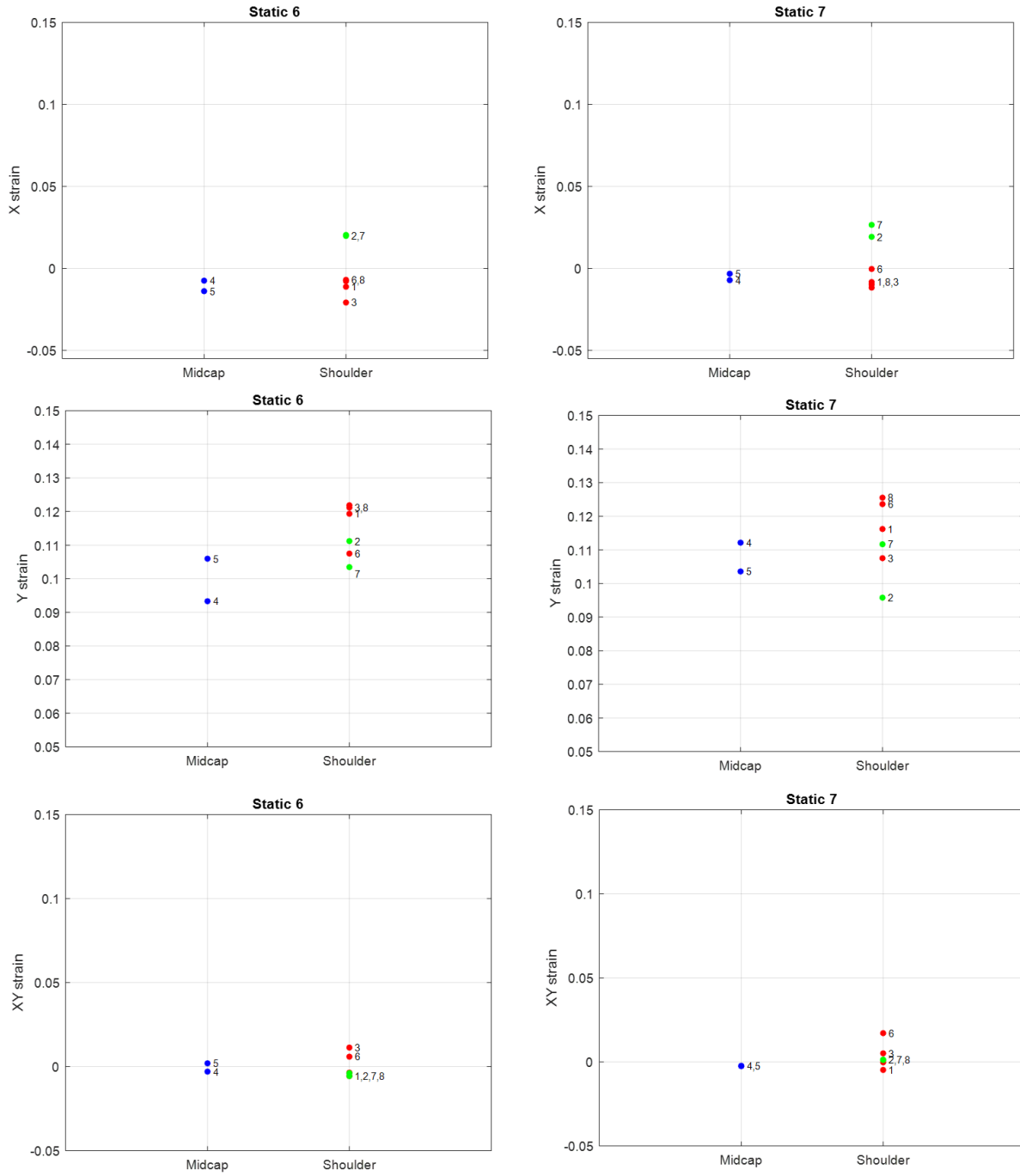


Figure E.27: Static constructs

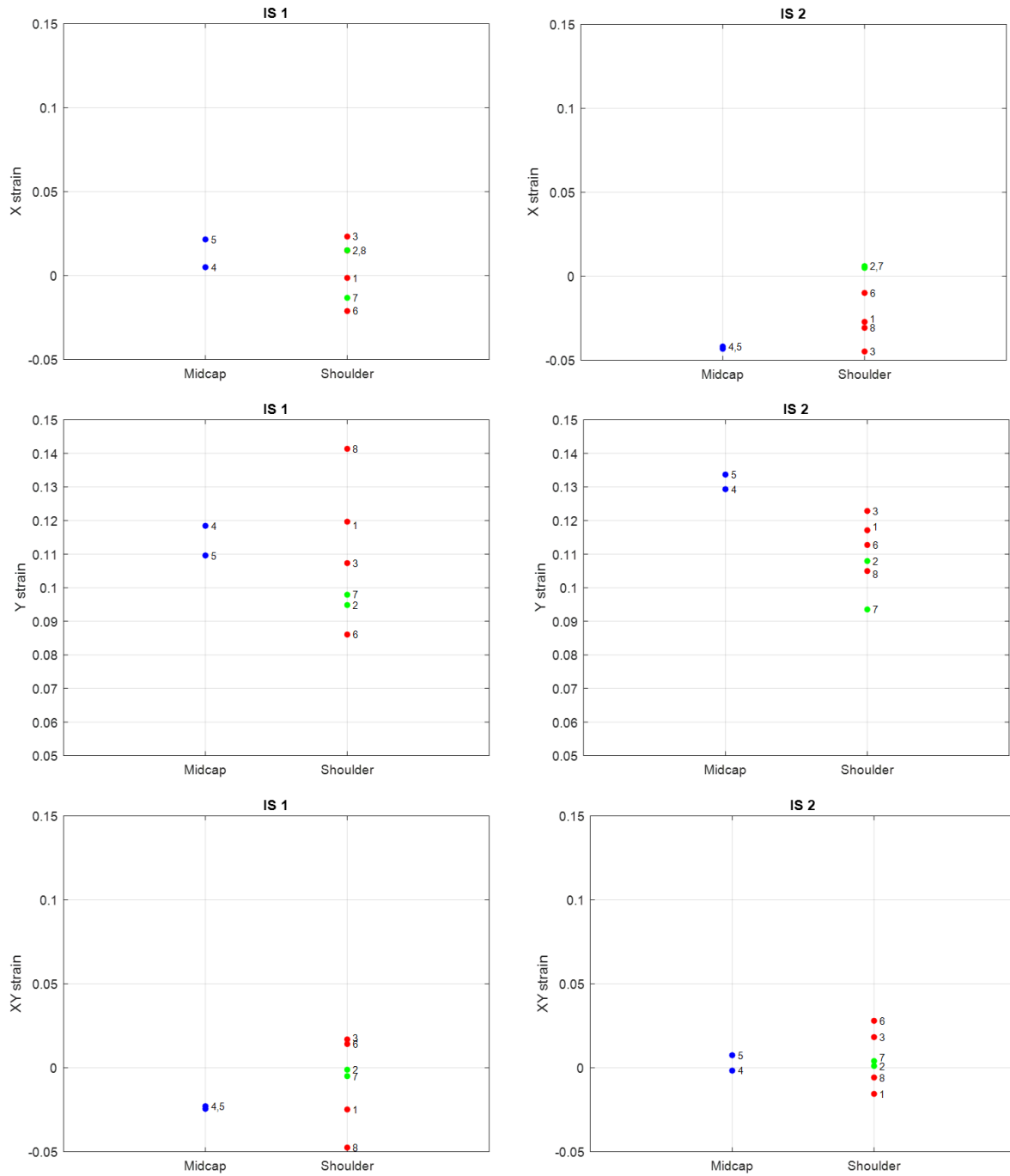


Figure E.28: IS constructs

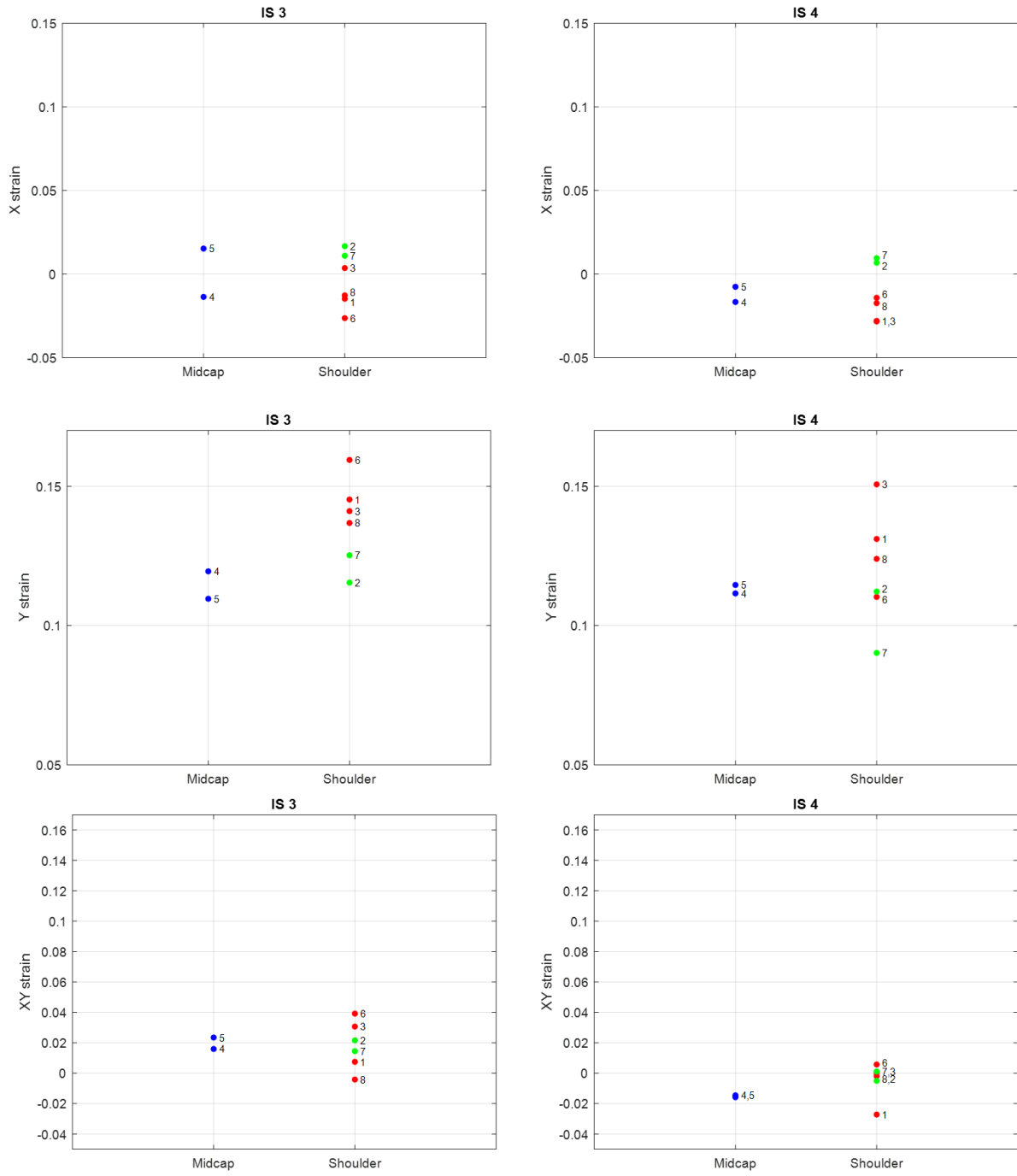
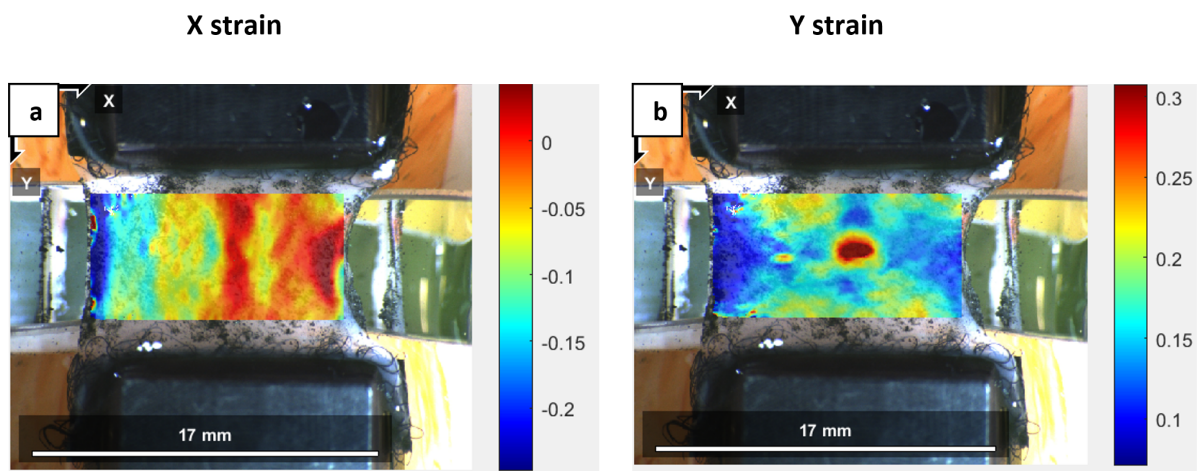


Figure E.29: IS constructs

## E.6 DIC analysis: SI region example

There were only two constructs that had a good correlation in the SI region ( $<0.7$ ), therefore analysis including the SI was not performed. Figure E.30 shows an example of the  $\epsilon_{xx}$  and  $\epsilon_{yy}$  maps of a construct which included the SI region before rupture. It can be seen that the  $\epsilon_{yy}$  is highest in the SI region and high  $\epsilon_{xx}$  values (tension) are seen within this region as well, with X compression occurring at the immediate left and right sides of the SI, following the same trend seen previously. This can possibly show that both X and Y strain play an important role in rupture at the interface between the SI and tissue.



**Figure E.30:** Static construct tested with commercial clamps including the SI region: a)  $\epsilon_{xx}$  map b)  $\epsilon_{yy}$  map

# F

## Matlab code

Appendix E includes the MATLAB code created in this study to perform analysis.

### F.1 Tissue Culture Analysis

#### F.1.1 Plotting average compaction

```
1 % The following code plots the average compaction in the X,Y,Z
   directions
2 % for both the static and IS constructs
3
4 X_Stat= -16.35;    % average values were calculated in Excel and
   imported
5 X_IS= -46.92;
6
7 Y_Stat= -12.52;
8 Y_IS= -2.05;
9
10 Z_Stat= -80.94;
11 Z_IS= -75.0;
12
13 X_Stat_sd= 6.07;    % standard deviation values were calculated
   in Excel and imported
14 X_IS_sd= 3.74;
15
```

```
16 Y_Stat_sd= 9.96;
17 Y_IS_sd= 6.67;
18
19 Z_Stat_sd= 3.92;
20 Z_IS_sd= 1.56;
21
22 figure(1)
23 % Plot X
24 x = 0.33 * ones(1, length(X_Stat));
25 plot(x, X_Stat, 'b.', 'MarkerSize', 12, 'LineWidth', 3); hold on
26 plot(x, X_IS, 'r.', 'MarkerSize', 12, 'LineWidth', 3);
27 errorbar(x, X_Stat, X_Stat_sd, 'b')
28 errorbar(x, X_IS, X_IS_sd, 'r')
29 grid on;
30 hold on;
31 % Plot Y
32 x = 0.66 * ones(1, length(Y_Stat));
33 plot(x, Y_Stat, 'b.', 'MarkerSize', 12, 'LineWidth', 3); hold on
34 plot(x, Y_IS, 'r.', 'MarkerSize', 12, 'LineWidth', 3); hold on
35 errorbar(x, Y_Stat, Y_Stat_sd, 'b')
36 errorbar(x, Y_IS, Y_IS_sd, 'r')
37 % Plot Z
38 x = 1 * ones(1, length(Z_Stat));
39 plot(x, Z_Stat, 'b.', 'MarkerSize', 12, 'LineWidth', 3); hold on
40 plot(x, Z_IS, 'r.', 'MarkerSize', 12, 'LineWidth', 3);
41 errorbar(x, Z_Stat, Z_Stat_sd, 'b')
42 errorbar(x, Z_IS, Z_IS_sd, 'r')
43 % Set up axes.
44 xlim([0, 1.33]);
45 ylim([-100, 10]);
46 ylabel('Average Compaction %');
47 ax = gca;
48 ax.XTick = [0.33, 0.66, 1];
49 ax.XTickLabels = {'X', 'Y', 'Z'};
50 grid on;
51 legend('Static', 'IS')
```

## F.2 DIC Parameter Analysis

### F.2.1 Subset size and strain radius selection

```
1 % This script plots the X-Y displacements and X-Y
2 % strains across the construct at one horizontal
3 % section and compares the subset sizes and strain
4 % radius sizes by calculating the average differences between
   each
5
6 %load analysis data with subset sizes 15,25,35,45,55
7
8 A = load ( 'sample#_subset15.mat' );
9 % load X-Y (u-v) displacement data
10 B= A.data_dic_save.displacements.plot_u_dic;
11 C= A.data_dic_save.displacements.plot_v_dic;
12 % determine section to investigate & convert pixels to mm
13 u_15 = B(279,151:263)*0.0093;
14 v_15 = C(279,151:263)*0.0093;
15
16 G = load ( 'sample#_subset25.mat' );
17 H= G.data_dic_save.displacements.plot_u_dic;
18 I= G.data_dic_save.displacements.plot_v_dic;
19 u_25 = H(279,151:263)*0.0093;
20 v_25 = I(279,151:263)*0.0093;
21
22 G = load ( 'sample#_subset35.mat' );
23 H= G.data_dic_save.displacements.plot_u_dic;
24 I= G.data_dic_save.displacements.plot_v_dic;
25 u_35 = H(279,151:263)*0.0093;
26 v_35 = I(279,151:263)*0.0093;
27
28 G = load ( 'sample#_subset45.mat' );
29 H= G.data_dic_save.displacements.plot_u_dic;
30 I= G.data_dic_save.displacements.plot_v_dic;
31 u_45 = H(279,151:263)*0.0093;
32 v_45 = I(279,151:263)*0.0093;
33
34 G = load ( 'sample#_subset55.mat' );
35 H= G.data_dic_save.displacements.plot_u_dic;
36 I= G.data_dic_save.displacements.plot_v_dic;
37 u_55 = H(279,151:263)*0.0093;
38 v_55 = I(279,151:263)*0.0093;
39
```

```

40 %load analysis data with strain radius(sr) 3,5,7,15
41
42 J = load ('sample#_subset35_sr3.mat');
43 % load X-Y strain data
44 K= J.data_dic_save.strains.plot_exx_ref_formatted;
45 L= J.data_dic_save.strains.plot_eyy_ref_formatted;
46 exx_35_3_3 = K(279,151:263);
47 eyy_35_3_3 = L(279,151:263);
48
49 M = load ('sample#_subset35_sr5.mat');
50 N= M.data_dic_save.strains.plot_exx_ref_formatted;
51 O= M.data_dic_save.strains.plot_eyy_ref_formatted;
52 exx_35_3_5 = N(279,151:263);
53 eyy_35_3_5 = O(279,151:263);
54
55 P = load ('sample#_subset35_sr7.mat');
56 Q= P.data_dic_save.strains.plot_exx_ref_formatted;
57 R= P.data_dic_save.strains.plot_eyy_ref_formatted;
58 exx_35_3_7 = Q(279,151:263);
59 eyy_35_3_7 = R(279,151:263);
60
61 P = load ('sample#_subset35_sr15.mat');
62 Q= P.data_dic_save.strains.plot_exx_ref_formatted;
63 R= P.data_dic_save.strains.plot_eyy_ref_formatted;
64 exx_35_3_15 = Q(279,151:263);
65 eyy_35_3_15 = R(279,151:263);
66
67 x1 = (1:113); %determine how many x values
68
69 %Plot the X-Y displacement and strains , comparing parameter
    sizes
70
71 figure (1)
72 plot (x1,u_15,'b',x1,u_25,'g',x1,u_35,'r',x1,u_45,'c',x1,u_55,'k
    ');
73 xlabel ('Lumen to soft inclusion')
74 ylabel('X displacement (mm)')
75 legend ('Subset=15','Subset=25','Subset=35','Subset=45','Subset
    =55')
76
77 figure (2)
78 plot (x1,v_15,'b',x1,v_25,'g',x1,v_35,'r',x1,v_45,'c',x1,v_55,'k
    ');
79 xlabel ('Lumen to soft inclusion')

```

```

80 ylabel('Y displacement (mm)')
81 legend('Subset=15','Subset=25','Subset=35','Subset=45','Subset
      =55')
82
83 figure(3)
84 plot(x1,exx_35_3_3,'b',x1,exx_35_3_5,'g',x1,exx_35_3_7,'r',x1,
      exx_35_3_15,'k');
85 xlabel('Lumen to soft inclusion')
86 ylabel('Exx')
87 legend('SR=3','SR=5','SR=7','SR=15')
88
89 figure(4)
90 plot(x1,eyy_35_3_3,'b',x1,eyy_35_3_5,'g',x1,eyy_35_3_7,'r',x1,
      eyy_35_3_15,'k');
91 xlabel('Lumen to soft inclusion')
92 ylabel('Eyy')
93 legend('SR=3','SR=5','SR=7','SR=15')
94
95 % Calculate the average difference between curves
96
97 % X displacement
98 PDif = u_25-u_15; %difference between subset size 15 & 25
99 PDif = abs(PDif); %absolute values taken from matrix
100 Pdif_uavg_15_25 = mean(PDif); %average determined
101
102 PDif = u_35-u_25;
103 PDif = abs(PDif);
104 Pdif_uavg_25_35 = mean(PDif);
105
106 PDif = u_45-u_35;
107 PDif = abs(PDif);
108 Pdif_uavg_35_45 = mean(PDif);
109
110 PDif = u_55-u_45;
111 PDif = abs(PDif);
112 Pdif_uavg_45_55 = mean(PDif);
113
114 % Y displacement
115 PDif = v_25-v_15;
116 PDif = abs(PDif);
117 Pdif_vavg_15_25 = mean(PDif);
118
119 PDif = v_35-v_25;
120 PDif = abs(PDif);

```

```
121 Pdif_vavg_25_35 = mean(PDif);
122
123 PDif = v_45-v_35;
124 PDif = abs(PDif);
125 Pdif_vavg_35_45 = mean(PDif);
126
127 PDif = v_55-v_45;
128 PDif = abs(PDif);
129 Pdif_vavg_45_55 = mean(PDif);
130
131 % X strain
132 PDif = exx_35_3_3-exx_35_3_5;
133 PDif = abs(PDif);
134 Pdif_xavg_3_5 = mean(PDif);
135
136 PDif = exx_35_3_5-exx_35_3_7;
137 PDif = abs(PDif);
138 Pdif_xavg_5_7 = mean(PDif);
139
140 PDif = exx_35_3_7-exx_35_3_15;
141 PDif = abs(PDif);
142 Pdif_xavg_7_15 = mean(PDif);
143
144 % Y strain
145 PDif = eyy_35_3_3-eyy_35_3_5;
146 PDif = abs(PDif);
147 Pdif_yavg_3_5 = mean(PDif);
148
149 PDif = eyy_35_3_5-eyy_35_3_7;
150 PDif = abs(PDif);
151 Pdif_yavg_5_7 = mean(PDif);
152
153 PDif = eyy_35_3_7-eyy_35_3_15;
154 PDif = abs(PDif);
155 Pdif_yavg_7_15 = mean(PDif);
```

## F.2.2 2D correlation coefficient maps

```
1 %% Creating 2D Correlation Coefficient Color-coded Plots
2
3 % 0<CC<=0.5 is strong correlation (green),
4 % 0.5<CC<=0.7 is moderate correlation (blue),
5 % 0.7<CC<1.0 is weak correlation (yellow),
6 % 1.0<=CC is bad data (red),
7 % CC=0 is background (white)
8
9 % Sample #
10
11 CC = load ('sample#-subset#.mat'); %load analysis data
12 %load correlation coefficient data
13 CC= CC.data_dic_save.displacements.plot_corrcoef_dic;
14 %create color codes
15 rgb = [0,1,0; 0,0,1; 1,1,0; 1,0,0; 1,1,1];
16 %assign colors to correlation coefficient ranges
17 idx = 1*(0<CC & CC<=0.5) + 2*(0.5<CC & CC<=0.7) ...
18       +3*(0.7<CC & CC<1.0)+4*(1.0<=CC) +5*(CC==0);
19 idx(CC==0) = 5; %assign a white background
20 image(idx) %create color map
21 colormap(rgb)
```

## F.3 Data Analysis

### F.3.1 Determining the image for each construct at 10% average mid cap Y strain

```

1 % This script finds the image # of a construct where the average
  % Y strain=10%
2 % within a certain defined mid cap region in order to run
  % analysis and
3 % normalize the clamp regions
4
5 % To define this mid cap region, the rows and columns were
  % selected from the
6 % displacement mask output from Ncorr. The region's side
  % boundaries were
7 % selected as 20% from the edges, using the top and bottom of
  % the SI as the
8 % top/bottom boundaries
9
10
11 % load the Ncorr output file
12 A = load ('sample#.mat');
13
14 % load the Y strains per pixel for all images (i.e.389) until
  % rupture
15 for i=1:389
16 E{i}= A.data_dic_save.strains(i).plot_eyy_ref_formatted;
17 end
18
19 % Create the region in each image (cut the matrices)
20 AMCR = cell(size(389));
21 for i=1:389
22     E{1,i}(256:312, 350:404);           % example of box
  % boundaries
23     AMCR{: , i} = ans;
24 end
25
26 % nan all zeroes to calculate mean
27 for i=1:389
28     AMCR{1, i}(AMCR{1, i}==0)=nan;
29 end
30
31 for i=1:389
32     a{1, i} = mean(AMCR{1, i}, 'omitnan'); % take mean of all

```

```

33     rows
        a2{1,i} = mean(a{1,i}, 'omitnan'); % take mean of all
        columns
34 end
35
36 a2=cell2mat(a2); % convert cell to
    array
37 val = 0.1000; % interested in 10% Y
    strain
38 [ d, ix ] = min( abs( a2-val ) ); % find the image #
    closest to 0.1
39 a2(ix-1:ix+1); % ix = image #
    closest to 0.1
40 ix_value = a2(ix); % ix_value = actual y
    strain at ix
41
42 % Plot image # vs average Y strain for all constructs (mark 10%
    Y strain)
43 x = 1:length(a2); hold on
44 plot (x, a2, 'k');
45 ylabel('Average Y strain')
46 xlabel('Image #')
47 title({'Midcap region w/ most homogenous strain pattern', '(20%
    away from edges/SI)'}))
48 ylim ([0 0.45]);
49 legend ('Static 1', 'Static 2', 'Static 3', 'Static 4', 'IS 1', 'IS 2
    ', 'IS 3', 'IS 4', 'location', 'northeastoutside')
50 plot(ix, ix_value, 'k.', 'HandleVisibility', 'off'); hold on
51 text(ix-30, ix_value+0.025, 'x=81', 'FontSize', 7)

```

### F.3.2 Plotting the average $\epsilon_{xx}$ , $\epsilon_{yy}$ and $\epsilon_{xy}$ values across the width of the constructs

```

1 % This script plots the average X, Y and XY strain across the
    width of the
2 % construct with the origin at the center of the SI
3
4 A = load ('sample#.mat'); % load the Ncorr output file
5
6 % Mid cap region
7
8 % Right side
9 % load X (and Y: eyy) strains per pixel for the pre-determined

```

```

    image # for this
10 % construct 's analysis (i.e. 175)
11 D= A.data_dic_save.strains(175).plot_exx_ref_formatted;
12
13 F = D(213:268, 335:410);           % determine boundaries of
    region
14 F(F==0)=nan;                       % nan all zeroes to calculate
    average
15 avg = mean(F, 'omitnan');           % calculate the averages for
    each column
16
17 % set the X axis values
18 Xf= (75/25);
19 x_avg = linspace((1/25),Xf,length(avg));
20
21 % plot the strain values (with center of SI=0)
22 plot (x_avg,avg, 'b', 'LineWidth',2); hold on
23 ylabel('X strain')
24 xlabel('Distance from center of SI to lumen (mm)')
25 % title('IS 2- mid cap, x strain averages')
26 ylim ([-0.1 0.14]);
27 legend ('Right side','Left side','location','northeastoutside')
28
29 D= A.data_dic_save.strains(175).plot_exx_ref_formatted;
30
31 F_2 = D(213:268, 410:459);
32 F_2(F_2==0)=nan;
33 Avg = mean(F_2, 'omitnan');
34
35 Xf_2= (124/25);
36 x_Avg = linspace((75/25),Xf_2,length(Avg));
37
38 plot (x_Avg,Avg, 'b', 'LineWidth',2, 'HandleVisibility','off');
    hold on
39 legend ('Right side','Left side','location','northeastoutside')
40
41 % Left side
42 D= A.data_dic_save.strains(175).plot_exx_ref_formatted;
43
44 % flip the data to represent it on the left side of the SI
45 F = fliplr(D(213:268, 258:335));
46 F(F==0)=nan;
47 avg = mean(F, 'omitnan');
48

```

```

49 Xf= (77/25);
50 x_avg = linspace((1/25),Xf,length(avg));
51 x_avg=-x_avg;
52
53 plot (x_avg,avg,'r','LineWidth',2); hold on
54 legend ('Right side','Left side','location','northeastoutside')
55
56 D= A.data_dic_save.strains(175).plot_exx_ref_formatted;
57
58 F_2 = fliplr(D(213:268, 207:258));
59 F_2(F_2==0)=nan;
60 Avg = mean(F_2,'omitnan');
61
62 Xf_2= (128/25);
63 x_Avg = linspace((77/25),Xf_2,length(Avg));
64 x_Avg=-x_Avg;
65
66 % Plot the right and left side mid cap average values along
    construct
67 plot (x_Avg,Avg,'r','LineWidth',2,'HandleVisibility','off')
68 legend ('Right side','Left side','location','northeastoutside')
69 x1= xline(1.04,'k-','HandleVisibility','off'); % 30/25, SI
    region
70 x2= xline(-1.08,'k-','HandleVisibility','off'); % 30/25, SI
    region
71
72 %% Shoulder region
73
74 % Right top
75 D= A.data_dic_save.strains(175).plot_exx_ref_formatted;
76
77 F = D(126:212, 335:410);
78 F(F==0)=nan;
79 avg = mean(F,'omitnan');
80
81 Xf= (75/25);
82 x_avg = linspace((1/25),Xf,length(avg));
83
84 plot (x_avg,avg,'b','LineWidth',2); hold on
85 ylabel('X strain')
86 xlabel('Distance from center of SI to lumen (mm)')
87 % title('IS 2- shoulder regions, x strain averages')
88 ylim ([-0.1 0.14]);
89 legend ('Top right side','Top left side','Bottom right side',

```

```

    Bottom left side', 'location', 'northeastoutside')
90
91 D= A.data_dic_save.strains(175).plot_exx_ref_formatted;
92
93 F_2 = D(126:212, 410:459);
94 F_2(F_2==0)=nan;
95 Avg = mean(F_2, 'omitnan');
96
97 Xf_2= (124/25);
98 x_Avg = linspace((75/25), Xf_2, length(Avg));
99
100 plot (x_Avg, Avg, 'b', 'LineWidth', 2, 'HandleVisibility', 'off');
    hold on
101 legend ('Top right side', 'Top left side', 'Bottom right side', '
    Bottom left side', 'location', 'northeastoutside')
102
103 % Left top
104 D= A.data_dic_save.strains(175).plot_exx_ref_formatted;
105
106 F = fliplr(D(126:212, 258:335));
107 F(F==0)=nan;
108 avg = mean(F, 'omitnan');
109
110 Xf= (77/25);
111 x_avg = linspace((1/25), Xf, length(avg));
112 x_avg= -x_avg;
113
114 plot (x_avg, avg, 'r', 'LineWidth', 2); hold on
115 legend ('Top right side', 'Top left side', 'Bottom right side', '
    Bottom left side', 'location', 'northeastoutside')
116
117 % Left top
118 D= A.data_dic_save.strains(175).plot_exx_ref_formatted;
119
120 F_2 = fliplr(D(126:212, 207:258));
121 F_2(F_2==0)=nan;
122 Avg = mean(F_2, 'omitnan');
123
124 Xf_2= (128/25);
125 x_Avg = linspace((77/25), Xf_2, length(Avg));
126 x_Avg= -x_Avg;
127
128 plot (x_Avg, Avg, 'r', 'LineWidth', 2, 'HandleVisibility', 'off');
    hold on

```

```

129 legend ('Top right side', 'Top left side', 'Bottom right side',
          'Bottom left side', 'location', 'northeastoutside')
130
131
132 % Right bottom
133 D= A.data_dic_save.strains(175).plot_exx_ref_formatted;
134
135 F = D(269:371, 335:410);
136 F(F==0)=nan;
137 avg = mean(F, 'omitnan');
138
139 Xf= (75/25);
140 x_avg = linspace((1/25), Xf, length(avg));
141
142 plot (x_avg, avg, 'k', 'LineWidth', 2); hold on
143 legend ('Top right side', 'Top left side', 'Bottom right side',
          'Bottom left side', 'location', 'northeastoutside')
144
145 D= A.data_dic_save.strains(175).plot_exx_ref_formatted;
146
147 F_2 = D(269:371, 410:459);
148 F_2(F_2==0)=nan;
149 Avg = mean(F_2, 'omitnan');
150
151 Xf_2= (124/25);
152 x_Avg = linspace((75/25), Xf_2, length(Avg));
153
154 plot (x_Avg, Avg, 'k', 'LineWidth', 2, 'HandleVisibility', 'off');
      hold on
155 legend ('Top right side', 'Top left side', 'Bottom right side',
          'Bottom left side', 'location', 'northeastoutside')
156
157 % Left bottom
158 D= A.data_dic_save.strains(175).plot_exx_ref_formatted;
159
160 F = fliplr(D(269:371, 258:335));
161 F(F==0)=nan;
162 avg = mean(F, 'omitnan');
163
164 Xf= (77/25);
165 x_avg = linspace((1/25), Xf, length(avg));
166 x_avg= -x_avg;
167
168 plot (x_avg, avg, 'g', 'LineWidth', 2); hold on

```

```

169 legend ('Top right side', 'Top left side', 'Bottom right side',
          'Bottom left side', 'location', 'northeastoutside')
170
171 D= A.data_dic_save.strains(175).plot_exx_ref_formatted;
172
173 F_2 = fliplr(D(269:371, 207:258));
174 F_2(F_2==0)=nan;
175 Avg = mean(F_2, 'omitnan');
176
177 Xf_2= (128/25);
178 x_Avg = linspace((77/25), Xf_2, length(Avg));
179 x_Avg= -x_Avg;
180
181 % plot the top right and left shoulders and bottom right and
          left shoulders
182 plot (x_Avg, Avg, 'g', 'LineWidth', 2, 'HandleVisibility', 'off')
183 legend ('Top right side', 'Top left side', 'Bottom right side',
          'Bottom left side', 'location', 'northeastoutside')
184 x1= xline(1.04, 'k-', 'HandleVisibility', 'off'); % add lines to
          define the sides of the SI
185 x2= xline(-1.08, 'k-', 'HandleVisibility', 'off');

```

### F.3.3 Determining the average $\epsilon_{xx}$ , $\epsilon_{yy}$ and $\epsilon_{xy}$ values for the 8 regions

```

1 % This script determines the average X, Y and XY strain values
  of each of the
2 % 8 regions and plots these values to compare
3
4 % The rows/columns of the sections were determined manually from
  the
5 % displacement mask output from Ncorr (1-8 regions)
6
7 A = load ('sample#.mat'); % load the Ncorr output file
8
9 % load the X ("exx") and Y ("eyy") strains per pixel for the pre
  -determined
10 %image # for this construct's analysis (i.e. 175)
11 D= A.data_dic_save.strains(175).plot_exx_ref_formatted;
12
13 % find the average for each of the 8 regions
14 D1= D(126:212, 258:308); % boundaries of the region
15 D1(D1==0)=nan; % nan all zeroes to calculate

```

```

    averages
16 D1 = mean(D1, 'omitnan');      % take mean of all rows
17 D1 = mean(D1, 'omitnan');      % take mean of columns
18
19 D2= D(126:212, 308:361);
20 D2(D2==0)=nan;
21 D2 = mean(D2, 'omitnan');
22 D2 = mean(D2, 'omitnan');
23
24 D3= D(126:212, 361:410);
25 D3(D3==0)=nan;
26 D3 = mean(D3, 'omitnan');
27 D3 = mean(D3, 'omitnan');
28
29 D4= D(213:268, 258:308);
30 D4(D4==0)=nan;
31 D4 = mean(D4, 'omitnan');
32 D4 = mean(D4, 'omitnan');
33
34 D5= D(213:268, 361:410);
35 D5(D5==0)=nan;
36 D5 = mean(D5, 'omitnan');
37 D5 = mean(D5, 'omitnan');
38
39 D6= D(269:371, 258:308);
40 D6(D6==0)=nan;
41 D6 = mean(D6, 'omitnan');
42 D6 = mean(D6, 'omitnan');
43
44 D7= D(269:371, 308:361);
45 D7(D7==0)=nan;
46 D7 = mean(D7, 'omitnan');
47 D7 = mean(D7, 'omitnan');
48
49 D8= D(269:371, 361:410);
50 D8(D8==0)=nan;
51 D8 = mean(D8, 'omitnan');
52 D8 = mean(D8, 'omitnan');
53
54 % Plot the averages of each of the 8 regions
55 figure(1)
56 % Plot mid cap region averages
57 Midcap = [D4,D5];
58 x1 = 0.5 * ones(1, length(Midcap));

```

```

59 plot(x1, Midcap, 'b*', 'MarkerSize', 4, 'LineWidth', 3);
60 grid on;
61 hold on;
62 % Plot shoulder region averages
63 Shoulder = [D1,D3, D6, D8];
64 T_B= [D2,D7];
65 x = 1 * ones(1, length(Shoulder));
66 x2 = 1*ones(1, length(T_B));
67 plot(x, Shoulder, 'r*', 'MarkerSize', 4, 'LineWidth', 3);hold on
68 plot(x2, T_B, 'g*', 'MarkerSize', 4, 'LineWidth', 3);
69 xlim([0, 1.5]);
70 ylim([-0.05, 0.15]);
71 ylabel('X strain'); % do the same for the Y strains
72 title('IS 2');
73 ax = gca;
74 ax.XTick = [0.5, 1];
75 ax.XTickLabels = {'Midcap', 'Shoulder'};
76 grid on;
77
78 % Add the region# next to each point
79 text(1+0.02,D1,'1', 'FontSize', 8)
80 text(1+0.02,D2,'2', 'FontSize', 8)
81 text(1+0.02,D3,'3', 'FontSize', 8)
82 text(1+0.02,D6,'6', 'FontSize', 8)
83 text(1+0.02,D7,'7', 'FontSize', 8)
84 text(1+0.02,D8,'8', 'FontSize', 8)
85 text(0.5+0.02,D4,'4', 'FontSize', 8)
86 text(0.5+0.02,D5,'5', 'FontSize', 8)

```

### F.3.4 Plotting the actuator Y displacement vs Y force and calculating the tangential stiffness for each construct

```

1 % This script plots the actuator Y displacement vs Y force
  % extracted from
2 % the Excel files for each construct
3
4 % extract the specific rows/columns from each Excel file
5 S_1=xlsread('Static_1.xlsx','G907:I1300');
6 S_1(:,2) = [];
7
8 S_2=xlsread('Static_2.xlsx','G907:I1212');
9 S_2(:,2) = [];
10

```

```

11 S_3=xlsread('Static_3.xlsx','G909:I1301');
12 S_3(:,2) = [];
13
14 S_4=xlsread('Static_4.xlsx','G907:I1509');
15 S_4(:,2) = [];
16
17 S_5=xlsread('Static_5.xlsx','G907:I1256');
18 S_5(:,2) = [];
19
20 S_6=xlsread('Static_6.xlsx','G907:I1109');
21 S_6(:,2) = [];
22
23 S_7=xlsread('Static_7.xlsx','G907:I1197');
24 S_7(:,2) = [];
25
26 IS_1=xlsread('IS_1.xlsx','G907:I1228');
27 IS_1(:,2) = [];
28
29 IS_2=xlsread('IS_2.xlsx','G907:I1138');
30 IS_2(:,2) = [];
31
32 IS_3=xlsread('IS_3.xlsx','G908:I1380');
33 IS_3(:,2) = [];
34
35 IS_4=xlsread('IS_4.xlsx','G908:I1255');
36 IS_4(:,2) = [];
37
38 % plot the graphs for the static constructs
39 figure(1)
40 plot(S_1(:,1),S_1(:,2),'k',S_2(:,1),S_2(:,2),'r',S_4(:,1),S_4
    (:,2),'r—',S_3(:,1),S_3(:,2),'k',S_5(:,1),S_5(:,2),'r—',S_6
    (:,1),S_6(:,2),'r—',S_7(:,1),S_7(:,2),'r—'); hold on
41 hold on
42 ylabel('Y force (mN)')
43 xlabel('Actuator Y displacement (um)')
44 title('Static Constructs')
45 xlim([0 3500]);
46 ylim([0 3500]);
47 legend('Static_{new, SI rupture}','Static_{new, clamp rupture}'
    , 'Static_{old, clamp rupture}','location','northwest')
48 % add marker to the point where average Y strain in mid cap =
    10%
49 x = [527 614 230 1445];
50 y = [342 424 13 611];

```

```

51 plot(x,y,'k.','MarkerSize',10,'HandleVisibility','off')
52
53 % plot the graphs for the IS constructs
54 figure(2)
55 plot (IS_2(:,1),IS_2(:,2),'k—',IS_1(:,1),IS_1(:,2),'r—',IS_3
    (:,1),IS_3(:,2),'r—',IS_4(:,1),IS_4(:,2),'k—'); hold on
56 hold on
57 ylabel('Y force (mN)')
58 xlabel('Actuator Y displacement (um)')
59 title('Intermittently Strained Constructs')
60 xlim ([0 3500]);
61 ylim ([0 3500]);
62 legend ('IS_{old, SI rupture}','IS_{old, clamp rupture}','
    location','northwest')
63 x = [1396 1682 1784 2166];
64 y = [408 719 652 1108];
65 plot(x,y,'k.','MarkerSize',10,'HandleVisibility','off')
66
67 % plot all constructs on one graph
68 figure(3)
69 plot (S_1(:,1),S_1(:,2),'k',S_4(:,1),S_4(:,2),'k—',S_2(:,1),S_2
    (:,2),'k',S_3(:,1),S_3(:,2),'k',IS_1(:,1),IS_1(:,2),'r—',
    IS_2(:,1),IS_2(:,2),'r—',IS_3(:,1),IS_3(:,2),'r—',IS_4(:,1)
    ,IS_4(:,2),'r—',S_5(:,1),S_5(:,2),'k—',S_6(:,1),S_6(:,2),'k
    —',S_7(:,1),S_7(:,2),'k—'); hold on
70 hold on
71 ylabel('Y force (mN)')
72 xlabel('Actuator Y displacement (um)')
73 title('New vs old clamps')
74 xlim ([0 3500]);
75 ylim ([0 3500]);
76 legend ('New clamps','Old clamps','location','northwest')
77 x = [527 614 230 1445 1396 1682 1784 2166 1274 1479 1471];
78 y = [342 424 13 611 408 719 652 1108 633 541 838];
79 plot(x,y,'k.','MarkerSize',10,'HandleVisibility','off')
80
81
82 %% Calculating the tangential stiffness for each construct
83 % at 10% average mid cap Y strain location
84
85 x = 1+S_1(:,1)/10000; % convert to stretch ratio from Y
    displacement
86 y = S_1(:,2)/4.6; % convert to kPa from Y force(mN): area
    = initial width*avg_thickness

```

```

87
88 % Derived 5 parameter mooney rivlin stress equation for strain
    energy density
89 %  $f(x) = 2*C10*(x-(1/x))+2*C01*(1-(1/x.^3))+6*C11*(x.^2-x$ 
     $-1+(1/x.^2)+(1/x.^3)-(1/x.^4))+4*C20*x*(1-(1/x.^3))*(x.^2+(2/$ 
     $x)-3)+4*C02*(2*x+(1/x.^2)-3)*(1-(1/x.^3))$ 
90 % Coefficients (with 95% confidence bounds):
91     C01 =      -3942
92     C02 =  1.009e+06
93     C10 =      5760
94     C11 = -1.797e+06
95     C20 =  7.994e+05
96
97 y_stretch = 342/4.6;
98 [ d, ix ] = min( abs(y-y_stretch ) );           % find the
    image # closest to 0.1000
99 y(ix-1:ix+1);                               % ix = image #
    closest to 0.1000
100 ix_value = y(ix); % stress @ 10%
101 stretch = x(82,1); % stretch @ 10 %
102
103 % differentiated Mooney Rivlin fit stress equation (TM:
    tangential modulus)
104 TM = 2.*C10 + (2.*C10)./stretch + (6.*C01 - 18.*C11 + 4.*C20
    .* (3.*stretch.^6 - 6.*stretch.^4 + 6)). ./stretch.^4 + 12.*C11.*
    stretch + (24.*C11)./stretch.^5 - (12.*C11)./stretch.^3 - 6.*
    C11 - 12.*C20 + (4.*C02.*(2.*stretch.^3 - 9.*stretch.^2 + 5))
    ./stretch.^6 + 8.*C02 ;

```

### F.3.5 Statistical analysis

```

1 % This script tests the (X, Y and XY strain) regional data sets
    for normality ,
2 % tests for homogenous variances , performs independent ttests ,
    and creates boxplots
3
4 S=xlsread('Section avgs.xlsx', 'B3:G32');      % extract the
    data sets from Excel file
5
6 alpha = 0.05;                                % Shapiro-Wilk
    test (test normality of each data set at p=0.05)
7 [H, pValue, W] = swtest(new_stat_MC, alpha)   % H = 0 :
    normal distribution , H = 1 : not normal

```

```

8
9 % Extract the cells for each regional data set
10 S=xlsread('Section avgs.xlsx','B3:J47');
11
12 % X strain
13
14 new_stat_MC = S(1:5,1); % normal, n=4
15 new_stat_MC(any(isnan(new_stat_MC),2), :) = [];
16
17 new_stat_SE = S(1:5,4); % normal, n=4
18 new_stat_SE(any(isnan(new_stat_SE),2), :) = [];
19
20 new_stat_TB = S(1:5,7); % n=2, no stats
    , low power
21 new_stat_TB(any(isnan(new_stat_TB),2), :) = [];
22
23 old_stat_MC = S(7:25,1); % n=8, normal
24 old_stat_MC(any(isnan(old_stat_MC),2), :) = [];
25
26 old_stat_SE = S(7:25,4); % not normal, n
    =16
27 old_stat_SE(any(isnan(old_stat_SE),2), :) = [];
28
29 old_stat_TB = S(7:25,7); % n=8, normal
30 old_stat_TB(any(isnan(old_stat_TB),2), :) = [];
31
32 IS_MC = S(27:45,1); % normal, n=8
33 IS_MC(any(isnan(IS_MC),2), :) = [];
34
35 IS_SE = S(27:45,4); % normal, n=16
36 IS_SE(any(isnan(IS_SE),2), :) = [];
37
38
39 %% Boxplots created for X, Y, and XY stain for the mid cap (left
    /right SI), shoulder, and top/bottom SI regions
40 %static_redesigned vs static_commercial (MC)
41 % equal variance?
42 X = [-0.0039 1;0.0172 1;0.042 1;-0.0102 1; -0.0512 2;-0.0185
    2;0.0122 2;-0.0072 2;-0.0075 2;-0.0139 2;-0.0072 2;-0.0033
    2];
43 Levenetest(X,alpha) % yes
44
45 group = [repmat({'First'}, 4, 1); repmat({'Second'}, 8, 1);
    repmat({'Third'}, 8, 1)];

```

```

46 boxplot([new_stat_MC;old_stat_MC;IS_MC],group,'Labels',{ 'Static
      (R), n=4', 'Static (C), n=8', 'IS (C), n=8'}, 'Whisker',1)
47 % title('Midcap region')
48 ylabel('Average X strain')
49 ylim([-0.06 0.06]);
50
51 [h,p] = ttest2(new_stat_MC,old_stat_MC) % P=0.085 (
      statistically comparable)
52
53 % static_commercial (MC) vs IS_commercial (MC)
54 X = [0.005 1;0.0215 1;-0.0418 1;-0.0432 1;-0.0137 1;0.0153
      1;-0.0167 1;-0.0076 1; -0.0512 2;-0.0185 2;0.0122 2;-0.0072
      2;-0.0075 2;-0.0139 2;-0.0072 2;-0.0033 2];
55 Levenetest(X,alpha) % yes
56 [h,p] = ttest2(old_stat_MC,IS_MC) % P=0.085 (statistically
      comparable)
57
58
59 %% static_new, static_old, IS (SE)
60 % equal variance?
61 X = [0.0025 1;0.0117 1;0.0018 1;-0.0026 1; -0.043 2;-0.0194
      2;-0.0496 2;-0.0192 2;0.0033 2;-0.0114 2;0.0025 2;-0.0102
      2;-0.0112 2;-0.0208 2;-0.0078 2;-0.007 2;-0.0083 2;-0.0117
      2;-3.80e-04 2;-0.0099 2; -0.0137 3;-0.0014 3;0.0233 3;-0.0211
      3;0.015 3;-0.0271 3;-0.0448 3;-0.01 3;-0.0307 3;-0.0147
      3;0.0036 3;-0.0264 3;-0.0128 3;-0.0283 3;-0.028 3;-0.0142
      3;-0.0174 3];
62 Levenetest(X,alpha) % yes
63
64 group = [ repmat({'First'}, 4, 1); repmat({'Second'}, 16, 1);
      repmat({'Third'}, 16, 1)];
65 boxplot([new_stat_SE;old_stat_SE;IS_SE],group,'Labels',{ 'Static
      (R), n=4', 'Static (C), n=16', 'IS (C), n=16'}, 'Whisker',1)
66 % title('Shoulder region')
67 ylabel('Average X strain')
68 ylim([-0.06 0.06]);
69
70 [h,p] = ttest2(new_stat_SE,old_stat_SE) % P=0.03 (
      statistically different, but old has few samples)
71 % [h,p] = ttest2(new_stat_SE,IS_SE) % P=0.065 (statistically
      comparable)
72 [h,p] = ttest2(old_stat_SE,IS_SE) % P=0.91 (statistically
      comparable)
73

```

```
74 %% static_new, static_old, IS (TB)
75 % equal variance? static_old vs IS_old
76 X = [5.4468e-04 1;-0.0066 1;0.0244 1;0.004 1;0.0198 1;0.0204
      1;0.0192 1;0.0265 1; 0.015 2;-0.0132 2;0.006 2;0.005 2;0.0166
      2;0.0109 2;0.0068 2;0.0095 2];
77 Levenetest(X,alpha) % yes
78
79 group = [repmat({'First'}, 2, 1); repmat({'Second'}, 8, 1);
          repmat({'Third'}, 8, 1)];
80 boxplot([new_stat_TB;old_stat_TB;IS_TB],group,'Labels',{'Static
          (R), n=2','Static (C), n=8','IS (C), n=8'},'Whisker',1)
81 % title('Top/Bottom SI Shoulder region')
82 ylabel('Average X strain')
83 ylim([-0.06 0.06]);
84
85 [h,p] = ttest2(old_stat_TB,IS_TB) % P=0.26 (statistically
          comparable)
```